

Development of Photoacoustic Spectral Response Technique For Biomedical Applications

Ph.D Thesis

By

Deblina Biswas



**DISCIPLINE OF ELECTRICAL ENGINEERING
INDIAN INSTITUTE OF TECHNOLOGY INDORE**

June 2017

Development of Photoacoustic Spectral Response Technique For Biomedical Applications

A THESIS

*Submitted in partial fulfillment of the
requirements for the award of the degree
of*

DOCTOR OF PHILOSOPHY

By

Deblina Biswas



**DISCIPLINE OF ELECTRICAL ENGINEERING
INDIAN INSTITUTE OF TECHNOLOGY INDORE**

June 2017



INDIAN INSTITUTE OF TECHNOLOGY INDORE

CANDIDATE'S DECLARATION

I hereby certify that the work which is being presented in the thesis entitled **“Development of Photoacoustic Spectral Response Technique For Biomedical Applications”** in the partial fulfillment of the requirements for the award of the degree of **DOCTOR OF PHILOSOPHY** and submitted in the **DISCIPLINE OF ELECTRICAL ENGINEERING, INDIAN INSTITUTE OF TECHNOLOGY INDORE**, is an authentic record of my own work carried out during the time period from July 2012 to May 2017 under the supervision of Dr. Srivathsan Vasudevan, Assistant Professor, Discipline of Electrical Engineering, IIT Indore. The matter presented in this thesis has not been submitted by me for the award of any other degree of this or any other institute.

Signature of the student with date
Deblina Biswas

This is to certify that the above statement made by the candidate is correct to the best of our knowledge.

Signature of Thesis Supervisor with date
Dr. Srivathsan Vasudevan

Deblina Biswas has successfully given her Ph.D. Oral Examination held on.....

Signatures of Thesis Supervisors
Date:

Convener, DPGC
Date:

Signature of PSPC Member #1
Date:

Signature of PSPC Member #1
Date:

Signature of External Examiner
Date:

***Dedicated to God,
my dearest Dadu,
my family and my teachers***

Acknowledgement

“A journey of thousand miles starts with a single step.- Lao Tzu”

And yes, Ph.D is that “single step” of the “thousand mile journey” of my research career. In this journey, I have been accompanied by many people who helped me to make this journey happy and memorable. Now I would like to express my appreciation to all of them.

Firstly, I would like to express my sincere gratitude to my advisor Dr. Srivathsan Vasudevan for the continuous support of my Ph.D study and related research, for his patience, motivation, and immense knowledge. His guidance helped me in all the time of research and writing of this thesis. I could not have imagined having a better advisor and mentor for my Ph.D study.

Besides my advisor, I would like to convey my heartiest thanks to Dr. George C. K. Chen for his suggestions and guidance throughout my Ph.D. His help and support kept me motivated and enthusiastic in my toughest days.

I would also like to thank my thesis committee: Dr. Amod Umarikar and Dr. Krushna Mavani for their insightful comments and encouragement, but also for the hard question which motivated me to widen my research from various perspectives.

I would like to express my sincere gratitude to my parents, my sisters for all the sacrifices they made on my behalf. My mother and father was always been a source of encouragement and inspiration to me throughout my life. My sisters were always with me during my hard times. This thesis was not possible without their support and help.

My sincere thanks also go to Dr. Sharad Gupta (IIT Indore), Dr. Debasis Nayak (IIT Indore), Dr. Preeti Bhoje, Dr. I. M. Palani, Dr. Trapti Jain, Dr. Sendhil Raja (RRCAT) and Mr. Shyam Sundar (RRCAT) who provided me an opportunity to join their team, and who gave access to the laboratory and research facilities. Without their precious support it would not be possible to conduct this research.

I would like to express my gratitude to Prof. Pradeep Mathur. He always goes out of the way to help students of IIT Indore.

I would take this opportunity to thank my collaborators Dr. Norman Sharma, Dr. Priyanka Bhagat, Dr. Chitnis, Dr. Satish Phatak, Mr. Sheel from Choitram Hospital and Research Centre, Indore for providing me samples as well as helping me in understanding and analysing the results. I would like to thank Dr. M J. Paul for his advices that helped

me to in my experimental studies. I want to thank to Dr. Supriya Shukla (College of Veterinary Sciences and Animal Husbandry, Mhow) for providing me animal tissue samples.

My sincere thanks to my colleagues Abhijeet, Karthik, Avay, Shiva, Akash, Krishna, Smriti, Suchismita, Mithun, Sayan, Anshu, Nandini, Dr. Kesav for their enormous help in my research work. A special thanks to Dr. Swarup Roy for his extensive help in experiments, technical discussions and thesis writing.

I would like to express my thanks to Mr. Anand Pitare, Mr. P.K. Parthivan, Mr. Satish Kausal, Mr. Deepak Dhepte, Mr. Pawan Chawhan and Mr. Pavanendra Mucchal for their enormous help in my research work.

I would like to thank Mr. Siddhartha Dhawale and his team members for helping me in all possible ways.

I would expand my special thanks to my best friend Shreya for her constant support and motivation during my hard times. I would also like to thank all my friends Smriti, Suchi, Anuradha, SmritiPriya, Surbhi, Shanu, Tulika, Shailendra, Vikash, Krishna, Tejendra, Yogesh, Shivendra, Anupam, Mithun, Sayan, Vishnu for providing me a homely environment in IIT Indore. Very special thanks to Dr. Swarup Roy for his support and encouragement in my toughest period of Ph.D.

I would like to sincerely thank Mrs. Meghna and her family for love and care. I would also thank Srini Sir and Archana Madam for their care and affection.

I want to thank all staff member of IIT Indore for providing all comfort and convenience.

Last but not at all the least, I want to express my gratitude towards Dr. Shilpa, Dr. P. Matkar and other staff members of IIT dispensary who kept me physically fit. Beside this, several people have knowingly and unknowingly helped me in successful completion of my thesis.

I also acknowledge MHRD for providing me financial assistance.

Deblina Biswas

LIST OF PUBLICATIONS

A. Journals:

1. **D. Biswas et al.**, “Quantitative photoacoustic characterization of blood clot in blood: A mechanobiological assessment through spectral information Quantitative assessment of blood clotting mechanism using Photoacoustic spectral response technique”, *Review of Scientific Instruments*, **AIP** (Doi: [10.1063/1.4974954](https://doi.org/10.1063/1.4974954)).
2. **D. Biswas et al.**, “Quantitative differentiation of pneumonia from normal lungs: diagnostic assessment using photoacoustic spectral response”, *Applied Spectroscopy* (OSA) (Doi: [10.1177/0003702817708320](https://doi.org/10.1177/0003702817708320)).
3. **D. Biswas et al.**, “Time-Frequency Based Photoacoustic Spectral Response for Differentiating Human Breast Masses”, *Biomedical Physics and Engineering Express*, (IOP) (Doi: [10.1088/2057-1976/aa6b06](https://doi.org/10.1088/2057-1976/aa6b06)).

B. Conferences:

1. **D. Biswas, et. Al.**, “Photoacoustic imaging for Biomedical Applications”, in **DAE- BRNS National Laser Symposium (NLS) – 22nd**, January 2014.
2. **D. Biswas, et al.**, “Investigation of diseases through red blood cells' shape using photoacoustic response technique”, in *SPIE BiOS*, 2015, pp. 93220K-93220K-5.
3. **D. Biswas, et. al.**, “Gold Nanoparticles as Photoacoustic tomography contrast agent”, in **ICONSAT**, IISER Pune-2016.
4. **D. Biswas, et. al.**, “Quantitative Charecterisation of biological tissues using Photoacoustic spectral response”, in **Photonics 2016**, OSA, IIT Kanpur.

Contents

Acknowledgment	i
List of publication	iii
List of figures	x
List of tables	xvi
List of abbreviations	xvii

Chapter 1: Motivation and objectives

1.1 Motivation	1
1.2 Objective	6
1.3 Major contribution of the thesis	8
1.4 Overview of the thesis	10

Chapter 2: Introduction to photoacoustic technique

2.1 Brief history of tissue imaging	11
2.2 Physics of photoacoustics	14
2.2.1 PA wave generation and propagation	15
2.2.1.1 Laser safety standard	19
2.2.2 PA signal detection and image reconstruction	20
2.2.3 Ultrasound sensor	20
2.2.4 Characteristics of time domain PA signal	21
2.3 Image reconstruction	22
2.3.1 PA signal processing	22
2.3.2 Image reconstruction algorithm	24

2.4 Types of PA technique	25
2.4.1 PA imaging	25
2.4.1.1 Photoacoustic tomography (PAT)	25
2.4.1.2 Photoacoustic microscopy (PAM)	26
2.4.2 PA signal analysis and spectroscopy	27
2.5 Biomedical application of PA technique	28
2.5.1 Brain imaging	29
2.5.2 Arthritis detection	30
2.5.3 Arterial plague detection	30
2.5.4 Hematological diseases	31
2.5.5 Cancer diagnosis	33
2.6 Summary and potential advancement in conventional PA technique	36

Chapter 3: Photoacoustic spectral response experimental development and characterisation

3.1 Introduction and motivation	37
3.2 Materials and instrumentation	38
3.2.1 PASR experimental setup	38
3.2.2 Software interface and signal conditioning	40
3.2.2.1 PA signal acquisition	41
3.2.2.2 Signal conditioning	42
3.2.2.3 Signal processing	45
3.2.3 Different parameter and their effect on PA signal: An analysis	49
3.2.3.1 Effect of absorption and laser energy	49
3.2.3.2 Spot size of laser	51
3.2.3.3 PA sample container	53

3.2.3.4 Distance between sample and sensor	53
3.3 PASR experiment with biological sample	54
3.3.1 Change in PA signal amplitude by varying RBC concentration	55
3.3.2 RBC shape analysis using PA signal amplitude	57
3.4 Elastic property study using PASR	60
3.4.1 Simulation study	60
3.4.2 Tissue mimicking phantom study	61
3.4.3 Elastic property study using biological samples	67
3.5 Summary	69

Chapter 4: Application of Fast Fourier Transform based PASR technique for different disease diagnosis

4.1 Introduction	71
4.1A Problem statement and motivation	71
4.2A Mechanism of clot formation	74
4.3A Materials and methods	75
4.3A.1 Sample preparation	75
4.3A.2 PASR experiments	76
4.4A Results	76
4.5A Discussion	79
4.1B Motivation and hypothesis	81
4.2B General introduction	83
4.2B.1 About Pneumonia	83
4.3B Materials and methods	84
4.3B.1 Biological sample preparation	84
4.3B.2 PASR experiment	85

4.3B.3 Frequency spectrum analysis of PA response	85
4.3B.4 Histology of lung tissues	86
4.4B Results	86
4.5B Discussion	88
4.2 Summary	93

Chapter 5: Application of Time-frequency based PASR technique for quantitative assessment of human breast masses

5.1 Introduction	95
5.2 Motivation	96
5.3 Introduction to breast tumours	98
5.3.1. About human breasts	98
5.3.2 Type of breast masses	100
5.3.2.1 Benign breast tumours	100
5.3.2.2 Types of malignant tumours	101
5.4 Qualitative differentiation of normal and malignant breast masses	102
5.4.1 PASR experiments for normal and malignant tissue diagnosis	103
5.4.1.1 About Wigner-Ville distribution	103
5.4.1.2 Histology study	105
5.4.2 Results and discussions	105
5.5 Quantitative breast masses classification by EWT-PASR technique	107
5.5.1 Tissue sample preparation and EWT-PASR experiments	109
5.5.2 Empirical wavelet transform	109

5.5.3 Results	113
5.5.3.1 Frequency spectrum analysis of photoacoustic signals of human breast masses	113
5.5.3.2 EWT extracted mono-component analysis of breast masses	115
5.5.3.3 Feature based differentiation of breast masses	117
5.5.3.4 Histopathology of human breast masses	119
5.5.4 Discussions	120
5.5.4.1 Spectral magnitude of frequency components	120
5.5.4.2 Energy analysis of mono-components	120
5.6 Summary	121

Chapter 6: PASR technique for therapeutic application: differentiating normal and thermally coagulated tissues

6.1 Introduction and motivation	123
6.2 Conventional non-invasive monitoring techniques	124
6.3 Applying PASR to monitor therapeutic process	124
6.4 Basics of tissue coagulation	125
6.5 Sample preparation for coagulation study	126
6.6 Differentiation of normal and coagulated tissues using PASR technique	127
6.7 Coagulation with external absorber	131
6.7.1 Sample preparation	131
6.7.2 PASR experiments with chicken liver and black ink	132
6.7.3 Alternative external absorber for targeted thermal therapy and monitoring	134

6.7.3.1 Gold nanoparticle characterization	134
6.7.3.1.1 Field emission scanning electron microscopy (FESEM) study	134
6.7.3.1.2 UV-Visible spectroscopy	135
6.7.3.2 PASR experiments of gold nanoparticles	136
6.8 Summary	137
Chapter 7: Conclusions and future scope	
7.1. Conclusion	139
7.2. Future prospects of PASR technique	142
Appendix	
Appendix I	145
Appendix II	147
References	149

List of Figures

Fig. 2.1. An overview of different tissue imaging modalities	11
Fig. 2.2. PA wave generation and propagation schematic	20
Fig. 2.3. A typical PA signal from circular numerical target	21
Fig. 2.4. Photoacoustic tomography detection geometry (a) spherical (b) cylindrical (c) planar	25
Fig. 2.5. Schematic of (a) AR-PAM and (b) OR-PAM	26
Fig. 2.6. Optical absorption spectra of different tissue chromophores	27
Fig. 2.7. Photoacoustic tomography (PAT) cylindrical scanner for small animal brain imaging (a) image showing cerebral vasculature and surgically induced lesion (b) sectional image of skull after taking PAT image	29
Fig. 2.8. Images obtained from human finger (a) and (b) PA image, (c) and (d) histopathology images	30
Fig. 2.9. PA image of human artery in which dotted circle denotes the lipid rich plaque	31
Fig. 2.10. Absorption spectra of oxygenated and deoxygenated haemoglobin	32
Fig. 2.11. PA images of (a) acute and (b) chronic clot in phantom study	32
Fig. 2.12. Images acquired from human breast using (a) mammogram (b) ultrasound (c) PAT	34
Fig. 2.13. PA images of cyst and malignant tumour in human subject that clearly illustrated malignant tissue with higher contrast	34
Fig. 2.14. Functional PA images of mouse brain in which circled part indicates the hypoxia region	35
Fig. 3.1. Block diagram of developed PASR setup	38
Fig. 3.2. Absorption spectra of whole blood	39
Fig. 3.3. Schematic diagram of PASR setup for liquid samples	40

Fig. 3.4. PA signal acquired from (a) black rubber sample (b) simulated numerical target	41
Fig. 3.5. Signal acquired from developed PASR system with and without averaging	44
Fig. 3.6. Front panel of LABVIEW based software interface	45
Fig. 3.7. (a) PA response from test sample (b) PA frequency spectrum without zero padding (c) PA frequency spectrum with zero padding	46
Fig. 3.8. Type of signal processing techniques used in the thesis	47
Fig. 3.9. (a) Signal with different frequency components (b) frequency spectrum of “a” obtained using FFT (c) WVD of signal illustrated in “a” The conversion factor for Y-axis is (coordinate position / 3000)*(Fs/2) and X-axis is ((co-ordinate position+5000)/3000)*(Fs/2). Fs is the sampling frequency (500 Hz). The unit of time and frequency is s and Hz respectively.	49
Fig. 3.10. Frequency spectrum from simulated target with varied absorption (absorption increased by 1.5 times and 2 times), corresponding time domain signal given in inset (a) without normalisation (b) after normalisation of PA time domain signal	50
Fig. 3.11. Laser energy vs PA signal amplitude plot	51
Fig. 3.12. Simulation study performed on numerical targets of different diameter to depict different sample size that provide (a) PA responses and (b) PA frequency spectrum	52
Fig. 3.13. Frequency spectrum of black rubber sample with sensor position varied by 5 mm (inset image provides PA time domain signal of the same sample (a) without normalisation (b) after normalisation	54
Fig. 3.14. PA response vs blood concentration plot	56
Fig. 3.15. Absorption spectra of water and NaCl	56
Fig. 3.16. Microscopy images of (a) isotonic (b) hypertonic (c) hypotonic samples	58
Fig. 3.17. PA response Vs isotonic, hypotonic and hypertonic sample plot	59
Fig. 3.18. Absorption spectra of PA response Vs isotonic, hypotonic and hypertonic samples	59
Fig. 3.19. Spectral information of two numerical targets with (a)	61

sound speed 1600 m/s and sound speed 1900 m/s (density 1500 kg/m³) (b) density 1600 kg/m³ and density 2000 kg/m³ (sound speed 1500 m/s)

Fig. 3.20. UV-VIS absorption spectra of black ink	62
Fig. 3.21. Plot of gelatine concentration and PASR median frequency	62
Fig. 3.22. PA frequency spectrum of black ink and beetroot sample when the samples placed in glass cuvette	63
Fig. 3.23. PA response obtained from (a) beetroot juice placed in glass cuvette (b) black rubber sample	64
Fig. 3.24. Schematic of PA response reflection in glass cuvette and response of band pass filter	65
Fig. 3.25. PA response of beetroot sample placed in silicone rubber tube that exhibits no oscillation	66
Fig. 3. 26. PA frequency spectrum of black ink and beetroot sample when the samples placed in silicone rubber tube which illustrates shift in frequency	66
Fig. 3.27. Spectral information of muscle and liver tissues obtained through PASR technique	68
Fig. 3.28. Box plot of (a) dominant frequency (b) spectral magnitude. The shaded box represent 25 - 75 % of the data set. The line in the box is the median and mean value is shown as square box. The whiskers (cross sign) show the maximum and minimum of data set	69
Fig. 4.1. (a) PA response of blood and blood clots of donor 1, (b) PA response of blood and blood clots of donor 2	73
Fig. 4.2. Schematic of prothrombin to thrombin conversion and polymerization of fibrinogen for fibrin fibers formation	75
Fig. 4.3. PA time domain signal from blood and blood clot	77
Fig. 4.4. Monitoring of clot formation using dominant frequency of PA frequency spectrum	77
Fig. 4.5. PA spectral response dominant frequency of 20 sets of blood and blood clots	78
Fig. 4.6. (a) PA response and (b) Spectral information of control,	87

Group 1 and Group 2 goat lungs

Fig. 4.7. Histopathology of Pneumonia affected goat lung in which green circle shows Group 1, yellow circle indicates Group 2, blue arrows show the oedematous fluid and green arrows indicate the air	88
Fig. 4.8. Schematic of spring-mass damper system	90
Fig. 4.9. Underdamped oscillatory behaviour	91
Fig. 5.1. Anatomical structure of human breast	99
Fig. 5.2. Contour plot of typical PA time domain signal in which dotted circle represent the low frequency component and the other indicate the high frequency component. The conversion factor for Y-axis is $(\text{coordinate position} / 3000) * (F_s/2)$ and X-axis is $((\text{coordinate position} + 5000) / 3000) * (F_s/2)$. F_s is the sampling frequency (200 MHz). The unit of time and frequency is s and MHz respectively	105
Fig. 5.3. WVD contour plot of human breast masses from different patient. Figures 4(a), (c), (e), (g) illustrate normal and figures 4(b),(d), (f), (h) illustrate malignant breast tissues. The conversion factor for Y-axis is $(\text{coordinate position} / 3000) * (F_s/2)$ and X-axis is $((\text{coordinate position} + 5000) / 3000) * (F_s/2)$. F_s is the sampling frequency (200 MHz). The unit of time and frequency is s and MHz respectively	107
Fig. 5.4. (a) Fourier spectrum of a typical PA signal (b) Boundary segmented Fourier spectrum (c) & (d) First and second mono-components of the PA signal obtained from Empirical Wavelet Transform	108
Fig. 5.5. Flow chart of EWT technique. The equations mentioned in flow chart are detailed in Section 5.5.1.1	112
Fig. 5.6. EWT analysis of PA signal (a) Boundary segmented Fourier spectrum (b) First mono-component (frequency 0.99 MHz) (c) Second mono-component (frequency 3.3 MHz) (d) Third mono-component (frequency 11.2 MHz)	113
Fig. 5.7. PA response of Normal tissue, Fibroadenoma and Malignant breast tissues	114
Fig. 5.8. Boundary segmented Fourier spectrum of Normal tissue, Fibroadenoma and Malignant breast tissues	114
Fig. 5.9. EWT extracted mono-components of benign tissue, fibroadenoma and malignant tumour (a) First mono-component (b)	116

Second mono-component

- Fig. 5.10.** Energy of mono-components (E1 and E2) of Normal, fibroadenoma and malignant tissues 117
- Fig. 5.11.** Box Plot of EWT based features of normal, benign and malignant breast masses. The Y-axis is shown in log scale. The shaded box represent 25 - 75 % of the data set. The line in the box is the median and mean value is shown as solid box. The whiskers (cross sign) show the maximum and minimum of data set. 118
- Fig. 5.12.** Microscopic images of histopathology of (a) Normal, (b) Fibroadenoma and (c) Malignant tissue; The cells encircled are epithelial cells and the stromal population are pointed with arrows. 119
- Fig. 6.1.** Photograph of chicken tissues (a) muscle (b) liver. Discoloured part indicates the coagulated regions 126
- Fig. 6.2.** Chicken muscle tissue normal and coagulated (a) PA response (b) PA frequency spectrum 128
- Fig. 6.3.** Box plot of normal and coagulated muscle. The Y-axis illustrates dominant frequency in MHz. The shaded box represents 25 - 75 % of the data set. The line in the box is the median and mean value is shown as solid box. The whiskers (cross sign) show the maximum and minimum of data set 128
- Fig. 6.4.** Chicken liver tissue normal and coagulated (a) PA response (b) PA frequency spectrum 129
- Fig. 6.5.** Box plot of normal and coagulated liver. The Y-axis illustrates dominant frequency in MHz. The shaded box represent 25 - 75 % of the data set. The line in the box is the median and mean value is shown as solid box. The whiskers (cross sign) show the maximum and minimum of data set 130
- Fig. 6.6.** Absorption spectra of black ink 131
- Fig. 6.7.** PA frequency spectrum of liver tissue with and without ink 132
- Fig. 6.8.** PA frequency spectrum of liver tissue obtained from normal, coagulated and coagulated with ink region 133
- Fig. 6.9.** SEM micrograph of GNPs. The clustered nanoparticles are shown in red circle and the single nano particles are shown in green circle 135
- Fig. 6.10.** Absorption spectra of GNPs 135

Fig. 6.11. PA response obtained from GNPs 136

Fig. 6.12. PA response obtained from pure blood 137

List of Tables

Table 2.1. Medical imaging techniques and their features	13
Table 3.1. Composition of the solutions for varying tonacity of blood	57
Table 3.2. Composition of blood samples	58
Table 4.1. PA frequency spectral parameters of blood and clot samples	78
Table 4.2. Main compositions of different regions of goat lung	85
Table 4.3. PA frequency spectral parameters of goat lungs	88
Table 5.1. Spectral magnitude along with error of different breast masses (FC: Frequency component)	115
Table 5.2. cell population in different breast masses	121

Abbreviations

Electrocardiogram	ECG
Electromyogram	EMG
Photoacoustic	PA
Photoacoustic Spectral Response	PASR
Fast Fourier Transform	FFT
Wigner-Ville distribution	WVD
Empirical Wavelet Transform	EWT
Magnetic resonance imaging	MRI
Computer tomography	CT
Positron Emission Tomography	PET
Single photon emission computer tomography	SPECT
Optical coherence tomography	OCT
American National Standard Institute	ANSI
Maximum permissible exposure	MPE
Lead zirconate titante	PZT
Photoacoustic tomography	PAT
Photoacoustic microscopy	PAM
Acoustic resolution photoacoustic microscopy	AR-PAM
Optical resolution photoacoustic microscopy	OR-PAM
Red blood cells	RBCs
Circulating tumour cells	CTC

Near Infra red	NIR
Neodymium-doped yttrium aluminium garnet	Nd:YAG
Signal to noise ratio	SNR
short time Fourier transforms	STFT
Continuous wavelet transform	CWT
Empirical mode decomposition	EMD
Extracellular matrix	ECM
Ultrasound	US
Ductual carcinoma in situ	DCIS
Invasive ductal carcinoma	IDC
Hematoxylin eosin	HNE
Gold nanoparticle	GNP
Field Emission Scanning Electron Microscopy	FESEM

Chapter 1

Motivation and objectives

“Beginning at the beginning”, the king said gravely, “and go on till you come to the end; then stop”- Lewis Carroll

1.1 Motivation

Medical diagnostics, per se, has become an altogether a new area in the field of medical sciences. Increasingly, it has been realized that diagnosing a disease or any pathological condition plays a very important role in medical sciences. Identifying the right pathological condition, would lead to proper treatment and therapy and the patient would recover faster. Particularly, for many critical illnesses (e.g., cancer, immuno-suppressive diseases etc.) early diagnosis leads to prompt and effective therapy which could make a life and death difference for the patient.

Physicists and engineers work in tandem with clinicians to understand their diagnostic requirements and develop new instruments / techniques for diagnosis. These developments over the years, has led to many cellular / biochemical investigations on one side and tissue based diagnostics on the other side [1], [2]. Analysing the components of blood through biochemical ways and microscopic studies have led to diagnosis of many diseases through blood tests and it has become very common [3]–[7]. Similarly, developments made on the tissue side has led to many imaging techniques such as X-Ray, ultrasound (US) imaging, magnetic resonance (MRI) imaging and sensing techniques such as Electrocardiogram (ECG), Electromyogram (EMG) etc. [8]–[19].

With the advent of new diseases and the demand for early diagnosis of critical diseases for better treatment and therapy, these diagnostic techniques have been pressed hard to provide more information and not just positive / negative result. For example, in addition to the presence of a disease, clinicians need more information like the stage / grade of the disease and also the severity of the disease to provide targeted therapy. Due to these demands, evolution of new diagnostic techniques such as optical coherence tomography (mainly used for eye applications), novel confocal microscopy (detailed cellular level analysis), photoacoustic imaging (deep tissue imaging

Chapter 1

with high contrast) have been witnessed in the recent past [20]–[26]. Moreover, continuous monitoring of the disease and the progress of the therapy also needs to be monitored by diagnosis. Therefore, the requirement of any diagnosis techniques would be

- completely non-invasive to provide repetitive diagnosis
- provide functional information with details leading to specific therapy
- complement with the existing diagnostic technique to provide better diagnosis

In the realm of tissue diagnostics, this thesis would focus on a recently popular technique known as photoacoustic (PA) imaging and sensing technique. Photoacoustic (PA) technique, conventionally used for liquid and gas sensing applications, has recently been applied to biological tissue imaging and characterisation [27]–[33]. PA is a hybrid modality where the tissues are irradiated with a short laser pulse that leads to generation of ultrasound signals that characterize the sample [32], [34]–[36]. These ultrasound signals are either acquired by a single transducer or an array of transducers. Obtaining PA signals from different sensor locations and then feeding them to a time-reversal reconstruction algorithm would provide tomographical photoacoustic tissue images which are very similar to ultrasound images [37]. Since PA technique is a hybrid modality (blend of optics and acoustics), PA images provide high specificity (due to optical absorption of tissue) and high depth of penetration (ultrasound scattering in tissues is lower than optical). These advantages of PA, compared to the conventional techniques (ultrasound, X-RAY etc.), have prompted wide biomedical applications such as brain imaging, cancer diagnosis, arterial plaque detection, arthritis diagnosis etc. [32].

PA reconstructed image is representing the optical absorbers (probing different tissue chromophores at different optical wavelengths) as specificity in the image. For example, oxygenated haemoglobin and de-oxygenated haemoglobin would have different

optical absorption wavelengths, thereby showing as a contrast in a PA image taken at a specific optical wavelength [38]–[40]. Due to high specificity of PA images, many studies have reported screening of diseases using PA imaging. Detection of human breast cancer (correlated with biopsy studies), arthritis in animal models (correlated with standard diagnostics), plaque detection are some of the applications where this technique has shown an edge over traditional techniques [41], [42].

Even though photoacoustic imaging has sufficient promise, it has not moved from research bench to the clinical side yet because, mere detection of a disease itself is not sufficient. For example, providing critical information that can complement the existing detection and also continuous monitoring of the therapeutic process is an important part of a non-invasive clinical diagnostic system. PA technique is capable of providing these information which has not been explored so far. Conventional PA images would provide optical absorption parameter as a signature of the tissue. This is sufficient to provide a screening and give a positive / negative answer but could not go any further to accomplish the demands of the clinical fraternity [42].

One such application explored using PA imaging is to differentiate acute from chronic blood clots which is a very useful study for thrombosis applications (leading to stroke, heart attacks etc.). While PA imaging can successfully differentiate these two clots, it has also been reported that they could not differentiate acute clots from blood [26]. The reason is these two have almost identical optical absorption leaving little contrast in the PA images. Differentiating blood from the clots is essential because in real-time situations blood is an integral part of the clot and needs to be differentiated. This indicates the limitation of conventional PA imaging for in-vivo application as inside blood vessels clot will be immersed in blood. Therefore clots cannot be detected inside blood vessels. Moreover mechanism of clot formation and understanding viscoelastic property of blood is very

Chapter 1

important for early diagnosis of thrombotic diseases (e.g. deep vein thrombosis, ischemia, stroke etc.) [43].

In another application of detection of human breast cancer, PA can differentiate cyst from malignant tumour non-invasively. However, the same study also reported that benign tumour (fibroadenoma) and malignant tumour could not be differentiated and the reason being identical optical absorption. Therefore these two types of solid tumours cannot be diagnosed using conventional PA technique. Thus the clinicians have to depend on invasive techniques like biopsy for diagnosis that is highly inconvenient for the patient [42].

PA images completely depend on optical absorption as a parameter and the depth is governed by the ultrasound waves that exhibit less scattering compared to optical detection. However, PA can also provide important mechano-biological information that can be used as an aid for better understanding of the disease [44]–[46]. This information is contained in the time domain signal acquired from each transducer. The rise time, relaxation time and the amplitude are the important components of the PA signal. However, while forming the PA image, only the amplitude of the signal (corresponding to the optical absorption of the tissues) is taken into account. Other parameters would provide important mechano-biological information which can also be extracted [47]. By obtaining this information, the technique can not only screen but provide vital information from a diagnosis point of view. For example the relaxation time of the PA time domain signal is associated to the mechano-biological property i.e. elasticity of the sample. It is well known from literature that significant change in elasticity is observed in normal and pathological tissues especially in normal, benign and malignant breast masses. Since conventional PA imaging fails to differentiate benign and malignant breast masses, changing the focus from optical absorption based PA imaging to tissue elasticity based PA signal analysis would provide better diagnosis. This would be also pragmatic to detect clot

immersed in blood since clot and blood substantiates distinct change in elasticity.

Not only screening, tissue elasticity provides pathological as well as biophysical information about the sample. Thus, understanding the mechanisms involved in different diseases such as clot formation, viscoelasticity change in blood, identifying early stage of Pneumonia would be possible by analysing PA time domain signal which is not been explored yet.

Chapter 1

1.2 Objectives

Despite huge potential of PA technique, Conventional PA imaging alone would not bring out many advantages of this technique and would depend only on optical absorption as parameter. Obtaining different mechano-biological properties of the tissues would complement the screening and also aid in better understanding of the disease and the pathological conditions as well. In this context, instead of focussing on PA imaging, PA signals can be used to quantitatively extract the mechano-biological information of the biological tissues.

Therefore, the primary objective of the thesis would be to develop photoacoustic experiment for obtaining the signal response and explore diagnosis based on mechano-biological properties of the tissues like tissue elasticity, density etc. Followed by these information, the setup would be applied to tissue phantoms to elicit mechano-biological information. In this process, different signal processing techniques in time as well as frequency domain would be applied to elicit elasticity dependent information from tissues. Subsequently, some of the issues faced in conventional PA imaging would be addressed. Differentiating blood clot in the presence of blood would be the first application where the continuous process of clot formation is explained through elasticity information obtained through the developed photoacoustic Spectral Response (PASR). Following this, different applications such as pneumonia detection, breast cancer detection using time-frequency analysis would be explored and critical functional information of the tissues is obtained. The detailed objectives are given as follows:

- ❖ Development and characterisation of PA spectral response setup for different disease diagnosis and study
- ❖ Theoretical analysis to understand relation between PA spectral parameters and sample's elasticity

- ❖ To validate the theoretical analysis with simulation and tissue mimicking phantom study.
- ❖ Applying this technique for various applications such as blood and blood clot differentiation, early stage of Pneumonia (red hepatisation) detection, classifying human breast masses i.e. normal, benign and malignant and differentiating coagulated tissue from normal.
- ❖ Utilising advance signal processing tools to extract time domain and frequency domain features of PA signal and correlating with tissues elasticity. Comparing the obtained results with standard technique like histopathology.

Chapter 1

1.3 Major contribution of the thesis

The major contributions made by the candidate are:

- ✓ **Development of PASR technique:** The sample elasticity based PASR system was developed in-house by nano-second laser pumping and ultrasound probing of generated acoustic signals that is characterised with tissue mimicking phantom and real biological samples. Careful consideration was made to eliminate the effect of different experimental parameters and to improve the signal to noise ratio. Subsequently, different signal processing tools (solely frequency based and time-frequency based) were explored to extract PA spectral parameters. Then, simulations as well as experimental studies were performed to investigate the effect of elasticity change in PA spectral parameters.
- ✓ **Quantitative assessment of blood clotting mechanism and characterisation of blood and clot:** PA spectral parameters (dominant frequency, spectral energy) were observed to be sensitive towards change in sample elastic property. Hence the developed technique was applied to study clot formation using PA spectral parameters. Following this, blood and clot immersed in blood was differentiated by obtaining PA frequency spectral parameters. The obtained results were validated with theoretical study that explains relation between elasticity and PA spectral parameters.
- ✓ **Early stage Pneumonia diagnosis:** Detection of early stage Pneumonia (red hepatisation) was investigated on formalin fixed goat lungs using FFT based PASR technique. PA spectral parameters (dominant frequency, spectral energy) provide significant disparity among normal and pathological part of the lung sample. By comparing obtained results with standard histopathology, high correlation between tissue pathology and PA spectral parameters were obtained.

- ✓ **Human breast masses classification:** After qualitative differentiation of normal and malignant breast masses through time-frequency based Wigner-Ville distribution (WVD) based PASR, quantitative classification of normal, benign and malignant breast masses were performed by Empirical Wavelet Transform (EWT) based PASR technique. By obtaining time domain, frequency domain and time-frequency domain features, the breast masses were classified with very high accuracy. Following this, obtained EWT-PASR parameters were compared with standard histopathology to obtain tissue pathological information.
- ✓ **PASR technique for therapeutic application:** Normal and coagulated chicken tissues were quantitatively differentiated in an in-vitro study using PASR technique. This study is an application to monitor the response of tissues after therapy (photodynamic). Gold nanoparticles were explored as external absorbers for targeted and controlled ablation.

Chapter 1

1.4 Overview of the thesis

The thesis consists of total seven chapters. It is given as follows:

- ✓ Chapter 1 is the introduction that includes motivation and objectives of the thesis.
- ✓ Chapter 2 provides a literature survey on the developments in this field and the bottlenecks faced.
- ✓ Chapter 3 focuses on analysis of acquired PA signal and takes through the experimental development of PASR
- ✓ Chapter 4 describes applications of developed FFT based PASR technique for differentiating blood and clot immersed in blood and early stage Pneumonia diagnosis.
- ✓ Chapter 5 illustrates applications of Time-frequency based PASR technique quantitative classification normal, benign and malignant breast tissues.
- ✓ Chapter 6 describes therapeutic application of PASR technique for differentiate normal and coagulated tissues
- ✓ Chapter 7 summarise the important findings of the thesis and also details about the future prospective.

Chapter 2

Introduction to photoacoustic technique

“Research has to see what everybody else have seen, and to think what nobody else has thought”-Albert Szent Gyorgi

This chapter discusses photoacoustic technique and its various biomedical applications. It also describes the bottlenecks of the conventional PA technique and possible solution through the proposed PASR technique.

2.1 Brief history of tissue imaging

Tissue imaging is always fascinating for the clinicians since it has primary advantage to get information regarding the tissue and/or organ non-invasively. Therefore it can be applied to the patient repeatedly for continuous monitoring. In this regard, tissue imaging modalities are the most viable option for the clinicians for chronic diseases like cancer, Pneumonia, thrombotic diseases etc. [48]–[52]. Tissue imaging can be defined as a technique which creates visual representation of the tissues by utilising various excitation-detection (optical, radiation, magnetic field, acoustic etc.) techniques to perform clinical analysis. Conventional tissue imaging modalities can be classified into two broad categories based on sample excitation method such as non-optical techniques and purely optical techniques. Figure 2.1 illustrates some of the tissue imaging techniques.

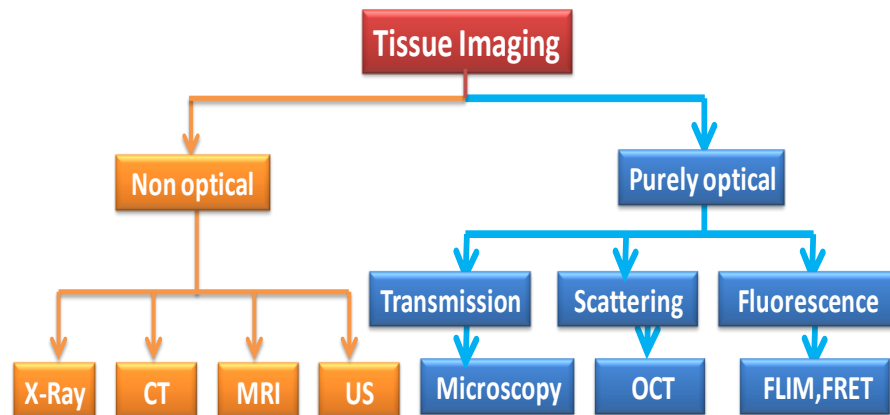


Fig. 2.1. An overview of different tissue imaging modalities

Chapter 2

Purely optical imaging modalities as mentioned in Fig. 2.1 utilise light as an excitation medium whereas the non-optical technique e.g. X-Ray, MRI, ultrasound involve various other excitation methods like ionisation radiation, magnetic field, acoustic waves etc. to generate image of the sample [53].

Purely optical techniques include mainly the microscopic techniques. It is well known that the first ever microscope was invented in the year 1590 by Janssen and his sons [54]. Thereafter, revolutionary changes have been witnessed in the field of microscopy by various researchers and it has become a highly essential tool for biologists. Apart from microscopy, optical coherence tomography (OCT), diffuse reflectance tomography (DRT) etc. also come under purely optical techniques. These techniques have numerous tissue imaging applications such as melanoma detection, ocular imaging, cervical cancer detection etc. [21], [55], [56]. However these techniques are limited by the depth of penetration as light gets highly scattered in the biological tissue. Therefore, the applicability of purely optical techniques is restricted to submillimeter depth beneath skin [9], [57].

The evolution in deep tissue imaging started with the discovery of X-Ray by William C. Rontgen in the year 1895 [58]. Ever since discovery of X-Ray clinicians have been using X-Ray as a regular diagnostic tool for many different disease diagnosis including breast cancer named as mammography [59]. Then approximately after 50 years, X-Ray based tomography imaging system i.e. computed tomography (CT) came up as an advanced imaging technique which was followed by nuclear medicine (gamma ray) based techniques like positron emission tomography (PET), single photon emission computer tomography (SPECT) etc. Despite these applications, these diagnostic techniques suffer from ionisation radiation that limits continuous monitoring in critical diseases [58]. Therefore it cannot be applied to the patient repeatedly for continuous monitoring and the younger age group patients as well. Later in 1970, a different approach i.e. sound

based imaging technique was introduced which came to be known as ultrasound. This new technique became very popular as it can image deep inside the tissues with micrometre resolution [9]. In addition ultrasound was non-ionising. Although ultrasound has all the features required for advanced tissue imaging, it suffers from lack of specificity since it totally relies on acoustic impedance mismatch. Therefore in case of tissues with insignificant change in acoustic impedance (e.g. fibroadenoma and malignant tumours), Ultrasound (US) generates false negative results for ultrasound [60]. Later in early 1980's, another very popular imaging modality, magnetic resonance imaging was introduced by P. Lautembur that uses magnetic field to generate the image of the sample. This technique became very popular due to its ability to provide very high contrast and penetration capability through skull. Therefore it came up as a brain imaging tool for the clinicians. Even though MRI illustrated several features that is essential for advanced tissue imaging, the cost of the technique hinder the use for continuous monitoring particularly in developing countries [58], [61]. The following table detail about features of conventional imaging modalities.

Table 2.1. Medical imaging techniques and their features

Techniques	Contrast	Penetration depth	Resolution
Ultrasound	Acoustic impedance mismatch	~60 mm	~300 micron
MRI	Magnetic field	~100 mm	~100 micron
OCT	Optical scattering	~1-2 mm	~10 micron
Confocal	Fluorescence/ scattering	~0.2 mm	~1-2 micron

Chapter 2

It is very evident that the conventional imaging techniques are not adequate to fulfil the requirement of advance diagnosis. Therefore researchers proposed a new technique which blends optical and non-optical eras to compliment the limitation of conventional techniques.

2.2 Physics of photoacoustics

Photoacoustic or optoacoustic imaging undoubtedly is an appealing image based diagnostic technique of the decade which has attracted the attention of scientists from different domains as well as clinicians. As the name suggests, PA technique is a unique blend of two different fields such as photo (optics) and the acoustics (sound). The features that make this technique most popular among researchers are non-invasive, non-ionising, high optical absorbance contrast and submicrometer resolution in deep (~5 cm) inside the tissues and organs which is desirable for advanced diagnosis [33], [62]. Unlike ultrasound, PA imaging is based on optical absorbance of the targeted tissue chromophores such as haemoglobin, lipid, water, melanin etc. (called contrast agent) which thereby enhances the specificity of the technique [57], [63]. The sample is probed with very short laser pulses (nano-second laser pulses) that generate non radiative, broad band acoustic signals due to thermoelastic expansion and compression of the sample. These acoustic signals are bipolar in nature known as PA response. Subsequent to acquisition, the PA responses are fed into reconstruction algorithms (e.g. time reversal, back projection) to form an image [37], [64], [65]. The primary advantage of this technique is it relies on detection of acoustic wave rather than photon (same as purely optical technique) as acoustic waves are less prone to scattering as well as attenuation compared to light. As a result, PA imaging yields higher spatial distribution of optical absorbance contrast deep inside the tissue that compliments the existing purely optical techniques. Not only high optical absorption contrast and penetration depth, PA imaging elucidate spatial resolution of ~10 μm which is ascendable with frequency of ultrasonic sensor similar to ultrasound imaging [66], [67].

2.2.1 PA wave generation and propagation

The basic physics behind photoacoustic technique was first observed by Alexander Graham Bell in the year 1880 during his experiment on photophone [68]. He observed that when the selenium cell was illuminated with modulated light, sound waves are generated. Since incidence of light caused sound generation, the physical phenomenon was named as photoacoustic effect.

In order to generate sound using light, the primary requirements are given as follows [30]:

- The sample should absorb the irradiated energy in terms of light or electromagnetic waves
- The energy should be in modulated form

If the above mentioned conditions are fulfilled then PA phenomenon can be observed. Usually for PA wave generation, short laser pulses are incident on the sample surface. The light penetrates through the sample depending upon the wavelength. Subsequently the light gets scattered and absorbed by the lattice specific molecules of the sample. PA works on the principle of short excitation which is shorter than two important time frames which are as follows [57], [69]:

- i. *Thermal relaxation time* is basically estimated by the thermal diffusion shown in Eq. 2.1.

$$\tau_{th} = \frac{d_c^2}{\alpha_{th}} \quad (2.1)$$

Where α_{th} is thermal diffusivity (m^2/sec) and d_c is the linear characteristic length of the heated regime of the sample.

- ii. The *stress relaxation time* is associated with pressure propagation i.e. the laser pulse duration should be less compared to time taken for release of stress from the heated regime. This is expressed as

Chapter 2

$$\tau_s = \frac{d_c}{V_s} \quad (2.2)$$

Where V_s is speed of sound.

Now if the laser pulse width is much smaller than the thermal relaxation time, then thermal confinement condition arises. If thermal diffusivity is considered to be $0.14 \text{ mm}^2/\text{sec}$ then for imaging a target with $100 \text{ }\mu\text{m}$ resolution, it would require 18 ns laser pulse according to Eq. 2.1. Consequently for stress confinement, the laser pulse width should be short compared to stress relaxation time. This is required for thermoelastic expansion of the sample which thereby causes acoustic signal generation. Similarly, to achieve $100 \text{ }\mu\text{m}$ spatial resolution in soft tissue imaging (sound speed $\sim 1500 \text{ m/s}$), the laser pulse width should be 60 ns according to Eq. 2.2. Thus it is clear from the above explanation that the laser pulse width should be in nano second duration in order to achieve submillimeter resolution. Fulfilment of these basic criteria initiates PA wave generation by enhancing the temperature of the sample followed by fractional volume change which is given as [57]

$$\frac{dV}{V} = -\kappa p + \beta T \quad (2.3)$$

Where κ is isothermal compressibility which is $\sim 5 \cdot 10^{-10} \text{ Pa}^{-1}$ for water and soft tissue, β represents thermal coefficient of volume expansion ($\sim 4 \cdot 10^{-4} \text{ K}^{-1}$ for muscle) [57], p and T represent the change in pressure and temperature.

The isothermal compressibility is expressed as [33]

$$\kappa = \frac{C_p}{dV_s^2 C_V} \quad (2.4)$$

here d is mass density and C_p , C_V are the specific heat constants at constant pressure and volume respectively. If both the criteria thermal

and stress confinements are fulfilled then there is negligible amount of volume expansion i.e. [57]

$$\frac{dV}{V} = -\kappa p + \beta T = 0 \quad (2.5)$$

The thermal expansion of the sample is followed by enhancement in initial pressure expressed as [33]

$$\Delta p_0 = \frac{\beta \Delta T}{K} = \frac{\beta}{\kappa d C_V} \eta_{th} A_e \quad (2.6)$$

Here A_e is denoted as optical absorption (J/m^3) and η_{th} is the percentage that is converted into heat. This can be represented as

$$\Delta p_0 = \Gamma A_e \quad (2.7)$$

$$\text{where } \Gamma = \frac{\beta}{K d C_V} = \frac{\beta V_s^2}{C_p} \quad (2.8)$$

The dimensionless parameter is named as Gruneisen coefficient that consists of thermal expansion coefficient, compressibility parameters and sound speed. The equation can be rewritten as

$$\Delta p_0 = \Gamma \eta_{th} A_e = \Gamma \eta_{th} \mu_a F \quad (2.9)$$

Here μ_a is optical absorption coefficient and F is fluence

This can be clearly observed that short laser pulse satisfies the confinement condition as well as ensure temperature rise to initial pressure increase when the Gruneisen coefficient is maximum. This initial pressure acts as a source of PA waves which depends on laser energy absorption and scattering property, thermal properties such as thermal diffusivity and thermal expansion coefficient as well as the elastic property of the material.

Chapter 2

The governing equation of photoacoustic wave generation and propagation in an acoustically homogeneous medium is given as follows [70]

$$\left(\nabla^2 - \frac{1}{V_s^2} \frac{\partial^2}{\partial t^2} \right) p(r,t) = - \frac{\beta}{\kappa V_s^2} \frac{\partial^2 T(r,t)}{\partial t^2} \quad (2.10)$$

Where $p(r,t)$ represents acoustic pressure at location r and time t , T indicates the rise in temperature.

The source term is detailed in the right side and wave propagation is illustrated in left part of the wave equation.

The generated PA waves are three dimensional (spherical) and time dependent signal which propagate through the sample in longitudinal mode (compression and rare fraction). Since PA waves are longitudinal waves, it is well associated with the particle velocity, density and the sound speed of the sample as well as the propagation medium that is given as [71], [72]

$$P(x, y, z, t) = v(x, y, z, t) \times \rho \times c \quad (2.11)$$

PA waves elucidate basic properties such as reflection and refraction at the boundaries of different density which follows Snell's law expressed as follows [73]:

$$\frac{\sin \theta_i}{V_{s1}} = \frac{\sin \theta_r}{V_{s1}} = \frac{\sin \theta_t}{V_{s2}} \quad (2.12)$$

Where θ_i , θ_r , θ_t are the angle of incidence, reflection and transmission with respect to the axis and V_{s1} , V_{s2} is the sound speed in the two mediums.

During propagation, generated PA waves are also affected by attenuation which is combined contribution of scattering and absorption of acoustic wave in the sample and the medium. The attenuation depends on the temperature and frequency that can be expressed as [74]–[76]

$$A' = A_0 e^{-a'z} \quad (2.13)$$

Where, a' is amplitude attenuation factor ($\text{dB/MHz}^{-1} \text{cm}^{-1}$), z is distance
 In case of biological tissues, the acoustic attenuation ($\sim 0.6 \text{ dB cm}^{-1} \text{MHz}^{-1}$) is very low compared to optical attenuation. However high frequency acoustic waves are more susceptible to attenuation. As a result, the acoustic signal would be very weak or die out before reaching the sensor. This will lead to decrease in penetration depth.

2.2.1.1 Laser safety standard

In order to ensure the safety of the subjects, certain limit of radiation exposure is decided by American National Standard Institute (ANSI). The limit depends on the laser wavelength, pulse duration, exposure duration and exposure aperture. The ANSI requirement policy states that “Exposure of the skin shall not exceed the MPE (Maximum permissible exposure) based upon a single-pulse exposure, and the average irradiance of the pulse train shall not exceed the MPE applicable for the total pulse train, duration T” (Laser Institute of America 2000). For example if a pulsed laser source generates a second harmonic laser pulse with 5 ns pulse width which irradiates the skin at the same region in area of 1 cm^2 for more than 10 s then safety standard for one single pulse would be 20 mJ (less than MPE). In addition the average power also should be less compared to MPE i.e. 200 mW. Basically long exposure is required for photoacoustic microscopy which needs raster scanning. In that case the safety limit can be expressed as follows [77]

$$E \times \sqrt[4]{F_r} \leq 2.75 \times 10^2 \pi d_a^{5/4} (\Delta / N_i)^{3/4} \quad (2.14)$$

where E is the pulse energy in mJ, F_r is the repetition rate in Hz, d_a represents the illumination spot diameter in cm, Δ denotes the scanning step size in cm and N_i is the number of pulses at each spot.

Chapter 2

2.2.2 PA signal detection and image reconstruction

The generated PA waves are propagated through the sample and the coupling medium (water, ultrasonic gel for biological tissue imaging). These signals are acquired by the ultrasonic sensor placed around the sample surface. The schematic of PA wave generation and propagation is illustrated in Fig 2.2.

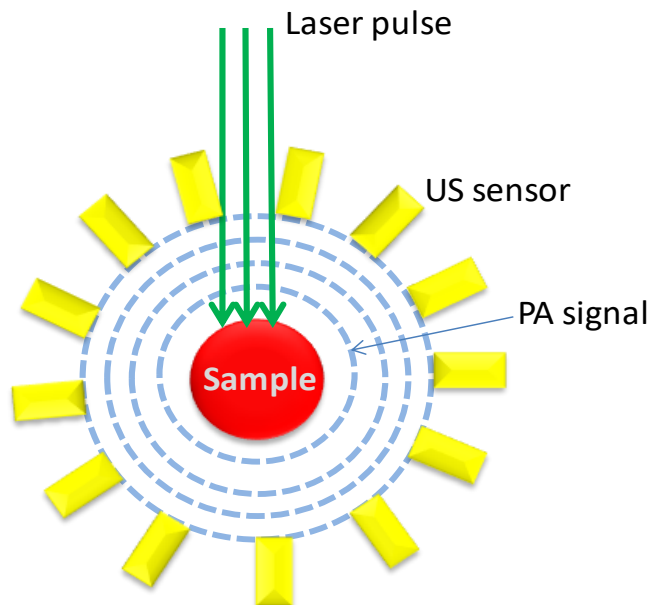


Fig. 2.2. PA wave generation and propagation schematic

2.2.3 Ultrasound sensor

For PA applications, commonly used ultrasonic sensors are made of Lead zirconate titanate (PZT) which is a piezoelectric crystal [69], [78], [79]. The basic principle of piezoelectric crystal relies on piezoelectric effect i.e. when potential difference is applied to opposite sides of the crystal surface, mechanical displacement is observed. Similarly application of mechanical force produces potential difference. Since acoustic waves can generate mechanical force, piezoelectric crystals provide voltage difference which is proportional to acoustic wave intensity [80]. The piezoelectric crystal is the primary component of the ultrasonic sensor which is placed at the forefront of the sensor. The bandwidth and centre frequency of the sensor is controlled by the thickness of the crystal. In order to ensure electrical

conduction, the crystal is coated with conducting material. Subsequently electrodes are placed at the front and back side of the crystal. This is followed by the backing material that provides damping to the sensor by absorbing reflected acoustic signal. The sensor contains an acoustic insulator to prevent detection of external acoustic wave and internally generated acoustic wave in the crystal [81]. The entire arrangement is placed inside insulated casing. The PA signals are sensed by the crystal which converts pressure waves to electrical signal.

2.2.4 Characteristics of time domain PA signal

Since PA waves are longitudinal waves, it consists of compression and rarefaction. Thus the piezoelectric ultrasonic sensor produces bipolar signal that has a resemblance with alphabet “N”. A typical PA signal from a circular simulated target is illustrated in Fig. 2.3.

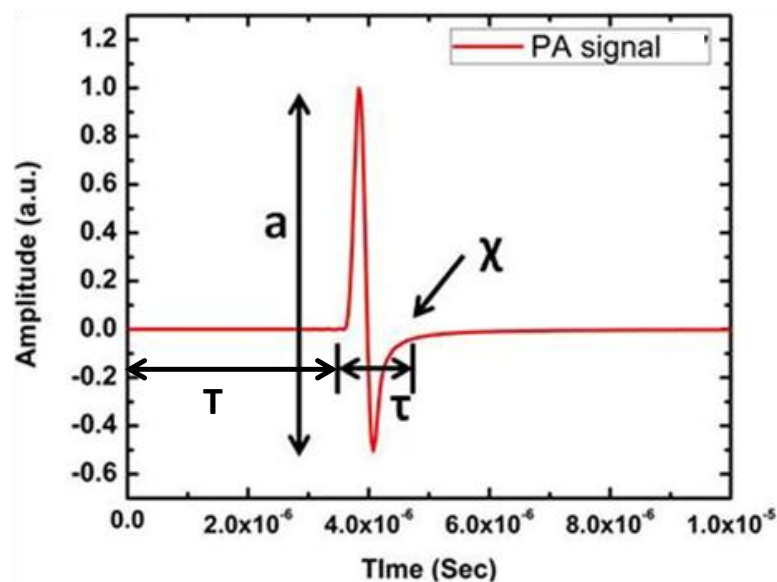


Fig. 2.3. A typical PA signal from circular numerical target

Figure 2.3 clearly shows the primary features of PA time domain signal. It consists of four dominating features namely amplitude (a), delay (T), width (τ) and relaxation time (χ). Among these features, width and relaxation time are related to each other.

Chapter 2

These features of PA time domain signal indicates very important properties of the sample. For example, PA signal amplitude is related to sample's optical absorption and laser energy irradiated onto the sample, delay provides information about the position of the absorber, width of the signal represents the size of the absorber and relaxation time depicts the elastic property of the sample [33], [82], [83]. Therefore PA signal consists of critical information about the sample. For image reconstruction, only two features such as amplitude and delay are utilised. Signal amplitude appears as contrast in the image and time delay provides the depth information of the absorber. Since normal and pathological tissues exhibit distinct change in optical absorption, PA imaging provides high contrast among these tissues [84], [85].

2.3 Image reconstruction

2.3.1 PA signal processing

The PA time domain signal acquired by the ultrasonic sensor is highly affected by the noise as well as the bandwidth of the sensor which alter the actual profile of the PA signal. Hence denoising and deconvolution with sensor response is essential to improve the signal to noise ratio (SNR) of reconstructed image since PA image contrast depends on the amplitude of PA signal [77], [86], [87].

The PA signal denoising can be performed by any of these techniques like averaging, filtering, wavelet based denoising etc. [88]–[90]. The random noise is usually eliminated by performing time averaging of the signal by performing multiple acquisitions from same point. However averaging is affected by different artefacts such as patient's movement, heart beat etc. Therefore different other techniques such as moving time averaging and frequency filtering can be performed to remove the noise [77]. The moving averaging method is substantially used for eliminating high frequency noise when the signal is in low frequency regime, whereas frequency filtering is applied to the signal with minimum overlap in noise and signal. Since

presence of multiple targets broaden the PA frequency spectrum, application of moving averaging removes the high frequency component and frequency filtering eliminates the useful frequency components overlapped with noise. Hence wavelet based denoising has gained a lot of attention. In contrast to Fourier transformation and other signal processing technique, Wavelet decomposes the time domain signal into scalable window function with different coefficient values [91]–[94]. A mother wavelet function is used for deriving wavelet window functions by performing transformation and scaling. Thus wavelet transform is applied to the PA time domain signal which removes the noise. Subsequently the inverse wavelet transform is performed to recover the denoised signal.

The other important factor which affects the PA signal characteristics is the limited bandwidth of the sensor. This may distort the actual profile of the PA time domain signal as the acquired PA time domain signal is the convolution of generated acoustic pressure and sensor's impulse response expressed as [77]

$$p_d(r, t) = p(r, t) * d_\delta(t) \quad (2.15)$$

Where d_δ is the sensor's impulse response

In frequency domain initial pressure is expressed as

$$p(r, \omega) = \frac{p_d(r, \omega)}{d_\delta(\omega)} \quad (2.16)$$

In order to recover the original pressure profile, inverse Fourier transform can be performed. However this will magnify the noise many folds. Thus the PA signal is deconvoluted by performing zero routine and Wiener deconvolution. The following equations illustrate both zero routine and Wiener deconvolution [95]:

$$p(r, \omega) = \left[\frac{d_\delta^*(\omega) |p_d(r, \omega)|^2}{|d_\delta(\omega)|^2 |p_d(r, \omega)|^2 + \sigma_n^2} \right] p_d(r, \omega) \quad (2.17)$$

$$p(r, \omega) = \frac{d_\delta(\omega) p_d(r, \omega)}{d_\delta(\omega)^2 + \delta^2} \quad (2.18)$$

2.3.2 Image reconstruction algorithm

The denoising process of the acquired PA signal is followed by image reconstruction. The processed PA signals are fed into different reconstruction algorithms such as back projection, time reversal, Fast Fourier Transform algorithm etc. for image reconstruction [32], [33], [35]. The image quality as well as imaging speed depends on the reconstruction algorithm.

In the case of back projection, the sum of initial pressure is detected by each element. Each acquisition point provides information about the point source as well as total attenuation along the path. The acquired information is projected back to reconstruct the image [96].

Advancement in reconstruction algorithm provides more accurate reconstruction and better computational efficiency. For example, back projection algorithm is modified to filtered back projection which employs filtering before or after back projection step. This reduces the artefacts in the reconstructed image. However this algorithm is computationally efficient, it is limited by the spherical geometry in practical applications [97].

In contrast, the time reversal algorithm utilises the temporally reversed PA waveform collected from each detection point for image reconstruction [65]. Basically PA signals acquired by each sensing point is temporally reversed and retransmitted in the medium numerically to trace the origin of that particular point source. The primary advantage of this algorithm is it relies on least number of assumptions and applicable for any geometry [98], [99]. However time reversal algorithm demands huge memory for computation that limits the practical application of this algorithm. The memory requirement of conventional time reversal technique is reduced by an efficient

technique called pseudo-spectral K-wave propagation model [100], [101]. This employs a pre-computation of initial pressure by forward model. Then matrix based and simulated p_0 would reduce the memory requirement for computation.

2.4 Types of PA technique

In biomedical field, PA technique is mainly utilised for imaging applications. However this has been also explored for spectroscopy (gas and liquid analysis) and few applications on PA signal analysis.

PA technique can be categorised in three broad applications such as imaging, spectroscopy and PA signal analysis. PA imaging is further divided into two types such as PA tomography and PA microscopy.

2.4.1 PA imaging

2.4.1.1 Photoacoustic tomography (PAT)

Photoacoustic tomography can be considered as the traditional way of performing imaging. In case of photoacoustic tomography, a single transducer is moved around the sample in different geometric positions such as planar, circular and spherical to acquire the PA pressure waves as shown in Fig. 2.4 [32], [33]. The scanning time with single element sensor is quite high. Therefore array of sensors are also used for PA signal acquisition [72], [102], [103]. Since the cost of the array sensor is relatively high compared to single element sensor, these are used in limited manner.

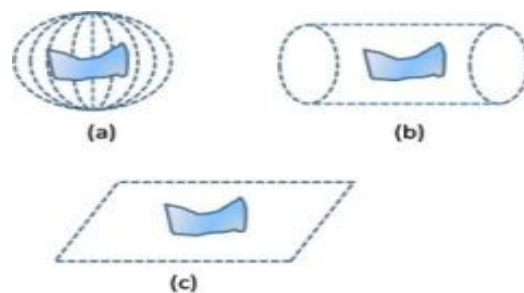


Fig. 2.4. Photoacoustic tomography detection geometry (a) Spherical (b) cylindrical (c) planar

Chapter 2

While considering the detection geometry, it mainly depends on the target tissue. For example for brain or breast imaging spherical and cylindrical geometry is used but for flat targets like bone or skin planar geometry is used [33], [37], [104], [105]. Subsequent to acquisition, PA signals are fed into suitable reconstruction algorithms for image reconstruction. Details of reconstruction algorithms are explained in earlier section.

2.4.1.2 Photoacoustic microscopy (PAM)

In contrast to PAT, photoacoustic microscopy does not require any robust image reconstruction algorithm to form an image. It utilises tightly focused laser beam or focused ultrasonic detector to form an image. In case of PAM, either the focused laser beam or focused acoustic detector is mechanically scanned through the sample. PA signals obtained from individual detection points directly form an image without aid of any reconstruction algorithm [67], [106].

Depending upon scanning methodology, PAM can be categorised as Acoustic resolution PAM (AR-PAM) and optical resolution PA microscopy (OR-PAM). The schematics of these two microscopy technique is illustrated as follows (Fig. 2.5) [32], [107]:

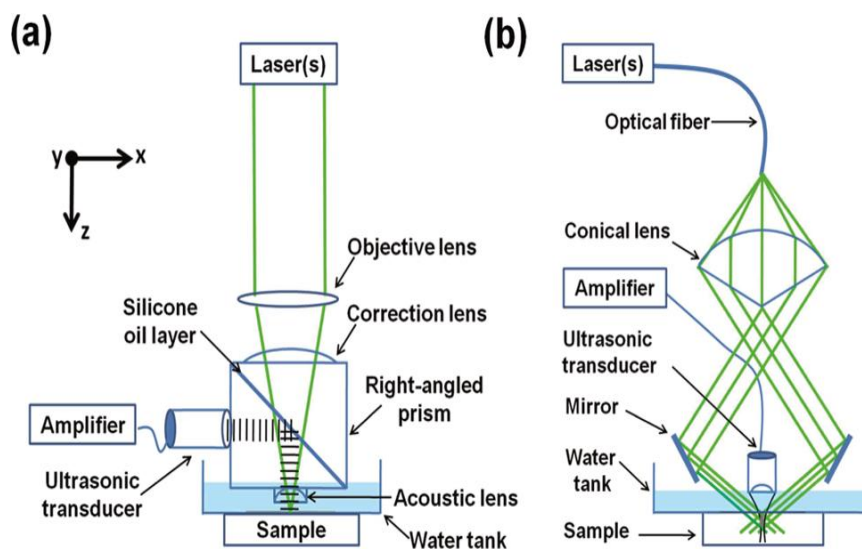


Fig. 2.5. Schematic of AR-PAM and OR-PAM [108]

AR-PAM utilises a focused ultrasound detector whereas OR-PAM relies on focused laser beam for scanning. The axial resolution of the

PAM depends upon the time resolved detection of the PA signal but the lateral resolution relies on either on acoustic focusing or optical focusing [33].

2.4.2 PA signal analysis and spectroscopy

PA time domain signal consists of many critical information about the sample. As mentioned in the previous section, it substantiates optical absorption, size, mechanobiological property of the sample by its amplitude, width and relaxation time [47], [63], [109]. Since PA signal amplitude primarily depicts the optical absorption of the sample which is wavelength dependent, different tissue chromophores such as haemoglobin, lipid, proteins, water, melanin (optical absorption spectra illustrated in Fig. 2.6) can be probed by varying the excitation wavelength [110], [111]. This is the fundamental principle of PA spectroscopy.

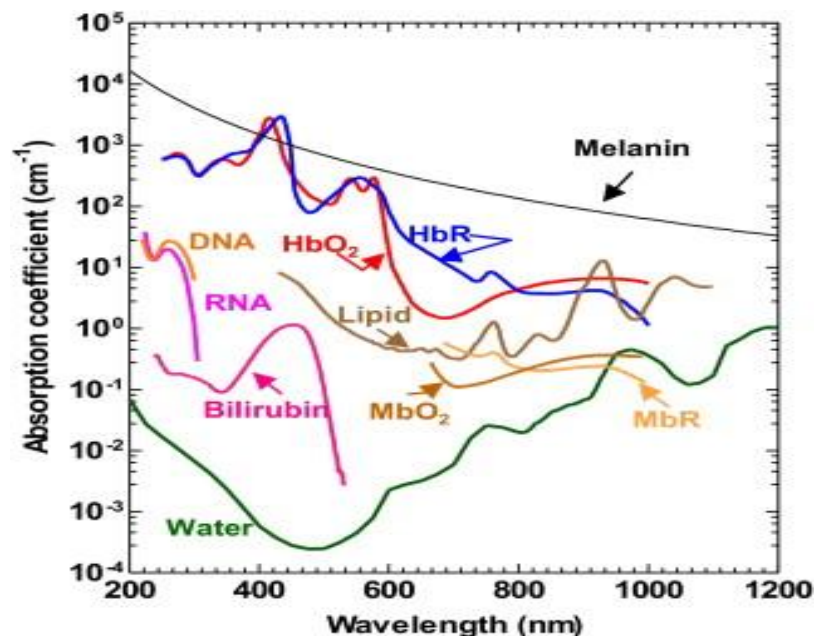


Fig. 2.6. Optical absorption spectra of different tissue chromophores [90]

For example, oxygenated haemoglobin and deoxygenated haemoglobin is signature for normal and malignant tissues and it has different optical absorption. Therefore by tuning the wavelength one

Chapter 2

can differentiate these two types of tissues by PA spectroscopy [112], [113].

In addition to amplitude, frequency domain features are also explored for extracting vital information such as size of microstructures in tissue, acoustic scattering property and different biophysical properties of the sample [114], [115]. Similar to ultrasound, linearly fitted PA power spectral features such as slope, midband fit and intercept has been primarily utilised to ascertain scattering property of the sample that serve as finger print of many diseases including cancer [115], [116]. For example the slope decreases due to enhancement in size of the absorber whereas intercept and midband fit increases with increase in absorber size. In addition, scatterer concentration is depicted by the intercept i.e. increase in concentration of the scatterer enhances the intercept due to increase in total optical absorption [114], [117].

The other approach of PA signal analysis was performed by Mahato et.al, in which different spectral parameters such as mean, median, standard deviation, total spectral energy etc. of magnitude spectra was used for tissue characterisation and classification [118]–[120]. These spectral features were correlated with change in different biophysical property (protein concentration, binding and unbinding of protein) of the sample [121], [122].

2.5 Biomedical application of PA technique

Around the globe, researchers have worked on PA technique to take it up from laboratory bench top to hospital. In last decade, PA technique has been applied onto various biomedical applications mainly for different disease diagnosis thorough imaging or signal analysis. Some of the major biomedical applications of PA technique are detailed as follows:

2.5.1 Brain imaging

Brain imaging in present scenario is an essential requirement for disease diagnosis as well as studying structural and functional operation of brain. However there are imaging modalities especially MRI which is often used by clinicians, delineates certain disadvantages like exposure to strong magnetic field and the cost. On the other hand PAT can provide a cost effective, non-ionic, real time, high resolution brain imaging technique [38], [123], [124]. It is capable of providing morphological as well as function information. A pioneer study performed by Dr. Wang and his group on mouse brain illustrated clear view of a lesion with intact skull. Figure 2.7 reveals certain resemblance between the PAT image and the open skull image [125]. Later this study was extended to observe tumour angiogenesis. This proves the capability of PAT for morphological brain imaging which will definitely be useful for brain tumour detection [126]. In another study done by the same research group elucidated functional information i.e. oxygen saturation in mouse brain [127]. The brain activity due to whisker movement of mouse is also studied by PAT. The above mentioned studies clearly illustrate that PAT has strong potential to become regular imaging tool for brain imaging.

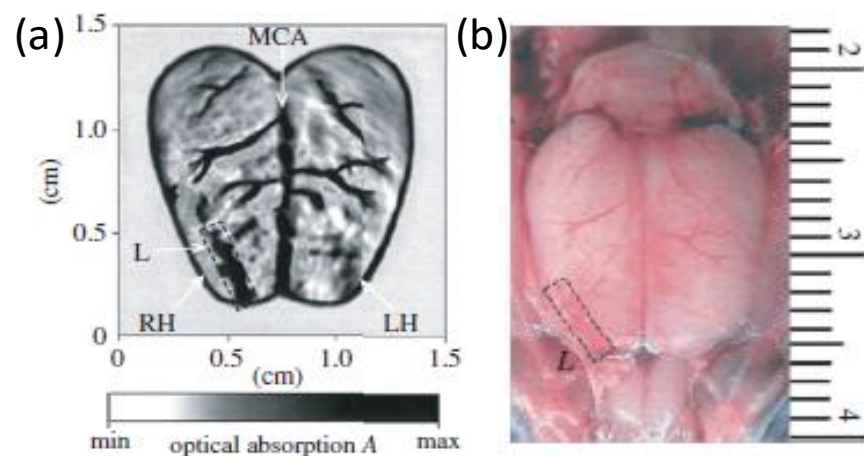


Fig. 2.7. Photoacoustic tomography (PAT) cylindrical scanner for small animal brain imaging (a) image showing cerebral vasculature and surgically induced lesion (b) sectional image of skull after taking PAT image [125]

Chapter 2

2.5.2 Arthritis detection

Nowadays arthritis is a major cause of disability around the globe. As PA imaging provides a high spatial resolution and deep penetration depth, it can be used for detection of arthritis as well. Xueding Wang et al., have studied joint structure of small animal using PAM. Further, they also imaged human peripheral joint by PAT [128]. In this study, they found that optical absorption contrast of PA imaging provides the information about the tissue at joint region better than the mechanical contrast of pulsed echo ultrasound imaging. The PAT images were compared with golden standard technique i.e. histopathology that illustrated very high correlation. Figure 2.8 exhibit the PAT and histopathology images of human finger.

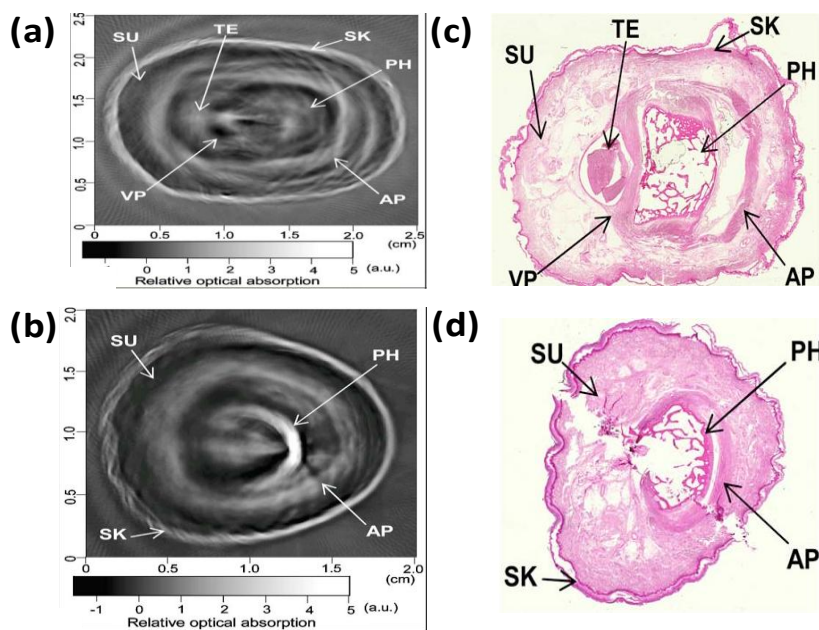


Fig. 2.8. Images obtained from human finger (a) and (b) PA image, (c) and (d) histopathology images [128]

2.5.3 Arterial plaque detection

Heart diseases are very common nowadays. The major cause of several heart diseases is deposition of lipid rich plaque in the arteries which has a tendency to rupture [129], [130]. These types of plaques may cause occlusive thrombus which may lead to heart attack or stroke [131], [132]. By using miniature intravascular sideways looking probe,

the coronary artery wall can be imaged which helps to detect the plaque. From the studies it has been observed that lipid has an affinity towards 1210 nm light. Therefore PA imaging could be helpful for lipid rich plaque detection [133], [134]. Although ultrasound imaging provide information about plaque but PA imaging provide more specific and quantitative information as it provides better contrast than the ultrasound images. A study done by Allen et al. research group on excised human aorta exhibited that PAT provide distinct contrast for lipid-rich plaque shown in figure Fig. 2.9 [133]. Not only lipid deposition but the other plaque forming causes such as calcium deposition, macrophage content, fibrous material can also be detected by PA imaging as calcium, macrophage, fibrous all have a distinct optical absorption [135]–[137].

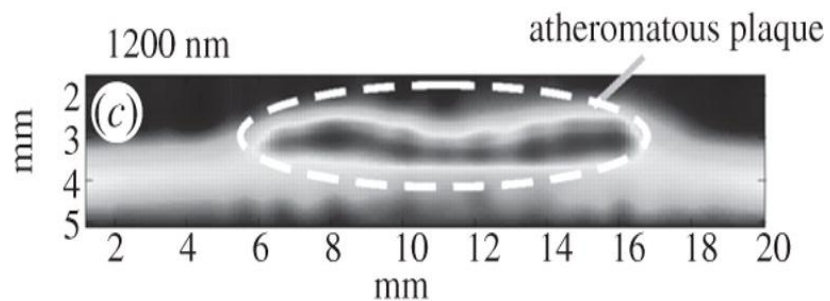


Fig. 2.9. PA image of human artery in which dotted circle denotes the lipid rich plaque [133]

2.5.4 Haematological diseases

One of the applications of PA technique is haematological disease diagnosis. Since haemoglobin (chromophore present in red blood cells (RBCs)) has strong affinity towards visible range wavelength (absorption spectra of haemoglobin illustrated in Fig. 2.10) [77], PA imaging has been explored for different disease diagnosis such as tumour angiogenesis, clot detection and differentiating acute and chronic clots in phantom study, RBC aggregation etc. [26], [138]–[144]. Tumour angiogenesis is the finger print for malignant tissue detection which is detailed in the later section. In this section, specifically haematological diseases are discussed.

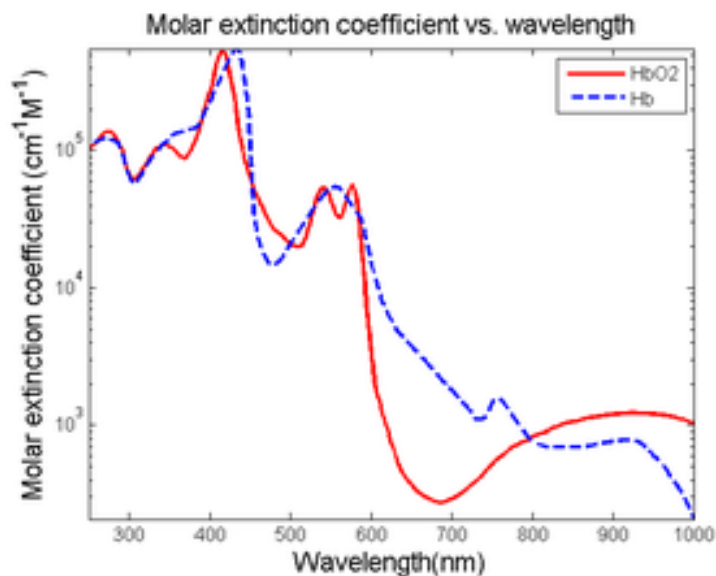


Fig. 2.10. Absorption spectra of oxygenated and deoxygenated haemoglobin [77]

Typical haematological diseases such as ischemia, myocardial infarction, deep vein thrombosis, stroke etc. mainly arise due to blockage of blood vessels by clots or other obstacles like lipid rich plaque, macrophages etc. [131], [145]. Therefore detection and analysis of blood clot is very important in terms of early diagnosis of these diseases [43]. Since haemoglobin strongly absorbs visible light, it will provide high contrast for clot in the PA images. Based on this hypothesis, Emelianov and his group applied PA imaging to study aging of blood clot in tissue phantom [26]. PA imaging of acute and chronic clot was performed in tissue phantom as illustrated in Fig. 2.11. This clearly indicates that acute and chronic clot exhibits distinct change in contrast which can be utilised for discrimination of clots.

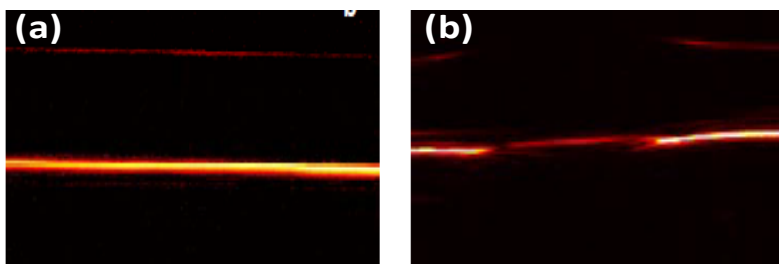


Fig. 2.11. PA images of (a) acute and (b) chronic clot in phantom study [26]

The other application of PA technique was explored by Kolios and his group in terms of PA spectrum analysis. They have studied RBC aggregation using simulation as well experimental studies through high frequency PA spectrum analysis [66], [146]. The same group has also extended the work to observe change in PA frequency spectrum due to oxygen saturation in pulsatile blood flow in an in vitro study. Not only RBC aggregation, probing of single RBC morphology was also performed by the same group [147]. This proves the potential of PA technique for haematological disease diagnosis.

2.5.5 Cancer diagnosis

Cancer is the deadliest disease that has taken millions of life around the globe. In order to control the mortality rate, early stage diagnosis as well as continuous monitoring is highly essential. Therefore non-invasive and non-ionising PA imaging would be a promising option. The features of PA imaging attracted the attention of many research groups worldwide. Since PA imaging relies on optical absorption of endogenous chromophores such as haemoglobin and melanin, malignant tissues exhibits very high contrast compared to normal tissues [33], [113]. In one of the study performed by Yang et al., growth of melanoma tumour was observed. This illustrated very high contrast between melanoma tumour and the surrounding tissues. Spectroscopic PA imaging of skin melanoma tumour was performed with 584 nm and 764 nm wavelength that provided very high resolution image of tumour vasculatures [148]. PA imaging has been taken up to the preclinical trials by Manohar and his group [42], [85]. Photoacoustic mammogram has been developed and applied on human subjects to detect malignant breast tumours as illustrated in Fig 2.12 [42]. Since vasculatures of malignant tissues are denser and abrupt compared to normal, it exhibits high contrast compared to normal tissues. In comparison of X-ray mammogram or ultrasound, PAT exhibits more contrast. The same study also detailed about

Chapter 2

differentiation of cyst from malignant tumour as shown in Fig 2.13 [42].

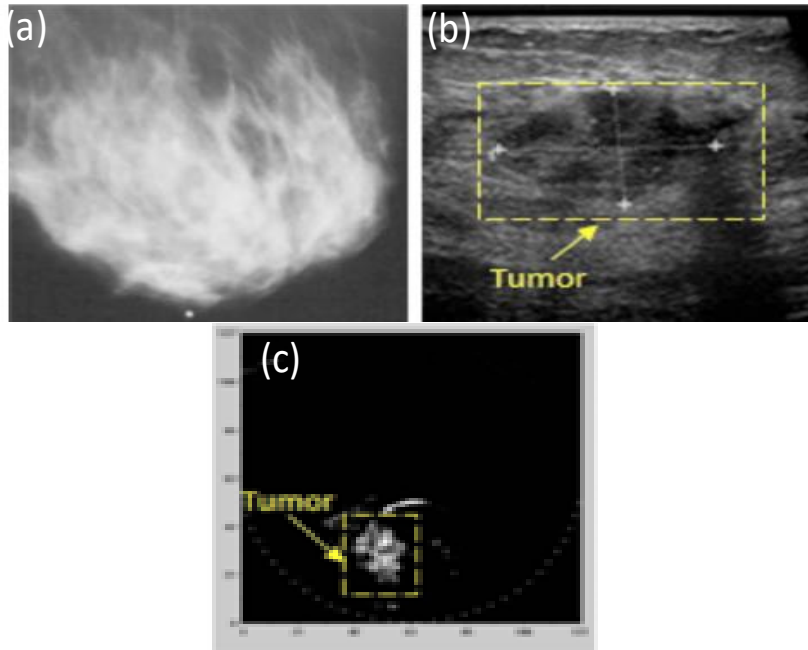


Fig. 2.12. Images acquired from human breast using (a) mammogram (b) ultrasound (c) PAT [42]

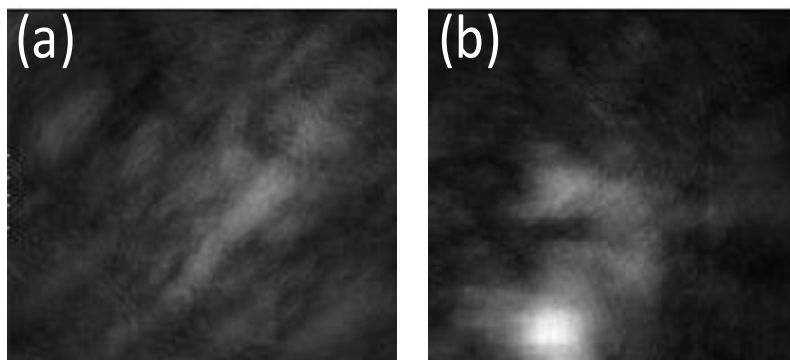


Fig. 2.13. PA images of cyst and malignant tumour in human subject that clearly illustrated malignant tissue with higher contrast [42]

In contrast to relying on tumour vasculature, PA imaging has been utilised to extract functional information of the tissue i.e. oxygen saturation in blood (hypoxia) is monitored [149]–[151]. Since hypoxia is a marker for detection of malignancy, it has been applied on to mouse brain glioblastoma. Obtained spectroscopic PA image is illustrated in Fig. 2.14 [150]. The malignant tumour inside mouse brain can be observed with high contrast (highlighted with blue circle) which indicates hypoxic region very prominently.

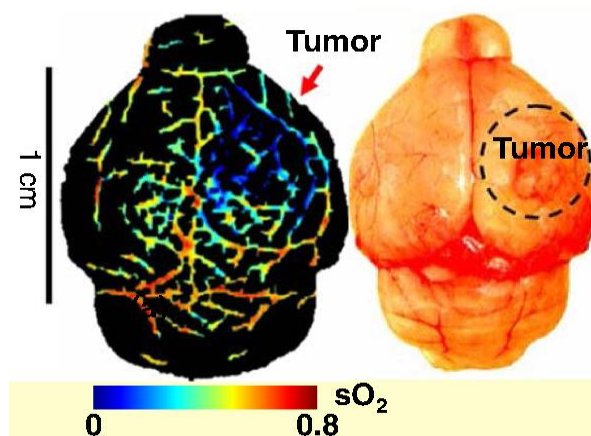


Fig. 2.14. Functional PA images of mouse brain in which circled part indicates the hypoxia region [150]

Another primary reason of cancer related death is due to metastatic spread of primary tumour. Identification of circulating tumour cells (CTC) would be very useful to slash down the mortality rate [152]. PA imaging is applied to detection of CTC in blood stream. In-vivo detection of CTC in blood stream provide many fold increase in sensitivity compared to existing in-vitro techniques [153]–[155]. Subsequently, use of exogenous contrast agents increases the sensitivity and specificity.

In order to enhance the imaging capability of PAI, different exogenous contrast agents are used. Different near infrared (NIR) absorbing dyes such as indocyanin green, Alexa flour750 and IRDye800CW is being commonly used as contrast enhancing agents [156], [157]. Besides these NIR dyes, gold nanoparticles (GNPs) are very popular as contrast enhancing agents. Different types of GNP such as nano rod, nano shell, nano cages and nano beacons are used for PAI imaging [157]–[160]. The major applications of these NP are for targeted imaging applications.

Besides PA imaging, PA spectroscopy is also explored for cancer diagnosis. It has been applied to ovarian, breast and solitary thyroid tissues for differentiating normal from malignant tissues [118],

Chapter 2

[162]. In these studies PA frequency spectral parameters such as mean, median, standard deviation, total spectral energy is utilised for tissue classification that exhibited high classification accuracy.

2.6 Summary and potential advancement in conventional PA technique

The primary advantage of PA technique is the non-ionising excitation that allows continuous monitoring and acoustic detection which enables deep tissue imaging. Even though optical absorption serve as a finger print for many diseases, but tissues with analogous optical absorption are difficult to be differentiated by the conventional PA techniques. Therefore the other intrinsic property of biological tissues i.e. mechano-biological property which is considered as finger print for different diseases, can be explored as a parameter to differentiate normal to pathological tissues.

Modern diagnosis claims understanding the mechanism of the disease for early stage diagnosis and treatment. Since mechano-biological property can be related to tissue pathology, PASR can be utilised for quantitative assessment of diseases mechanism (e.g. blood clot formation). However the existing studies are limited to conventional signal processing technique e.g. Fast Fourier Transform that provide limited information. Thus advanced signal processing tools can be used to extract critical information about tissue pathology that can be helpful to understand complex samples like benign and malignant tumours. These are some of the potential improvements that can lead conventional PA technique to regular clinical applications.

Chapter 3

Photoacoustic spectral response experimental development and characterisation

“If we know what we are doing it would not be called research, would it?”-Einstein

3.1 Introduction and motivation

Evolution in PA technique has proved its potential as a diseases diagnosis tool for various biomedical applications [33], [77]. Even though PA imaging has been mostly explored, PA signal analysis also has its unique features (real time, marker free, quantitative biophysical information of tissues) that are required for an advanced disease diagnostic tool. Despite these exciting features, PA signal analysis have not been explored so far in many biomedical applications. The number of studies related to sample elasticity through PA signal is even rarer. Therefore an attempt has been made in this thesis to develop tissue elasticity based PASR technique for different disease diagnosis and study.

The very first step of PASR technique development is designing the instrumentation. To develop the basic PASR setup, details of different experimental parameters such as laser energy, distance between sample and sensor, sample containers etc. are collected from the literatures as discussed in Chapter 2. This is the very first attempt to develop tissue elasticity based PASR technique. Hence system parameters should be obtained precisely from literatures and then simulation studies need to be carried out before performing characterising experiments. Subsequent to basic setup development, it is very essential to analyse different parameters of the setup that may affect PA signal and the frequency spectrum. The reason is PA frequency spectral parameters are the key features for tissue differentiation as well study. Thus it is essential to ensure the change in PA spectral parameters is solely due to change in the tissue property, not by any other experimental parameters. Otherwise this would lead to erroneous diagnosis. Subsequent to development of the PASR setup, testing of the setup is imperative to verify the sensitivity of the developed setup. Further, the developed setup is tested for detection of change in elasticity by employing different samples.

Chapter 3

The organisation of the chapter is as follows: Development of PASR experimental setup and software interface for real time monitoring followed by characterisation and elimination of different experimental parameters that affect PA frequency spectral parameters. Next verifying the response of the setup with tissue phantom and biological samples are illustrated. Following this, the response the developed setup towards change in sample elasticity is also verified with experimental studies with tissue phantom as well as real biological samples.

3.2 Materials and instrumentation

3.2.1 PASR experimental setup

The basic block diagram of developed PASR setup is shown in Fig. 3.1. The sample is irradiated with an Q-switched Nd:YAG pulsed laser (Ekspla, NT342c) which generates nanosecond laser pulses typically ~ 5 ns with 10 Hz repetition rate. The laser pulse width certainly satisfies the thermal confinement and stress confinement condition for PA wave generation as described in Chapter 2. The laser fluence on sample surface was limited to 10 mJ/cm^2 for all the studies that is well below the ANSI safety limit (20 mJ/cm^2) to ensure sample's safety [163]. More over for optical excitation, second harmonic wavelength of the laser was utilised for PA wave generation as haemoglobin is a strong absorber of this wavelength [164].

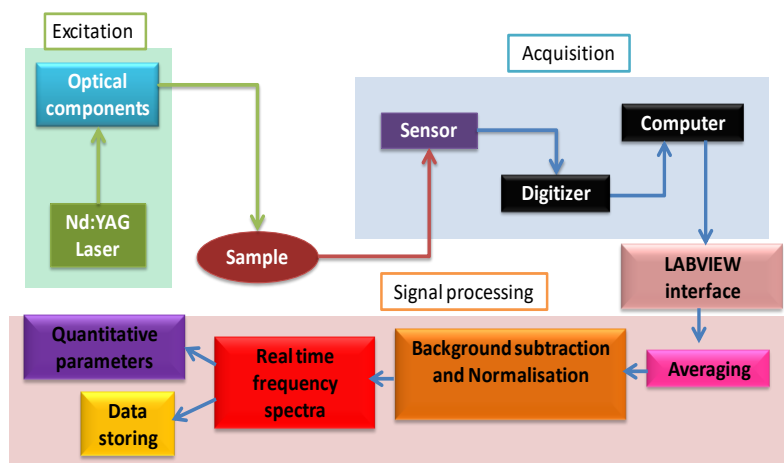


Fig. 3.1. Block diagram of developed PASR system

Absorption spectra of human blood illustrated in Fig. 3.2, clearly shows strong affinity of blood towards visible range particularly green. For PA experiments, the sample as well sensor should be coupled with water or ultrasonic coupling gel to avoid acoustic impedance mismatch [165].

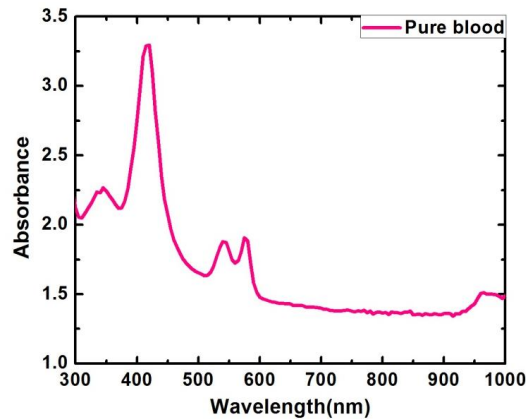


Fig. 3.2. Absorption spectra of whole blood

Therefore sample and sensor both were placed in a water tank filled with water. Since different types of samples (solid, gel and liquid) were used in different studies of the thesis, different arrangements of experimental setup was utilised. For example, solid samples like biological tissues, black rubber samples were wrapped in parafilm prior to placing in the water tank and the samples were stuck to the bottom of the tank to keep the sample stationary during experiments. In this case, the laser beam is irradiated from top whereas the liquid samples were filled in a glass container. The container is placed vertically inside the water tank and the sample is illuminated from sides. Figure 3.3 illustrates the schematic of PASR experimental setup for both solid and liquid samples. Firstly, the laser beam passes through a beam splitter which splits the beam into two parts. The main beam contains 96% of energy and splitted beam has rest 4%. The main beam passes through a lens in order to achieve a reduced the beam diameter in compared to main beam that is used for sample irradiation. The position of the lens is varied to adjust the beam diameter falling onto the sample. The splitted beam is utilised for laser energy

Chapter 3

monitoring during the experiment. Since energy fluctuation may cause error in the obtained results, energy monitoring is very essential. Subsequent to excitation of sample with laser pulses, acoustic signals are generated due to thermoleastic expansion and relaxation [63]. These acoustic signals (PA time domain signals) are known as PA response, traverse through the surroundings and coupling medium before reaching the sensor placed in the same water tank. The ultrasonic sensor converts the compression-rarefaction acoustic signal (PA response) into corresponding voltage signal. The output of the sensor is connected to high speed digitizer (National Instruments PXI-5124). The bandwidth of the digitizer was 150 MHz. An external triggering is provided to the digitiser through a photodiode (BPW34) for synchronised acquisition of PA signal.

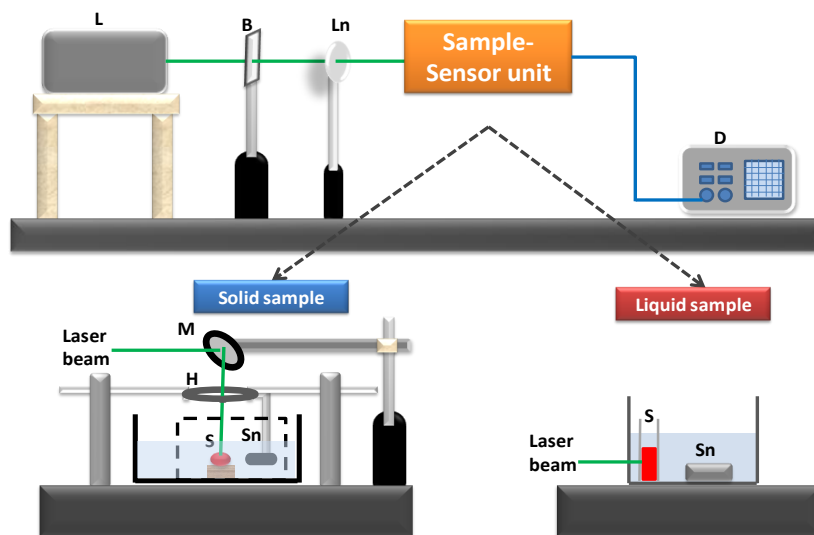


Fig. 3.3. Schematic diagram of PASR setup in which L- laser, B-beam splitter, Ln- lens, D-digitize, M-mirror, H-holder, S-sample, Sn-sensor

3.2.2 Software interface and signal conditioning

The data transfer between the digitizer and the computer was performed by an in house built LABVIEW program. Since the primary objective of this thesis is to develop an instrument for different biomedical applications, user friendly interface is desirable for easy use of non-technical person. In addition, miniaturisation of instrument also can be done by implementing the LABVIEW code in VLSI board.

The developed program performs data acquisition, signal conditioning, signal processing and saving the data in preferred memory location in computer that makes the PASR system automated.

3.2.2.1 PA signal acquisition

As a first step of acquisition, PA signal is digitized at sampling rate of 200 Msps. Since the bandwidth of the digitizer (150 MHz) is approximately five times higher compared to the maximum bandwidth (30 MHz) of the ultrasound sensors used for PA response acquisition, the aliasing effect is avoided [166]. Figure 3.4(a) illustrates PA signal from standard sample i.e. black rubber sample.

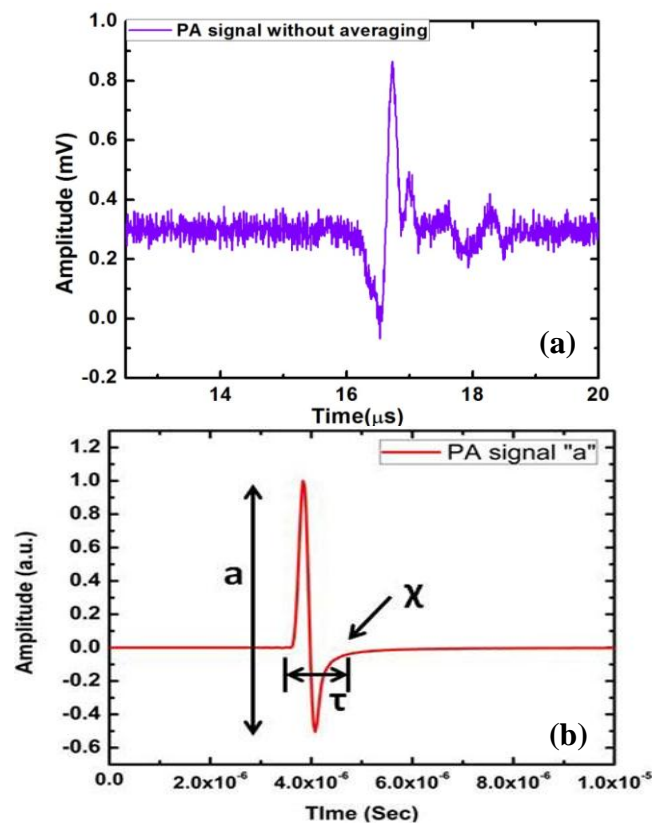


Fig. 3.4. PA signal acquired from (a) black rubber sample (b) simulated numerical target

It can be clearly observed from the above figure that signal is “N” shaped signal and have four distinct features such as amplitude (a), width (τ), time delay (T) and relaxation time (χ). This has high resemblance with the PA signal obtained from simulation as shown in Fig. 3.4(b). However the polarity of the signals is opposite to each other due to polarity of the transducer and digitizer. As mentioned

Chapter 3

earlier, the amplitude of the signal is related to sample's optical absorption, laser energy, sample's acoustic attenuation and distance between sample and sensor whereas the width and the relaxation time is associated to the size of the sample and the elastic property [32], [35]. The time delay indicates the position of the sensor and the sample (can be correlated to sound speed). This parameter is very important with respect to image reconstruction as this provides the depth information of the absorber [37]. However for signal analysis time delay is not required since the frequency spectral information is obtained from the N-shaped PA response. In order to generate detectable PA response, very high energy is used for this experiment. Since biological sample has limitation of energy dose, this energy might damage the sample. Thus lower energy is used to excite the samples. With lower energy density, PA signals are detected totally buried in noise. This certainly decreases the signal to noise ratio (SNR) of the PA response which makes the extraction of frequency components very difficult. Therefore acquired signal is conditioned prior to saving the data for frequency spectrum analysis.

3.2.2.2 Signal conditioning

The signal to noise ratio of the PA signals obtained is generally very low. The signal are most probably buried in noise and it is essential to remove or reduce the noise before the signal can be extracted for further signal processing. To reduce/eliminate noise, three approaches can be adopted.

- i. Increasing the irradiance of the laser
- ii. Using bandpass filters to reduce the noise
- iii. Using time averaging approach during acquisition

Increasing the laser irradiance causes heating which subsequently damage the sample. The second approach is to implement bandpass filters to eliminate noise from the signal. However bandpass filters are limited to eliminate noise that overlap with the bandwidth of the signal. Therefore time averaging technique is utilised [167]. This is basically

applicable for the signals buried with high amplitude noise within the bandwidth of the signal. Hence time averaging is implemented for PA signal's noise reduction. The following are the conditions for signal averaging [168]:

- i. The waveform of the signal must be repetitive.
- ii. Noise should be random.
- iii. Temporal position of each signal waveform must be accurately known.

If the input waveform $f(t)$ has signal portion $S(t)$ and noise portion $N(t)$ then

$$f(t) = S(t) + N(t) \quad (3.1)$$

Let us assume $f(t)$ has a sampling rate t second. Then the value of any sample point in the time epoch ($i = 1,2,3,\dots$) is the sum of noise and signal component

$$f(it) = S(it) + N(it) \quad (3.2)$$

All the sample points are stored in memory. The value stored in memory location i after m repetition is

$$\sum_{k=1}^m f(iT) = \sum_{k=1}^m S(iT) + \sum_{k=1}^m N(iT) \quad (3.3)$$

for $i = 1,2,3,\dots,n$

The signal position is same at each repetition if the signal is stable and the sweep are aligned together perfectly. Then the following equation is obtained:

$$\sum_{k=1}^m S(iT) = mS(iT) \quad (3.4)$$

The assumptions for this development are that the signal and noise are uncorrelated and noise is random with mean of zero. After many repetitions, $N(iT)$ has rms value of σ_n

Chapter 3

$$\sum_{k=1}^m N(iT) = \sqrt{m\sigma_n^2} = \sqrt{m}\sigma_n \quad (3.5)$$

Taking the ratio of equation 3.4 and 3.5 gives the SNR after m repetition is [168]

$$SNR_m = \frac{mS(iT)}{\sqrt{m}\sigma_n} = \sqrt{m}SNR \quad (3.6)$$

Thus the signal averaging improves the SNR by a factor of \sqrt{m} .

Since the noise from the PA experiments is random in nature, time averaging of the signal remarkably improves the SNR. By performing test experiments, it was observed that 200 times averaging provides adequate SNR for frequency spectrum analysis of PA response. Figure 3.5 illustrates a signal acquired from PASR experimental setup without averaging and the same signal after 200 times averaging is illustrated in Fig. 3.5. This certainly shows that the amplitude of the noise signal is 0.6 mV_{PP} for no averaging. However the amplitude is reduced to ~ 0.1 mV_{PP} after 200 times averaging. Hence in this thesis averaging of signal is performed to improve the SNR.

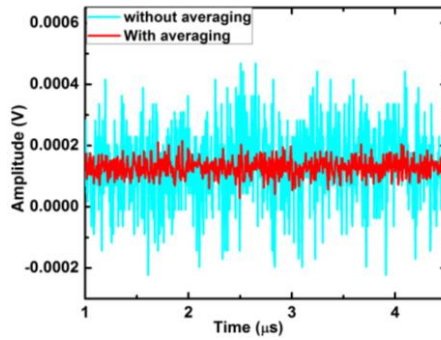


Fig. 3.5. Signal acquired from developed PASR system with and without averaging

As a part of software interface, averaging was implemented in the program using time averaging function of LABVIEW. This is a built in analog signal express VI of LABVIEW that provides both running mode as well as block mode averaging. In this thesis, running mode averaging is performed. Subsequent to time averaging, Fast Fourier Transform (FFT) of the PA signal is performed to visualise

real-time frequency spectrum of the sample that will help to discriminate samples instantaneously. In order to obtain FFT, signal analysis VI of LABVIEW is implemented that provides FFT magnitude spectrum. Thereafter the PA signal is stored in the computer using custom built LABVIEW program that stores the data in .CSV format for further processing and analysis. Figure 3.6 delineates the LABVIEW based software interface used in the thesis that illustrates real time PA response, averaged PA response and the real time frequency spectrum.

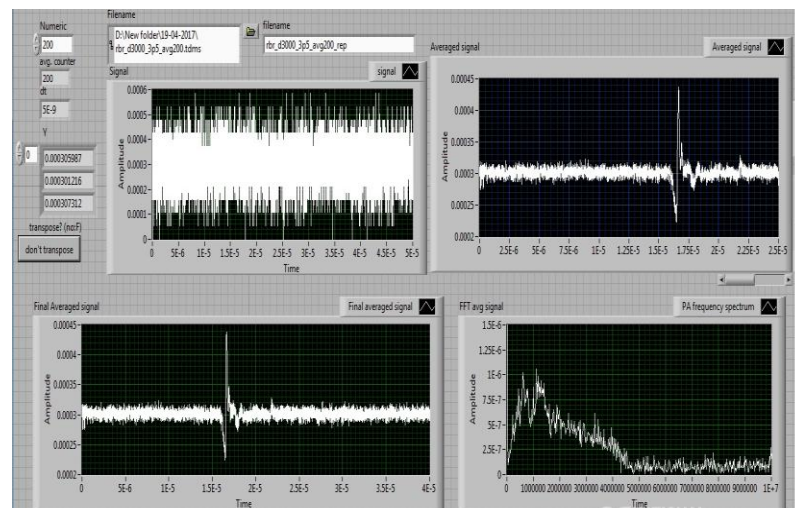


Fig. 3.6. Front panel of LABVIEW based software interface

3.2.2.3 Signal processing

Subsequent to acquisition, frequency spectra of PA signals are analysed using in house developed MATLAB program for sample differentiation as well as characterisation. In this thesis, mainly two types of signal processing techniques are applied to the PA signal for qualitative and quantitative assessment of tissue pathology given as follows:

- (a) Solely frequency based (FFT)
- (b) Time-frequency (EWT, WVD) based techniques

In case of solely frequency based techniques, FFT is the primarily used technique to obtain frequency spectrum of signals [169]. Therefore it has been used for extracting frequency domain

Chapter 3

information of the PA signals acquired from different samples. In order to perform FFT, the PA signal is first subtracted from the baseline to remove any offset arising out of sensor and amplifier (if used in future). Subsequently, windowing is employed to the signal for background noise reduction. Thereafter FFT is applied to the PA response. Figure 3.7(a) & 3.7(b) show a typical PA signal and its frequency spectrum from black rubber sample.

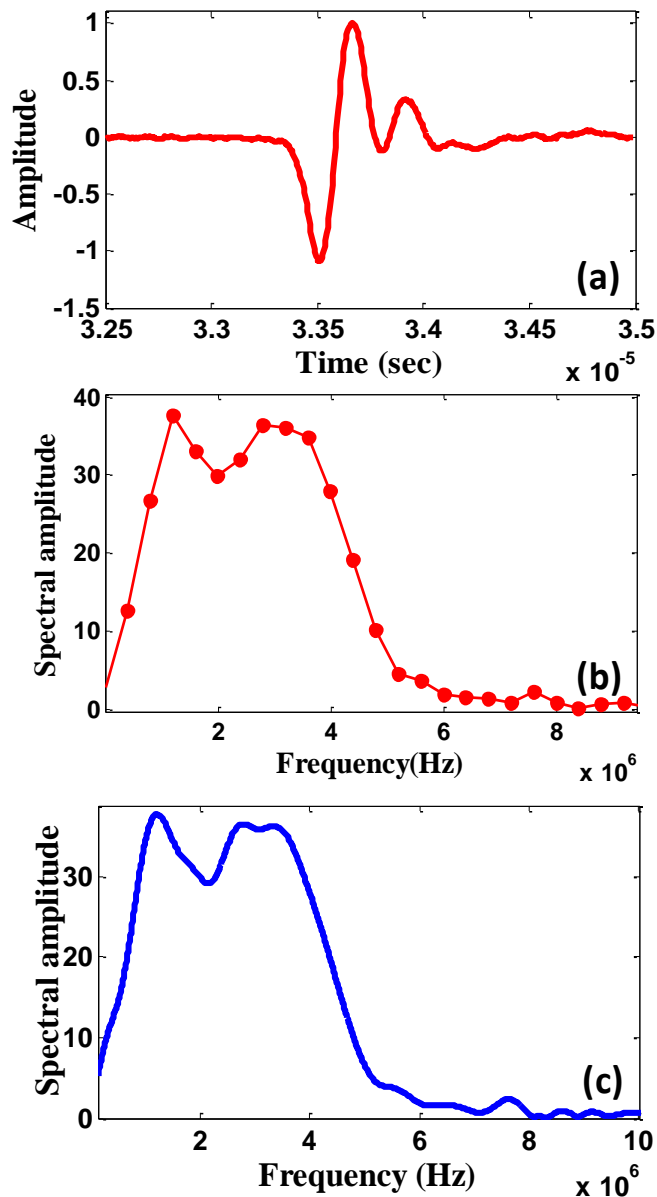


Fig. 3.7. (a) PA response from test sample (b) PA frequency spectrum without zero padding (c) PA frequency spectrum with zero padding

It clearly delineates that the spectrum has inadequate points for reconstruction as illustrated in Fig. 3.7(b). Therefore zero padding of

the signal is performed. The zero padding of signal signifies adding zeros at the end of the signal to increase the number of data points. Figure 3.7(c) shows the frequency spectrum of the zero padded signal in which the frequency peaks of the spectrum can be identified more precisely. Since the frequency peaks are one of the important parameters for analysis, precise identification is very essential. Apart from frequency components other frequency spectral parameters such as dominant frequency, total spectral energy, and variance are also obtained for quantitative analysis in later studies.

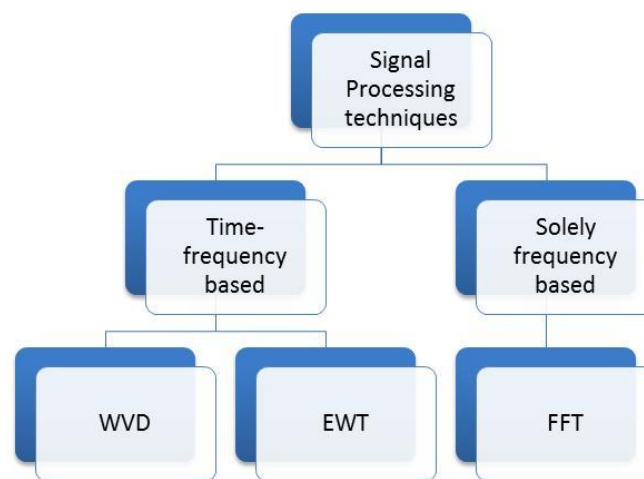


Fig. 3.8. Type of signal processing techniques used in the thesis

In this thesis, advanced signal processing techniques like time-frequency based techniques are also employed. The primary advantage of these techniques is these techniques provide frequency information along with the time. For example, signal illustrated in Fig. 3.7(a) has different frequency components that appear at different time points. Applying FFT, one can obtain the frequency components present in the signal. However at what point of time the components are appearing cannot be obtained from FFT [170]. The time information is very important as it can provide critical information about tissue property. Hence it can be considered as a parameter for normal and pathological tissue discrimination. In addition, PA signals are non-stationary in nature. Utilising FFT for extracting frequency components of the non-stationary signals would provide overlapped frequency components

Chapter 3

due to spectral leakage [171]. Since individual frequency components serve as primary spectral parameter, overlapped frequency components would lead to erroneous results. Therefore time-frequency techniques are applied to PA response for complex tissues like human breast masses. There are many time frequency techniques such as short time Fourier transforms (STFT), continuous wavelet transform (CWT), empirical mode decomposition (EMD), empirical wavelet transform (EWT), Wigner-ville distribution (WVD) etc. [172]–[174]. Among these techniques, WVD and EWT are employed in this thesis due to their unique advantages. For example, WVD provides qualitative information in terms of contour plots that shows the individual frequency components as concentric circles and corresponding energy density in colour variation whereas EWT is an adaptive technique that conform variation in processed signal by utilising adaptive algorithm (detailed in Chapter 5) [171], [175], [176]. These features are imperative for classification and studying pathology of human breast masses.

Now let's take an example to observe how time-frequency based techniques are advantageous over solely frequency based techniques. For this, WVD is applied to the signal illustrated in Fig. 3.9(a), it can be observed that the frequency components as well as the time information can be obtained which cannot be obtained from FFT technique as illustrated in Fig. 3.9(b). The contour plot (Fig. 3.9(c)) of WVD shows the increase in frequency with respect to time. The colour bar indicates the energy density of the frequency components. Since the frequency components present in the signal consists of identical energy density, there is no variation in colour. As time frequency based technique provide more information compared to FFT, theses technique are used in the thesis for detailed study of complex samples. In depth explanation of the time-frequency based techniques is given in the later chapters.

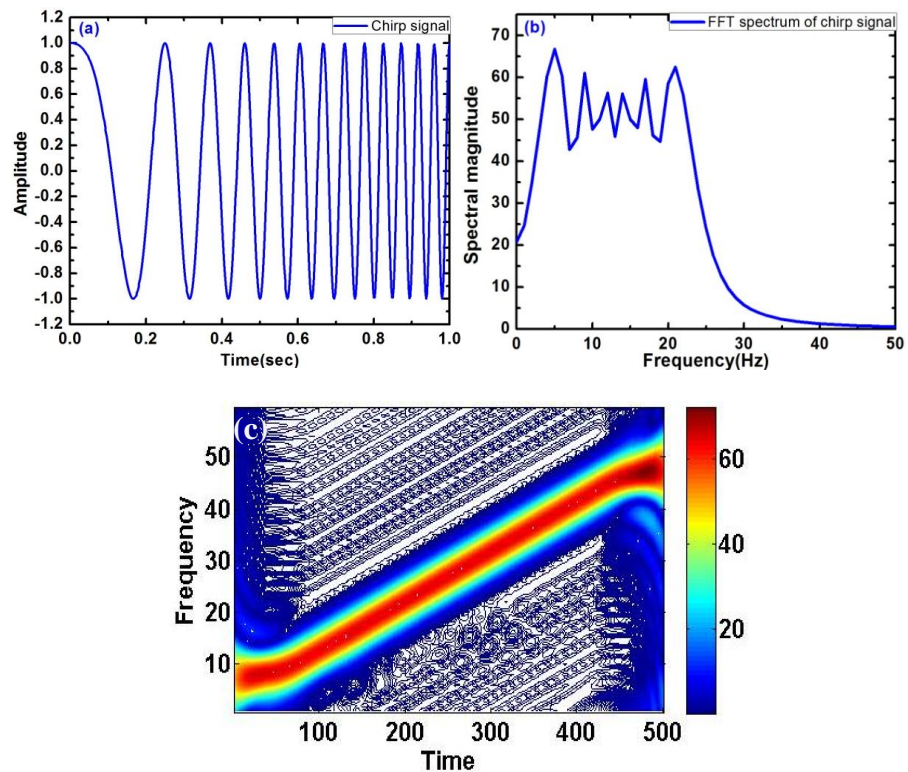


Fig. 3.9. (a) Signal with different frequency components (b) frequency spectrum of “a” obtained using FFT (c) WVD of signal illustrated in “a” The conversion factor for Y-axis is $(\text{coordinate position} / 3000) * (F_s/2)$ and X-axis is $((\text{co-ordinate position} + 5000) / 3000) * (F_s/2)$. F_s is the sampling frequency (500 Hz). The unit of time and frequency is s and Hz respectively

3.2.3 Different parameters and their effect on PA response: An analysis

Since one of the primary aims of the thesis is to perform frequency spectrum analysis of PA response, it is very important to investigate the effect of experimental parameters on PA response as well as the frequency spectrum. In this section, effect of different experimental parameters such as laser energy, spot size of the laser, sample container, distance between sample and sensor on PA signal frequency spectrum is explained. In order to remove the effect of the mentioned experimental parameters, the PA response is normalised.

3.2.3.1. Effect of absorption and laser energy

It is known that absorption and laser irradiance on the sample would change the amplitude of the PA response [32]. The higher the

Chapter 3

absorption and laser irradiance, higher the PA response's amplitude. If the signal amplitude is changed due to any of these factors, then the spectral amplitude of the signal changes. A simulation study by changing the optical absorption of the sample shows an increase in spectral amplitude as illustrated in Fig. 3.10(a). Here the absorption of the sample has been increased by 1.5 times and 2 times the original absorption as shown in the inset of Fig. 3.10(a). Thus it is essential to differentiate mechano-biological property from the optical absorption. In that sense normalisation would help.

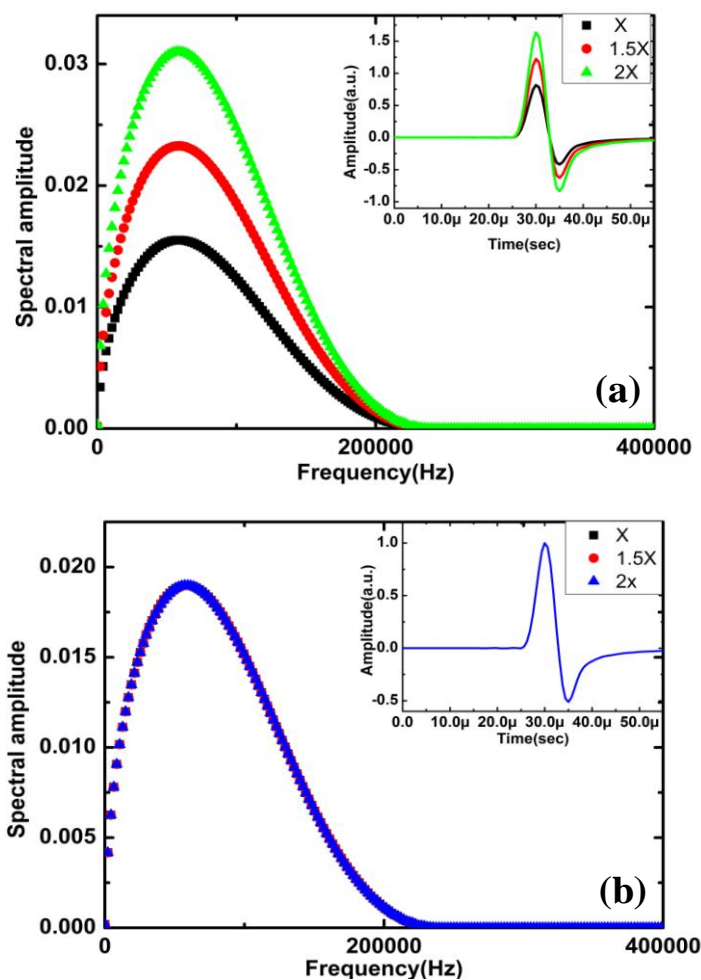


Fig. 3.10. Frequency spectrum from simulated target with varied absorption (absorption increased by 1.5 times and 2 times), corresponding time domain signal given in inset (a) without normalisation (b) after normalisation of PA time domain signal

Figure 3.10(b) illustrates PA response and the frequency spectra after performing normalisation. This clearly indicates that absorption/energy

variations in experiments are not affecting the normalized results and thereby the spectral information. Therefore, all the PA signals in this thesis are normalised before performing spectral analysis.

In addition, it is also worthwhile to investigate the effect of laser energy on PA response amplitude. The reason is during experiments if there is a variation in laser energy it would affect the PA signal. Therefore it is very important to verify the linearity of PA response amplitude with laser energy so that the effect of this variation can be nullified by normalisation. An experimental study is performed to verify the relation between laser energy and PA signal amplitude as illustrated in Fig. 3.11. The figure clearly elucidates a linear relationship within the experimental range of laser energy.

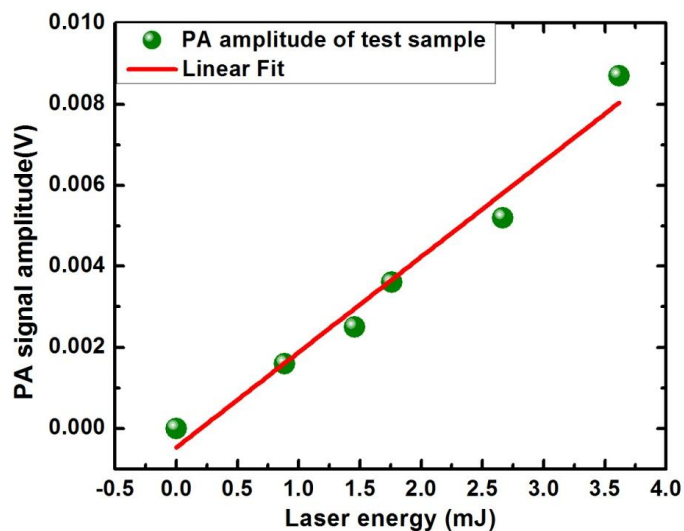


Fig. 3.11. Laser energy vs PA response amplitude plot

3.2.3.2 Spot size of the laser

Subsequent to laser energy, the spot size of the laser is another experimental parameter that affects PA response characteristics. The irradiated laser spot on the sample surface is considered as sample size. The spot size of the laser i.e. the sample size is related to the width of the PA response. The following equation (Eq. 3.7) illustrates the relation between sample size (diameter) and the PA response width (τ) [75].

$$\tau = \frac{2a}{V_s} \tag{3.7}$$

where a is radius of the absorber, V_s is the sound speed

It can be certainly observed that the PA response width is linearly related to the size of the sample. To verify the theoretical explanation, simulation study was performed. Figure 3.12(a) & 3.12(b) illustrate PA response and frequency spectrum of two numerical targets with different diameters (0.4 mm and 1 mm).

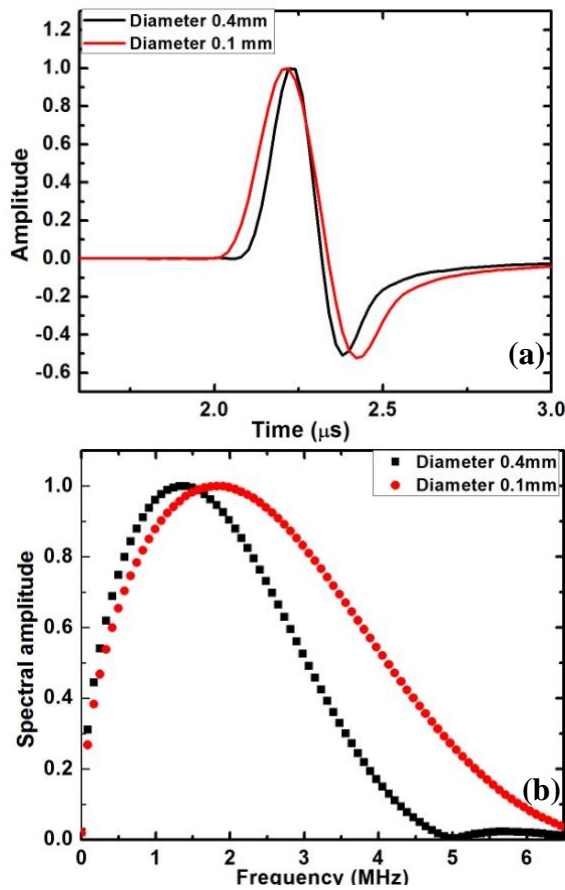


Fig. 3.12. Simulation study performed on numerical targets of different diameters to depict different sample size that provide (a) PA responses and (b) PA frequency spectrum

The width of the PA response is verified with theoretical and simulation studies that provides very high resemblance (Theoretical width of 0.4 mm target is $2.62\mu\text{s}$ and simulated width $2.6\mu\text{s}$). Since it very evident that change in sample size causes shift in dominant

frequency (frequency spectral parameter) from 1.5 MHz to 2.3 MHz, it should be taken care for accurate results. Therefore, the laser spot size was kept fixed for all the experimental studies to nullify the effect of this parameter.

3.2.3.3 PA sample container

As per literatures, glass container was utilised as sample containers [177], [178]. Investigating the effect of sample container on PA response is very essential as the container also can generate PA response that can merge with response from the sample. This would lead to erroneous result. Hence for this study, PA response was acquired from the sample container without pouring any sample into the container. It was observed that there is no PA response generated from the PA sample container. Therefore glass containers were used for PASR experiments with liquid samples.

3.2.3.4 Distance between sample and sensor

The distance between the sample and the sensor also have an effect on PA response. This is human error. While placing the sensor for repeating experiments, the sensor position i.e. the distance between sample and sensor may vary which can affect the PA response. Therefore this parameter should be verified and eliminated for more accurate results. To verify the affect of PA response due to variation in sample-sensor distance, experimental studies were performed. Here, the PA signal of a black rubber sample has been acquired and the sensor was moved away from the sample by 0.5 cm. The time domain signals shown in inset of Fig. 3.13(a) exhibits an amplitude change as well as change in the time delay. To eliminate the experimental errors that arise due to sample-sensor distance, the time domain signals are again normalised and the spectral information of the two signals becomes identical as shown in Fig. 3.13(b). This proves that experimental variations of the transducer at least upto 5 mm can be eliminated when the signals are normalized. In our experiments, the experimental error due to transducer positioning is lower than 2 mm.

Chapter 3

Therefore it can be stated that PA response normalisation would eliminate the effect of sample and sensor distance that will eliminate the positioning error of sensor.

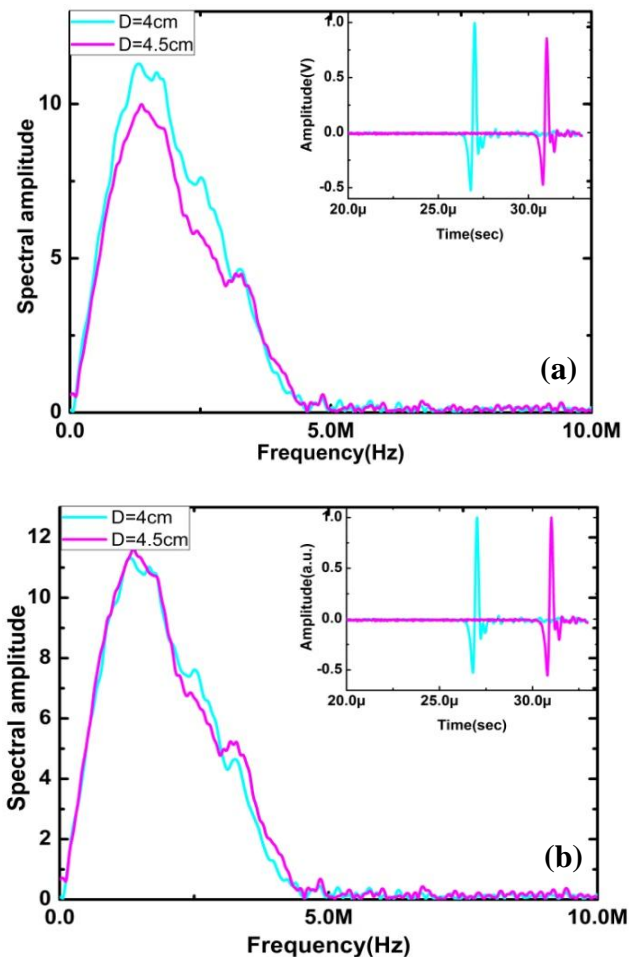


Fig. 3.13. Frequency spectrum of black rubber sample with sensor position varied by 5 mm (inset image provides PA time domain signal of the same sample (a) without normalisation (b) after normalisation

3.3 PASR experiment with biological sample

Subsequent to PASR experimental setup characterisation with simulation and tissue mimicking phantom study, it is very important to observe the response of the system towards biological samples. In order to do that, developed PASR setup is verified with blood samples. This study includes two parts which is given as follows:

- i. Change in PA response amplitude by varying red blood cells (RBC) concentration
- ii. Change in PA response amplitude by varying RBC shape

3.3.1 Change in PA signal amplitude by varying RBC concentration

The first set of study is to ascertain how sensitive is PA response technique's amplitude for a change in concentration of RBCs. For this experiment, different volume concentrations of whole blood samples were prepared and experimented immediately after sample preparation.

To prepare blood samples, fresh human blood was collected from healthy donor. For this experiment, concentration of RBC in whole blood sample was varied by diluting the whole blood with isotonic solution (0.9 gm NaCl in 100 ml water). Isotonic solution is used to maintain the tonacity of blood [179]. Four samples with different volume percentage of whole blood i.e. 20%, 60%, 80% and 100% were prepared. The variation in volume percentage of whole blood provided change in concentration of RBCs in the samples. The PASR experiments were performed immediately after sample preparation. The samples were poured in PA sample container and placed vertically into the water tank. The schematic of the experimental setup is already illustrated in Fig. 3.3. The sample was irradiated by a Nd:YAG laser with second harmonic pulses as mentioned in section. It was exposed to maximum 10 mJ with the spot size of 4 mm² laser beam. In this experiment, these PA responses are acquired by a single element ultrasound sensor with centre frequency 3.5 MHz and bandwidth 3.8 MHz. The other details of the experimental setup are given in section 3.2.1. PA response amplitude obtained from the samples is shown in Fig. 3.14. The signal amplitude has shown a change of 2.5 mV when the concentration was changed from 20% to 100%. The reason for this change in amplitude can be related to the number of cells that are irradiated by the laser. With the increase in concentration of the blood, number of cells that get irradiated also increases. As mentioned in Chapter 2, initial pressure (p_0) is proportional to absorbed absorption coefficient ($\mu_a(r)$) as shown in Eq. 3.8 [57]

Chapter 3

$$\Delta p_0 = \Gamma \eta_{th} \mu_a F \quad (3.8)$$

where $\mu_a(r)$ is absorption coefficient, η_{th} is the percentage that is converted into heat, Γ is Gruneisen coefficient and F is fluence, change in RBC concentration varies the absorption thereby changes the amplitude of PA response. Absorption spectra of water and NaCl were obtained to confirm that they do not contribute to absorption for second harmonic excitation. Figure 3.15 clearly shows very low absorbance (0.092) compared to blood (~ 2.3). Therefore the effect is negligible.

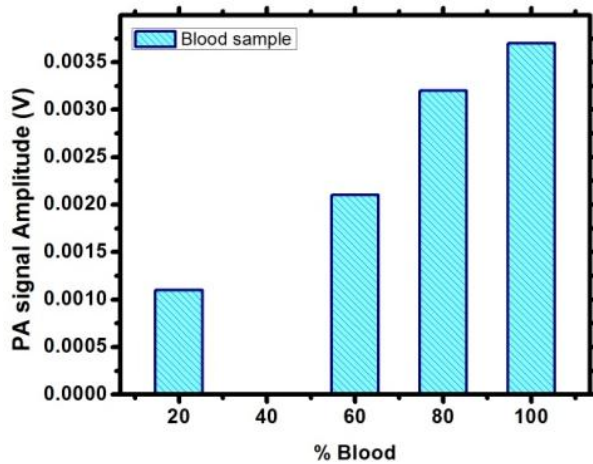


Fig. 3.14. PA response vs blood concentration plot

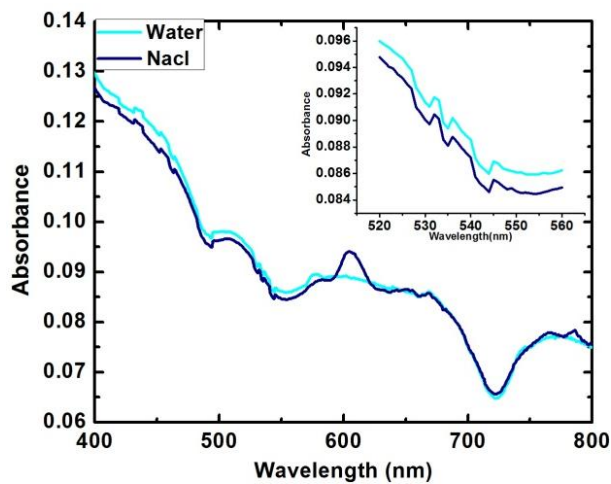


Fig. 3.15. Absorption spectra of water and NaCl

3.3.2 RBC shape analysis using PA signal amplitude

The second set of experiment would be to identify the effect of morphological changes on amplitude of PA response. For this set of experiment, the samples (test and control) were kept for 1 hr in room temperature to allow the RBCs to undergo morphological changes. For performing the experiments, three different solutions isotonic, hypotonic and hypertonic solution with different concentration of NaCl were prepared to dilute the blood sample with different tonicity. Among these solutions, isotonic solution maintains similar tonicity as blood plasma and rest causes osmotic pressure change in RBCs [180]. Table 3.1. illustrates the details about the composition of the solutions.

Table 3.1. Composition of the solutions for varying tonacity of blood

Sample	Water (ml)	NaCl (gm)	Osmolarity(Osm)
Isotonic	5	0.045	0.15
Hypotonic	5	0.001	0.006
Hypertonic	5	0.7	4.4

The samples were categorised into test and control. Two test samples named hypotonic sample and hypertonic sample were prepared by adding hypotonic and hypertonic solution with whole blood with mentioned proportion (Table 3.2.). The control sample was prepared by adding isotonic solution named as isotonic sample. The RBCs in test samples undergo morphological changes whereas the control sample maintains its original shape [181]. The RBCs with hypertonic solution get shrunk as the water inside the RBCs drain out since the solute concentration is high in the surrounding medium compared to cells. In contrast, the RBCs in the hypotonic solution allow diffusion of water from the surrounding medium to the cells due to lower concentration of solute in the medium. Due to diffusion of water into the RBCs, it gets swollen.

Chapter 3

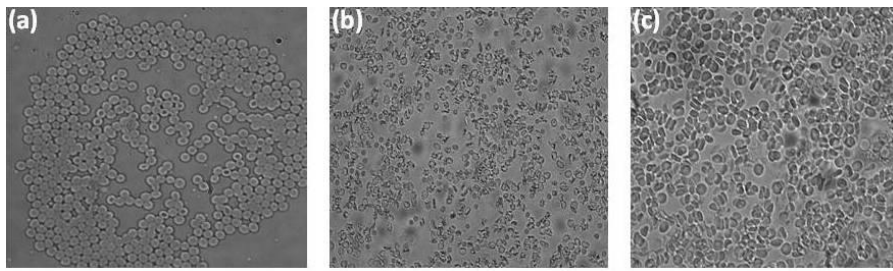


Fig. 3.16. Microscopy images of (a) isotonic (b) hypertonic (c) hypotonic samples

Table 3.2. Composition of blood samples

Blood sample	Blood (ml)	Solution (ml)
Isotonic sample (Control)	0.3 ml	0.2 ml isotonic solution
Hypotonic sample (Test)	0.3 ml	0.2 ml hypotonic solution
Hypertonic sample (Test)	0.3 ml	0.2 ml hypertonic solution

It was confirmed by microscopy that test as well as control samples have undergone morphological changes. Subsequent to sample preparation, microscopy of the samples was performed by microscope within an interval of 10 mins. Immediately after observing the shape change of the control samples, PASR experiments were performed by the same experimental setup as the first study. Figure 3.16 illustrate microscopy images of test and control samples. This clearly elucidates the shrunken RBCs in hypertonic solution and swollen RBCs in hypotonic solution. However the control sample i.e. the isotonic sample retains its original disc shape. The PAS experimental result shows a prominent change in amplitude when there is a change in shape of RBCs as shown in Fig .3.17. The signal amplitude increased almost two fold in the case of hypertonic solution whereas amplitude reduces (0.08 V) hypotonic solution where the RBCs swell and get lysed. The probable cause for this can be associated with number of cells under irradiated region. More number of shrunk RBCs would have been irradiated which increases the signal amplitude. The swollen RBCs lyses and disruption of haemoglobin inhibits the amplitude of

PA response. The obtained PAS results were compared with standard UV-VIS spectroscopy as illustrated in Fig. 3.18 Distinct change in absorption is clearly observed from the spectra that correlate very well with the obtained PASR results. This proves that the developed setup is sensitive towards change in biological samples. In addition it can provide quantitative analysis which is very important for clinical diagnosis and study.

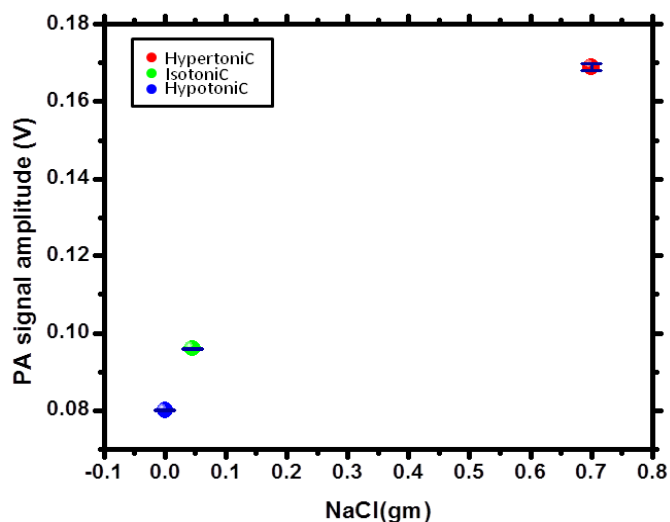


Fig. 3.17. PA response amplitude vs isotonic, hypotonic and hypertonic sample plot

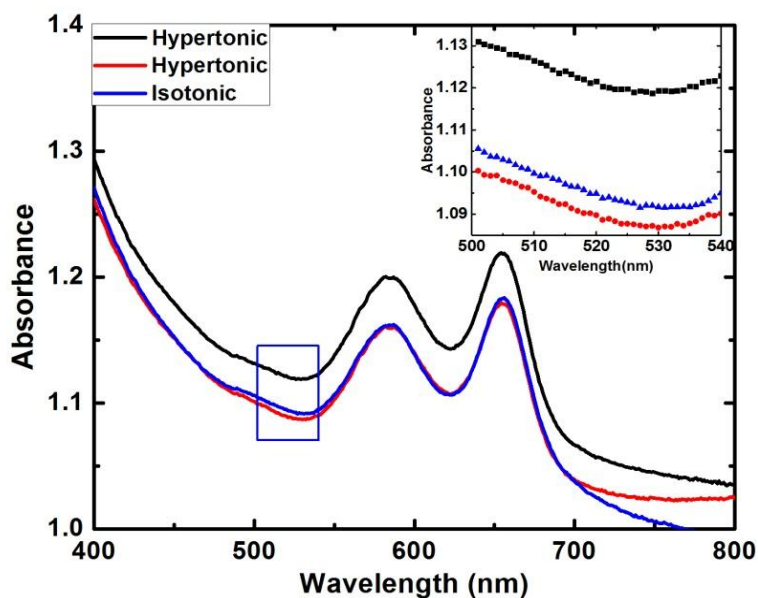


Fig. 3.18. UV-VIS absorption spectra of PA response Vs isotonic, hypotonic and hypertonic samples

Chapter 3

3.4 Elastic property study using PASR

Subsequent to PASR setup development and characterisation, the setup is verified with blood. The studies clearly delineate that the developed setup yield change in PA response amplitude due to change in optical absorption of biological samples. The next step is to verify that how change in mechano-biological property (elasticity) of the sample affects PA frequency spectrum. This has been verified with simulation as well we experimental studies (tissue mimicking and biological tissues). It is well known from literature that tissue elastic property is related to density and sound speed of the sample as illustrated in Eq.3.9 [182]

$$\xi = V_s^2 d \quad (3.9)$$

where, ξ is bulk modulus, V_s is sound speed and d is density of the sample. From Eq. 2.10 it is known that generation of PA time domain signal is related to initial pressure rise in the sample due to thermal expansion which serves as a strain source. Therefore it can be inferred that generated acoustic signals are related to sample's elasticity.

3.4.1 Simulation study

In order to understand how sound speed and density affects PA spectrum, a simulation study was performed in MATLAB using K-wave toolbox to investigate elasticity in biological tissues [65], [183], [184]. As it has been already explained that sample size and absorption affects the PA spectral response, the effect of these two parameters are avoided in the simulation by taking two numerical samples with identical size and absorption. The targets were simulated with a change in sound speed from 1600 m/s to 1900 m/s (arbitrary chosen values). Figures 3.19(a) shows there is a shift in centre frequency of the spectrum by 1 MHz. Similarly, keeping the sound speed constant, simulations were performed by varying sample density from 1600 kg/m³ to 2000 kg/m³. Similar to the previous study, Fig. 3.19(b) shows similar shift in frequency. Hence this study clearly

proves that mechanobiological property of the samples can be assessed through photoacoustic spectral analysis.

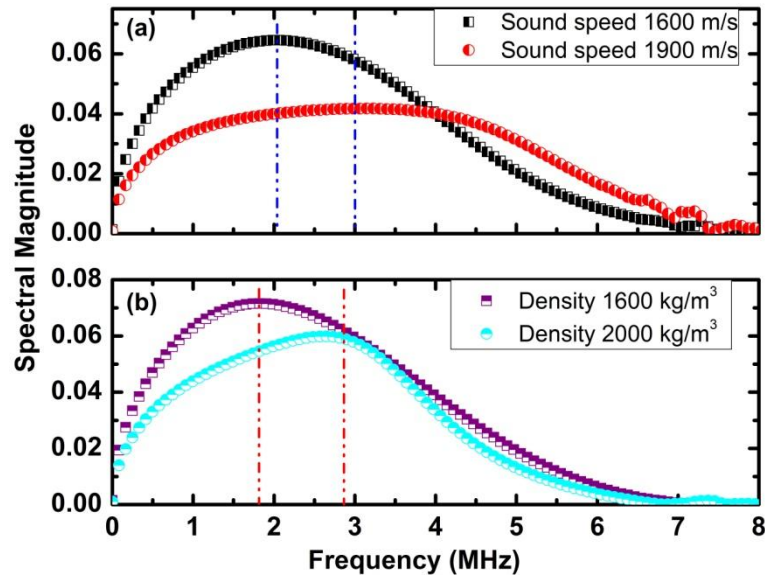


Fig. 3.19. Spectral information of two numerical targets with (a) sound speed 1600 m/s and sound speed 1900 m/s (density 1500 kg/m³) (b) density 1600 kg/m³ and density 2000 kg/m³ (sound speed 1500 m/s)

3.4.2 Tissue mimicking phantom study

Subsequent to simulation study, developed PASR technique is applied on to tissue mimicking phantoms to verify the hypothesis. In this thesis, Gelatine is used as tissue mimicking phantom as the properties of gelatine is very close to soft tissues [185]–[187]. Since optical absorption coefficient of gelatine is significantly low in second harmonic wavelength, absorber has been added to the gelatine gel. Black ink is used as absorber in this study which exhibits very high absorption in mentioned wavelength as illustrated in Fig. 3.20. Thus sample absorber is black ink and surrounding sample gelatine is a model that depicts absorption as well as mechano-biological property. Since the motivation of the study is to verify the effect of elasticity on PA frequency spectrum, change in elasticity is induced in the gelatine sample by varying the concentration of gelatine in the gel samples. Four samples were prepared with various concentration of gelatine such as 0 gm/ml (only black ink, 1 ml ink), 0.1 gm/ml (0.1 gm gelatine in 1 ml ink), 0.25 gm/ml (0.25 gm gelatine in 1 ml ink), 0.4 gm/ml (0.4

Chapter 3

gm gelatine in 1 ml ink), while the concentration of ink was kept constant to ensure identical absorption. Since increase in gelatine concentration increases the density of the phantom, dominant frequency reflect density change. In this thesis, dominant frequency represents the frequency component with highest spectral amplitude which is obtained from in-house developed MATLAB code.

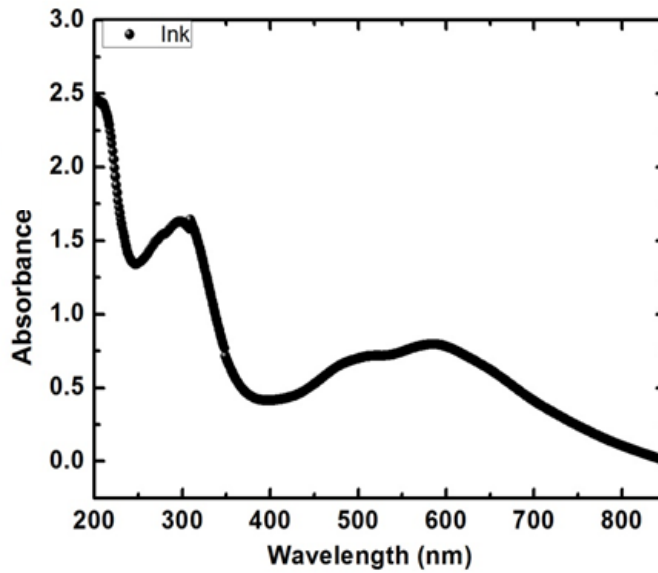


Fig. 3.20. UV-VIS absorption spectra of black ink

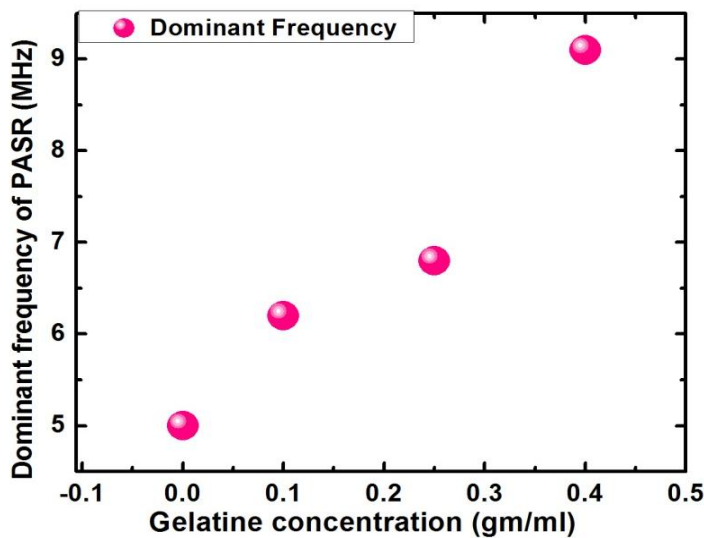


Fig. 3.21. Plot of gelatine concentration and PASR dominant frequency

Figure 3.21 shows a significant rise in PASR dominant frequency with increased gelatine concentration. In this study, 39 % increase in the

PASR dominant frequency was obtained for 1.5 times increase in gelatine concentration.

Subsequent to solid tissue phantoms, PASR technique was applied to liquid samples that exhibits change in elasticity in terms of variation in density. This is important to differentiate liquid samples based on elasticity as many diseases such as haematological diseases, Pneumonia deals with body fluids (blood, oedematous fluid etc.). For this study, beetroot juice and black ink is used as samples as both of them illustrate high absorbance in 532 nm wavelength and differs in density. The experimental parameters such as laser energy, spot size of laser is kept constant for this study. The only change was in the sample's density that signifies that elasticity. Figure 3.22 illustrates the PA frequency spectrum obtained from beetroot juice and black ink. Even though there is considerable change in sample's density, no change in PA frequency spectrum was observed for beetroot and black ink samples.

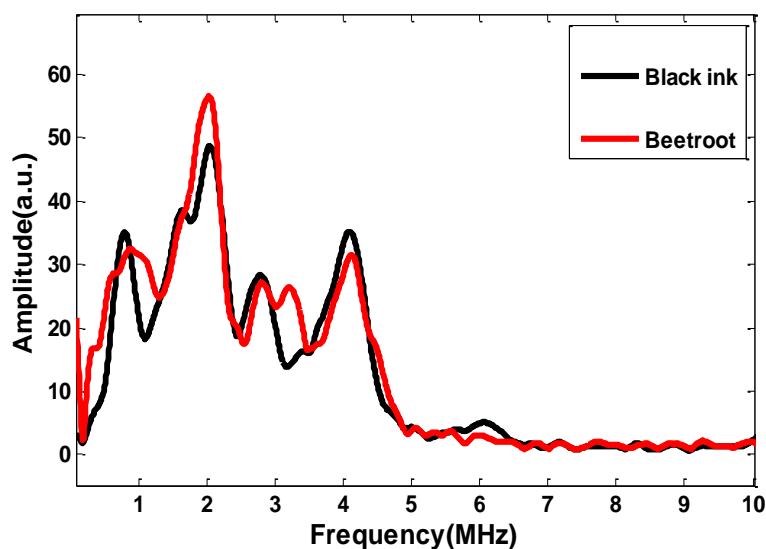


Fig. 3.22. PA frequency spectrum of black ink and beetroot sample when the samples placed in glass cuvette

In order to verify the results, PA response of beetroot sample (liquid) were closely investigated that illustrates oscillations as shown in Fig. 3.23(a). Then PA response of the rubber sample was acquired in similar experimental condition as shown in Fig. 3.23(b) (not placed in

Chapter 3

glass cuvette) was compared with PA response from beetroot sample as illustrated in Fig. 3.23. Since solid sample like black rubber is not placed in glass sample container, it is worth comparing liquid samples PA response with black rubber. By comparing PA responses of beetroot and rubber samples, it can be clearly observed that beetroot sample exhibits multiple oscillations compared to rubber sample. Since all the experimental parameters were constant during acquisition of PA response from beetroot and rubber sample except the glass cuvette, there is a possibility that glass cuvette plays an important role in PA response.

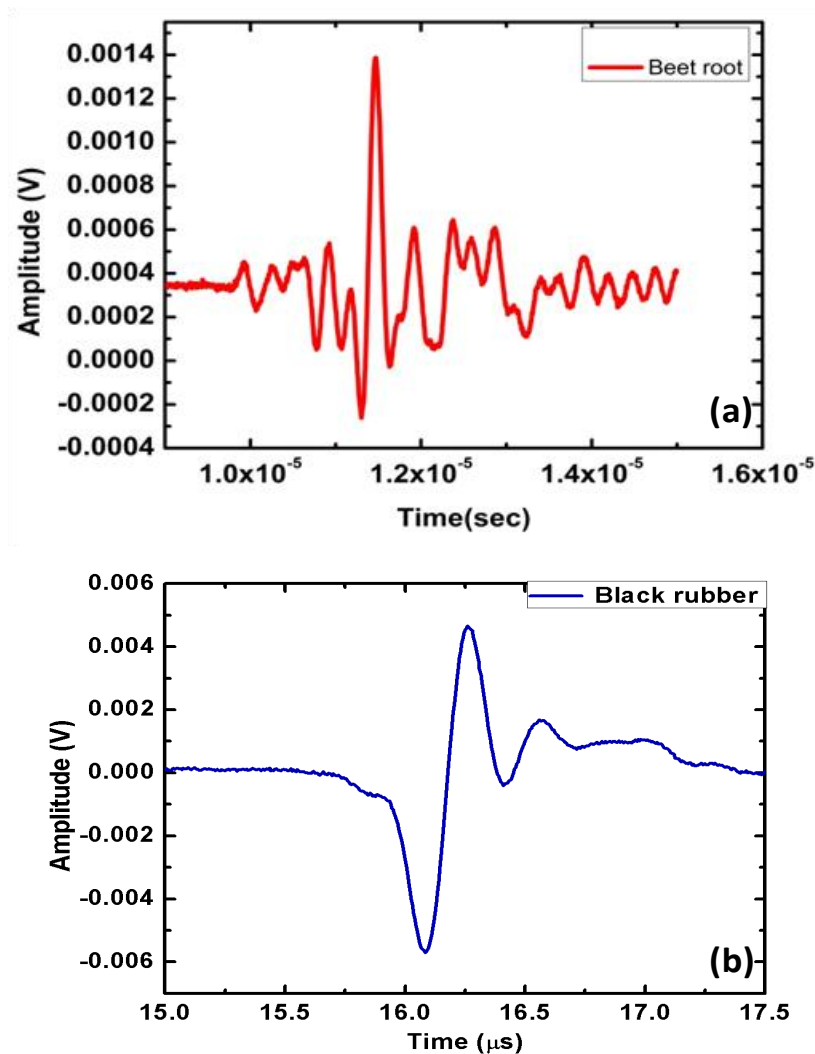


Fig. 3.23. PA response obtained from (a) beetroot juice filled in glass cuvette (b) black rubber sample

To investigate the effect of glass cuvettes on PA response, interaction of ultrasound waves with glass was studied. It is well known from literature, that glass is a very good reflector of ultrasound waves [188]. Since the glass container is cylindrical, it can be hypothesised that two opposite walls of the container act as reflectors as illustrated in Fig. 3.24 which forms a cavity. Due to the multiple reflections, oscillation in PA response is obtained. The cavity formed in the glass cuvette behaves as a band pass filter that allow only certain band of frequency to pass through the wall of the container. The frequency band which comes out of the container is similar to the pass band of the filter. The passband of the container depends on the diameter of the container. The reason is the distance between the two reflectors (walls of the container) is the primary factor for oscillations.

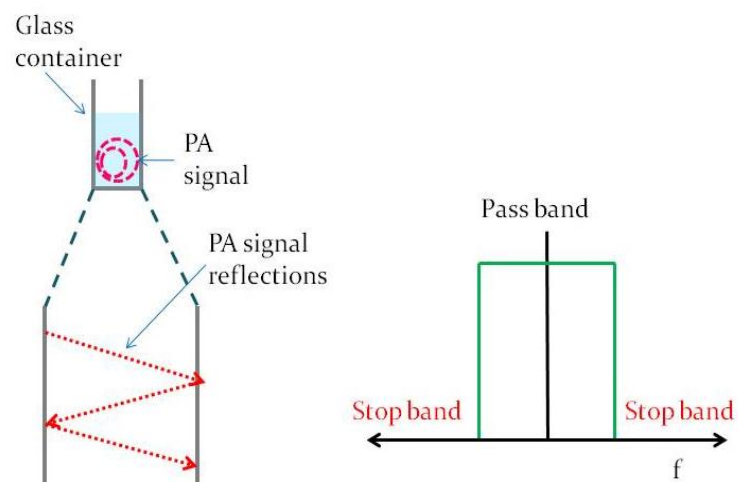


Fig. 3.24. Schematic of PA response reflection in glass cuvette and response of band pass filter

Therefore all the samples which is poured in the glass cuvette container, exhibit a certain band of frequencies thereby causes identical frequency spectrum.

Therefore utilising glass cuvettes for PASR experiments would provide erroneous results. To acquire the true PA response of the sample, cavity effect should be nullified. For this reason glass cuvettes were replaced by silicone rubber tubes. Since silicone rubber has inherent property to pass ultrasound [189], [190], generated PA signal

Chapter 3

from the samples can easily travel through the container and reach the ultrasound sensor. Figure 3.25 illustrates the PA response of same beetroot sample placed in silicone rubber container that exhibits no oscillations in the signal due to PA cell. This proves that the silicone container does not reflect PA response.

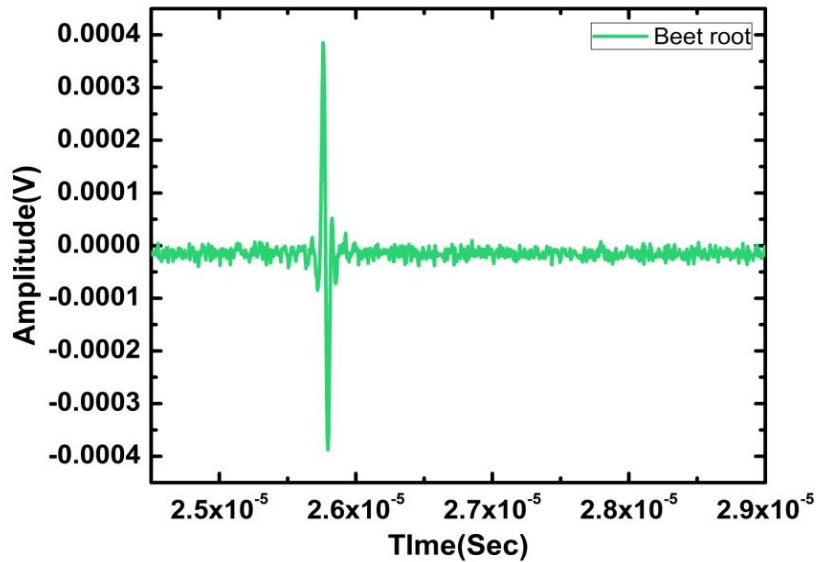


Fig. 3.25. PA response of beetroot sample placed in silicone rubber tube that exhibits no oscillation

Then the PASR experiments with beetroot and black ink samples were repeated with silicone rubber tube to observe the PA frequency spectrum which is shown in Fig. 3.26.

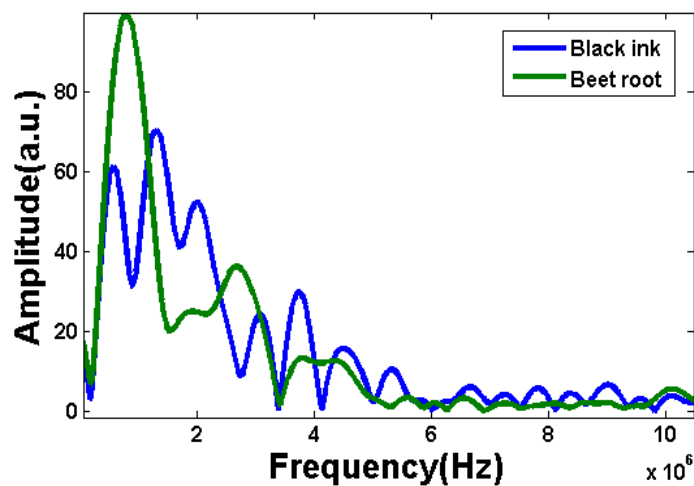


Fig. 3.26. PA frequency spectrum of black ink and beetroot sample when the samples placed in silicone rubber tube which illustrates change in frequency spectrum

From the spectrum it clear that there is a distinct shift in frequency components. For example beetroot sample exhibits two dominant peaks at 1 MHz and 2.3 MHz whereas black ink illustrates multiple peaks at 0.8 MHz, 1.7MHz, 2.1 MHz and so on. This certainly proves that silicone rubber tubes help to obtain true response of the sample. Thus for all the experiments with liquid sample were performed with silicone rubber tubes.

In case of solid samples, another approach has been utilised. To avoid contamination of water in which sample and sensor are immersed, the sample was wrapped with parafilm. As parafilm is a very thin membrane, it does not affect the PA signal. However the airgap present in between the film and sample exhibits oscillation in PA response. Thus the sample was coated with ultrasound gel in order to get rid of the air gap. This method of sample wrapping is followed in the all the studies.

3.4.3 Elastic property study using biological samples

Subsequent to tissue phantom study, the hypothesis is verified with biological samples. For this study, freshly excised chicken liver and muscle were experimented. The motivation behind choosing theses samples is liver and muscle exhibit distinct difference in elasticity. Therefore applying PASR onto liver and muscle would provide an idea about feasibility of PASR on biological samples. In order to perform the PASR experiments, tissues were cut into 1 cm × 1 cm pieces. Then the samples were coated with thin layer of ultrasound gel and wrapped with parafilm avoiding bubble formation. PA responses were acquired from three different areas of a sample by utilising the developed PASR setup as described in section 3.2.1. The PA frequency spectrum was obtained by applying FFT to the PA response. Figure 3.27 delineates the PA frequency spectrum of liver and muscle. It is known that liver and muscle have stark difference in their elastic property [185]. Hence, in this study, PASR is applied onto chicken liver and muscle to discriminate them based on tissue elasticity. It is clear from Fig. 3.28(a) that the dominant frequency of liver is at least 1 MHz more

Chapter 3

than that of chicken liver. To verify the consistency of the results, the same experiment has been repeated at different locations of the three biological specimens. Moreover, for quantitative differentiation, besides dominant frequency, spectral magnitude is also obtained. Both of the spectral parameters delineate distinct change which can be observed from the box plots illustrated in Fig. 3.28(b)

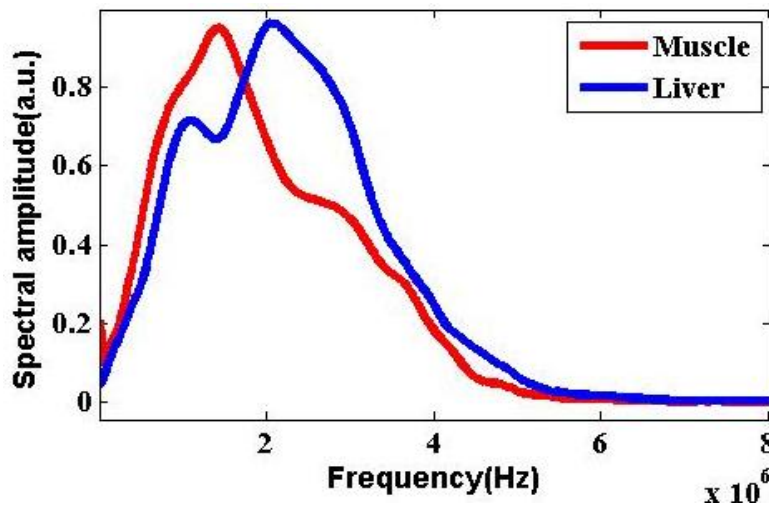


Fig. 3.27. Spectral information of muscle and liver tissues obtained through PASR technique

In order to understand the reason behind the obtained results, properties of liver and muscle should be analyzed. Liver is a cell continuous tissue which contains very low amount of extracellular matrix (ECM) and collagen content. Therefore liver is soft and friable tissue but high density. On other side, muscle is a matrix continuous tissue that possess high amount collagen [191]. Therefore tensile strength of muscle is high compared to liver which indicate high elasticity. Since elastic medium exhibits low sound speed, the dominant frequency of the spectrum shifts to lower value. This is the reason behind higher dominant frequency of liver compared to muscle. Subsequently muscle possess high acoustic attenuation (3.3 MHz/dB) compared liver (0.9 MHz/dB) [185]. Therefore spectral magnitude of muscle tissue is relatively low compared to liver tissue. Results obtained from PASR study of chicken muscle and liver clearly indicates that spectral parameters such as dominant frequency and

spectral magnitude exhibits distinct change for tissue types with different elastic property. Thus proposed PASR technique can be used for many critical applications such as differentiating benign and malignant tumors, different thrombotic diseases etc. which exhibits change in elastic property.

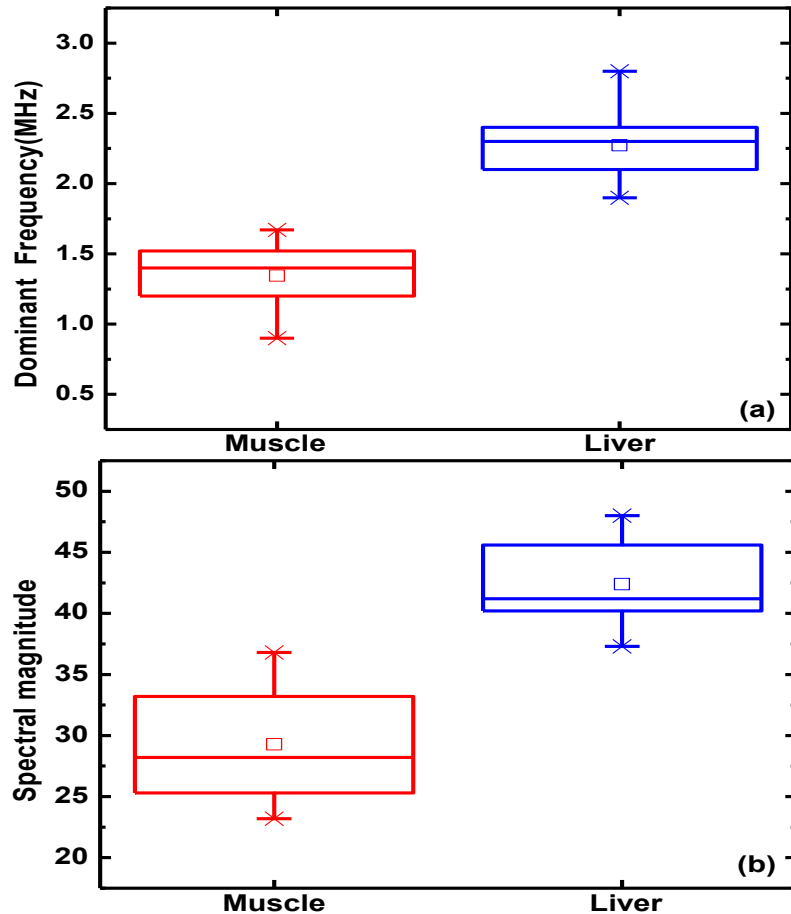


Fig. 3.28. Box plot of (a) Dominant frequency (b) Spectral magnitude. The shaded box represents 25 - 75 % of the data set. The line in the box is the median and mean value is shown as square box. The whiskers (cross sign) show the maximum and minimum of data set

3.5 Summary

An attempt was made to develop PASR instrument in-house that can serve as a tool for different disease diagnosis based on sample's elasticity. The experimental setup was developed and real time PA frequency spectrum of the sample is monitored by custom made LABVIEW interface. Since the technique relies on PA response and the frequency spectrum, the effect of different experimental parameters

Chapter 3

such as laser energy, sample's absorption, distance between sample and sensor sample size etc. on PA response should be performed. Therefore the developed system is characterised with simulation as well as experimental studies in order to eliminate the effect of the mentioned experimental parameters and obtain true response of the sample. Subsequent to characterisation, the developed PASR setup is applied on to blood samples to verify the sensitivity of the setup towards biological samples. PA response amplitude delineated distinct change due to change in RBC concentration as well as shape. After development and testing of PASR setup, developed setup was applied to tissue mimicking phantom made out of gelatine sample and black ink as absorber to verify the hypothesis that PA frequency spectrum is sensitive towards change in sample elasticity. The study illustrated significant change in PA frequency spectrum dominant frequency due to change in sample density. Consequently biological samples (chicken liver and muscles) were also experimented that also illustrated significant change in PA spectral parameters. This proves the applicability of the developed PASR setup for different diseases that exhibits change in elasticity. The setup can be useful to differentiate normal from pathological tissues with high efficiency. Application of PASR setup for different disease diagnosis is reported in the next chapter.

Chapter 4

Application of Fast Fourier Transform based PASR technique for different disease diagnosis

“If you can't explain it simply, you have not understand it well enough”

-Einstein

4.1 Introduction

In Chapter 3, development and characterisation of PASR technique is discussed. It also explains the potential of PASR technique in order to detect change in sample's mechanobiological property in details. The simulation, tissue phantom and biological samples (chicken liver and muscle) studies clearly signify that PA frequency spectral parameters are highly sensitive towards change in sample's elasticity. As described in Chapter 3, two types of signal processing tools such solely frequency based (FFT based) and time-frequency (WVD, EWT) are utilised depending upon the complexity of the samples. This Chapter describes two major applications of FFT based PASR techniques that include differentiation of blood and clot and detection of early stage Pneumonia. Chapter 4 is divided into two sections, section 4A and section 4B. Detection of blood and blood clot study is described in Section 4A end Section 4B detail about early stage diagnosis of Pneumonia.

Section-4A

4.1A Problem statement and motivation

Blood coagulation is a natural defence mechanism of human body to prevent blood loss during injury. While blood coagulation is a normal phenomenon, hyper-coagulation could lead to the formation of blood clots or thrombus in the vessels. These thrombi while moving through the blood vessels can reach vital organs like heart, lungs, kidney, brain etc. and can impede blood flow in the vessels. This process is the cause for many fatal diseases such as heart attacks, ischemia, pulmonary emboli, deep vein thrombosis etc. [192]–[194]. Hence scientists show a keen interest in understanding the process of thrombus formation.

Briefly, thrombi formation is a complex process where fibrinogen converts into fibrin and the subsequent covalent cross-

Chapter 4

linking of fibrin play important roles. Particularly, the mechanical properties of fibrin affect the criticality of thrombus [195], [196]. For example, if a blood vessel is partially occluded because of a clot, the viscoelastic properties would determine whether the flowing blood would deform the clot, rupture or embolize (occlusion of blood vessels). Interestingly, epidemiological studies involving patients suffering from myocardial infarction show tight and rigid fibrin network structures compared to controls [194], [197].

The mechanical properties of fibrin in clots are important for understanding, preventing and treating thrombosis and blood coagulation related disorders. However, there is little understanding of the clinical and even less known is the basic mechanical properties of clots necessary for haemostasis and thus, investigation is needed to understand the mechanism involved in haemostasis.

In this context, monitoring blood coagulation process as well as differentiate blood from blood clots (immersed in blood) by quantitatively assessing its mechanobiological properties using developed PASR technique, a non-invasive, marker-free technique suitable for real-time biomedical applications is proposed. As mentioned earlier, the advantage of this technique lies in specific optical absorption (increasing specificity by targeting sample's absorption) and also in diagnosis of deep tissues through less scattering ultrasound waves. Conventional PA imaging has shown the ability to detect blood clots in tissue phantoms and also aging of clots as optical absorption changes with respect to the age of the clot [26].

Despite the potential of conventional PA imaging, after clot detection in tissue phantoms, it could not go further in understanding the mechanism of clots. The main reason is that clots when present with blood would have many components like hematocrit concentration, fibrin concentration that contribute to optical absorption and acoustic attenuation, which is reflected in the amplitude of the PA signals. For example, PA response of blood and clot taken from a donor is shown in Fig. 4.1(a). The amplitude of the blood clot signal is

higher compared to the blood. However, the same study repeated on another donor reveals that the PA amplitude of the clot is lower than that of blood as shown in Fig. 4.1(b). There exists inconsistency in the amplitude. This problem becomes worse when moving on to in-vivo studies, thereby preventing conventional PA technique to perform in vivo studies and understand the mechanism of formation of thrombus.

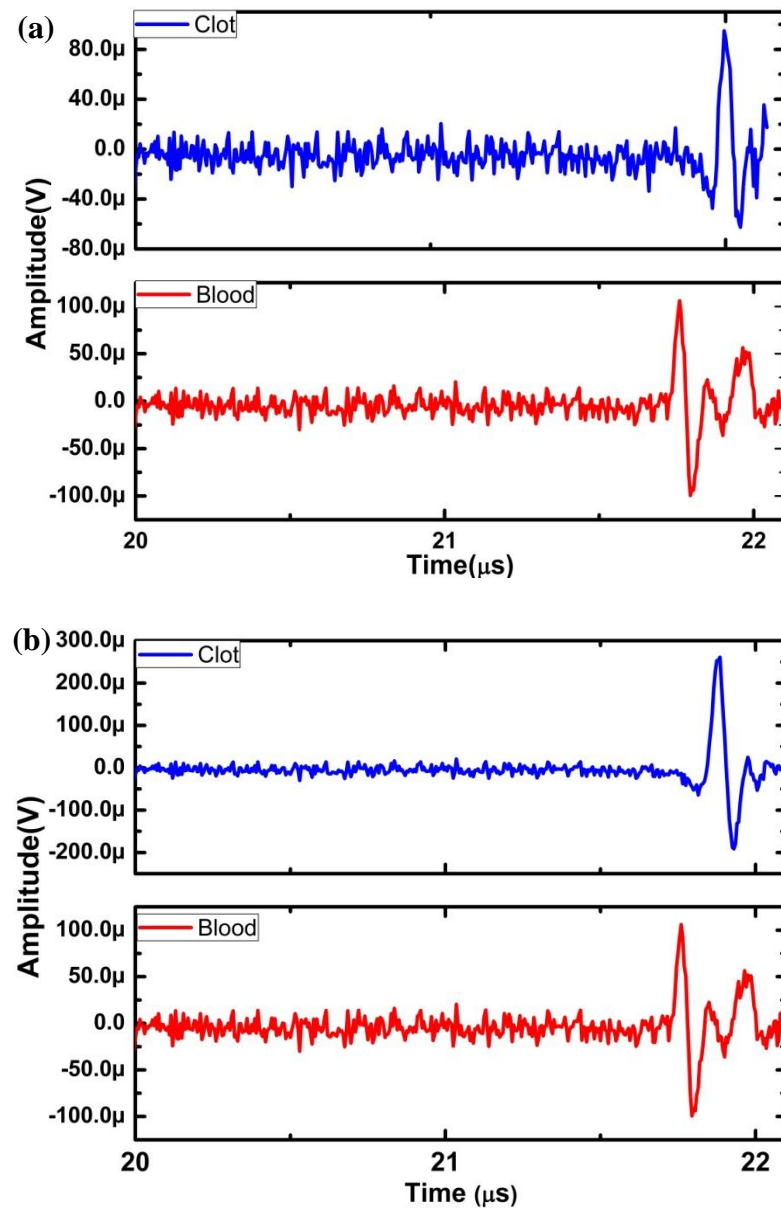


Fig. 4.1. (a) PA response of blood and blood clots of donor 1, (b) PA response of blood and blood clots of donor 2

This study attempts to solve the above-mentioned problem by calculating the spectrum of the acoustic signal. The proposed

Chapter 4

technique normalizes the signal (to eliminate amplitude effect) and then obtains the spectral information of the signals which is governed by the size, sound speed and density of the sample. Since elasticity is related to the sound speed and density by $\xi = v_s^2 d$ where ξ is modulus of elasticity, v_s is velocity of sound and d is density, PA signal can depict elasticity information, which is important to understand the mechanism of blood clots [47], [198], [199]. In this chapter, the PA spectral parameters such as dominant frequency and total spectral energy are utilized as primary parameters to assess the mechano-biological property change in the blood and clot samples.

4.2A Mechanism of clot formation

Blood coagulation is regulated by 50 important substances which initiate or affect blood coagulation [200]. The substances that promote blood coagulation known as procoagulant. The others which inhibit coagulation process known as anticoagulant. The blood coagulation totally relies on balance between procoagulant and anticoagulant. Among these two group of substances, anticoagulant are predominant to ensure proper circulation of blood in the vessels. The process of coagulation in normal condition is initiated by damage of blood vessels. This activates the procoagulant to dominate anticoagulants. Subsequently, solid clot is formed.

Blood coagulation follows basic three steps such as [201]

- i. Involving blood coagulation factors by complex cascades of chemical reaction in response to blood vessel rupture or damage of blood. It evolves many blood coagulation factors that forms activated substances called prothombin activator.
- ii. Prothombin is converted in thrombin by the prothombin activator
- iii. Thrombin work as an enzyme for fibrinogen to fibrin fiber conversion that forms mesh like structure to trap platelets, blood cells and plasma to form the clot.

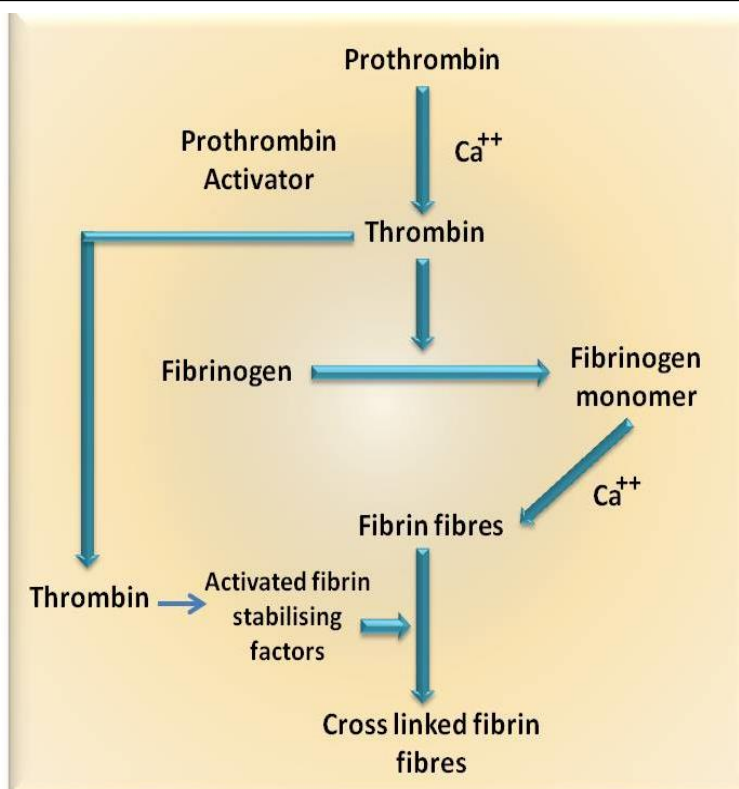


Fig. 4.2. Schematic of prothrombin to thrombin conversion and polymerization of fibrinogen for fibrin fibers formation [200]

4.3A Materials and methods

4.3A.1 Sample Preparation

For this study fresh human blood was collected from healthy voluntary donors by venipuncture into sodium citrate tube (tri sodium citrate solution 0.129 mol/l) in order to avoid coagulation [202]. The citrate ions basically bind to Ca ions present in blood by generating calcium citrate. This hinders blood coagulation as Ca ions are essential for prothombin to thrombin conversion. Subsequently, collected blood was divided into two equal proportions of hematocrit concentration to ensure identical absorption. One of the samples was used as pure blood sample and the other sample consists of clot along with blood. Blood was artificially clotted by adding 0.2M calcium chloride solution (CaCl_2) [193]. Since citrated blood blocks the calcium ions, excess of ions are provided by adding calcium chloride solution so that blood has free Ca ions for prothombin to thrombin conversion. After adding

Chapter 4

CaCl₂ solution to the blood samples, the sample was kept undisturbed until solid clot was formed. Clot formation took approximately 45 mins. In order to obtain the intermediate state reading, it was taken 20 mins after adding calcium chloride solution into blood. Even though a solid clot is formed, still it contains some amount of blood. The clot sample was used along with blood which depicts the original thrombotic disease condition where clot and blood both are present inside blood vessel.

4.3A.2 PASR experiment

Since the samples (blood) used in this study is liquid, PASR experimental setup for liquid sample was utilised as illustrated in Fig. 3.2. Samples were poured in to silicone rubber container and irradiated by laser pulses (energy 9 mJ/cm², wavelength 532 nm). Generated PA responses were acquired by an unfocused ultrasound transducer with centre frequency of 20 MHz placed ~3 cm away from the sample. Since blood exhibits low attenuation (0.17 dB/MHz) for high frequency compared to soft tissues (0.54 dB/MHz) [185], high frequency (20 MHz) transducer was employed for this study. Acquired PA responses were transferred to computer via digitizer. For quantitative analysis of the sample, frequency spectrum of PA response was obtained by applying FFT. The spectral features such as dominant frequency and spectral energy are obtained from PA frequency spectra. These are the key parameters which depicts change in tissue elasticity.

4.4A Results

The primary motive of this study is to understand the mechano-biological mechanism behind the formation of clots through PA frequency spectral information. Hence, PASR has been applied to blood, an intermediate state of formation of clots and properly formed blood clots in blood. Figure 4.3 illustrates the PA response obtained from blood and clot that delineates distinct disparity in relaxation time that is related to sample elastic property. After obtaining the response,

the spectral information of the signals was obtained for the three samples.

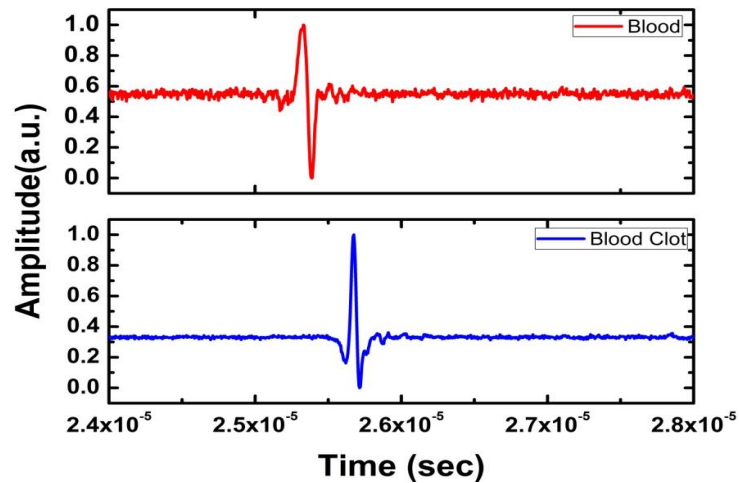


Fig. 4.3. PA time domain signal from blood and blood clot

It is clear from Fig. 4.4 that there is a gradual shift in the frequency response of PA signals when we move from blood to clot formation. The dominant frequency of blood is 5.1 MHz whereas for blood clot it is 11.5 MHz and during the formation of clot, the dominant frequency is at 6.4 MHz as observed from Fig. 4.4. Shifting of dominant frequency depicts an increase in density of the sample and it is a parameter to characterize the clots.

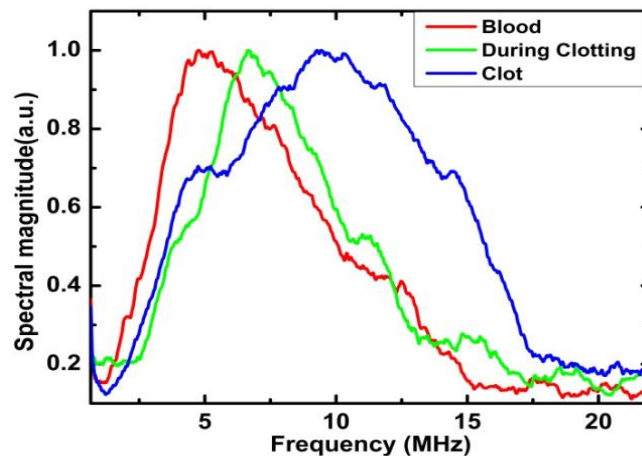


Fig. 4.4. Monitoring of clot formation using dominant frequency of PA spectral response

Chapter 4

To perform statistics, PASR has been applied to 20 samples of blood and formed clots. Figure 4.5 shows that PA spectral response dominant frequency for blood lies between 4.5 to 6 MHz whereas for clot the range is distinctly different i.e. 6.5 to 11 MHz. In addition to change in dominant frequency, total spectral energy was also obtained for the same samples. A change in these spectral parameters can also be used to differentiate sample with identical absorption.

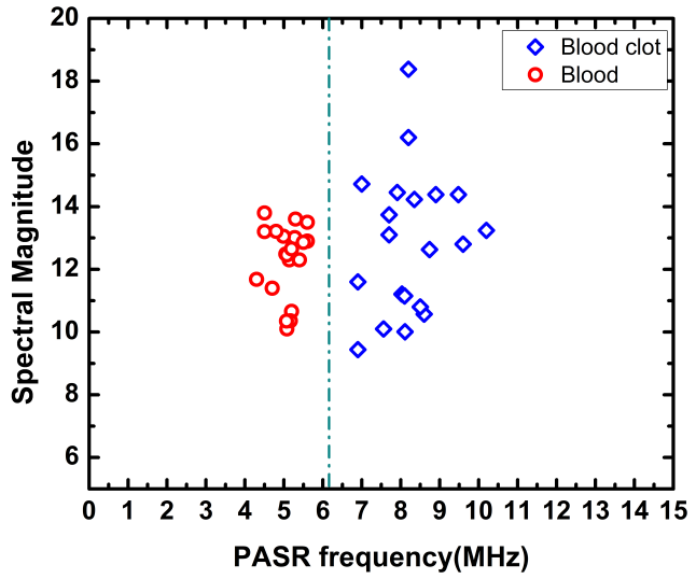


Fig. 4.5. PA spectral response dominant frequency of 20 sets of blood and blood clots

Table 4.1 shows the spectral parameters of blood and blood clot samples. From Table 4.1, it is clear that, in addition to dominant frequency, spectral energy can also be used as a parameter to identify the sample.

Table 4.1. PA frequency spectral parameters of blood and clot samples

Sample	Dominant frequency (MHz)	Energy(*10 ⁵)
Blood	5.14±0.45	1.4±1.7
Clot	7.7±1.3	1.7±0.9

There is a 21% increase in spectral energy of blood clots compared to blood samples. These parameters, which depend on mechanical

properties, show significant change in clots compared to blood and this would pave way to take this technique to in-vivo diagnosis.

4.5A Discussion

A theoretical discussion to understand the relationship between the frequency components and the mechano-biological properties of the sample is provided in this section. Subsequently, the reason for the change in the frequency during clot formation is also discussed.

Basically photoacoustic effect is the generation of sound waves due to absorption of light and the resulting rapid heating of a tissue. Upon light absorption by a nano-second laser pulse, a time-scale significantly lower than the thermal and stress confinement of the tissue, there is a localized temperature increase [33]. This temperature increase induces a transient pressure rise and the tissue undergoes thermoelastic expansion. The initial pressure rise depends on thermal expansion and the photoacoustic source can be treated as a strain source [35]. In other words, the variation of the elastic modulus of the irradiated tissue is related to the light induced strain source. Subsequently, in an elastic medium like tissues, the change in spatially varying pressure induces acoustic waves with a wide range of frequencies at the irradiated spots. Further these waves propagate through the tissue and the medium through momentum transfer. As mentioned in Chapter 2, the wave can be denoted by Eq.4.1. below [203].

$$\nabla^2 p(r,t) - \frac{d}{K} \frac{\partial^2}{\partial t^2} p(r,t) = -\frac{\beta}{C_p} \frac{\partial}{\partial t} H(r,t) \quad (4.1)$$

where $p(r,t)$ is the acoustic pressure, d is the density, C_p is the specific heat, β is the isobaric constant, K is the bulk modulus and $H(r,t)$ represents the source term which is related to the optical irradiance onto the sample due to the pulsed laser.

As detailed in Chapter 2, the PA response amplitude is related to the absorption coefficient of the tissue which has been extensively

Chapter 4

studied [25], [204]. The other two parameters such as width (τ) and relaxation time (χ) are related to mechanobiological property of the sample that affects the frequency spectrum of PA time domain signal. Some studies are performed to extract sample's mechanobiological properties from relaxation time of the PA time domain signal using models (for example Levenberg-Marquardt algorithm) [205], [206]. However this model fitting approach is limited to tissue mimicking phantoms and would the model need to be more complex for real tissues due to complicated tissue structure. Hence, an alternative approach of exploring the frequency content is attempted in this paper. The following equations provide a theoretical background on how the spectral information is related to the mechanical properties of the tissues.

The frequency spectrum of a PA response can be obtained by applying Fourier Transform to PA response. Therefore if we apply Fourier Transform, the pressure wave can be denoted as

$$P(r, \omega) = \int_{-\infty}^{+\infty} p(r, t) \exp(-i\omega t) dt \quad (4.2)$$

After taking Fourier transform, the Fourier transformed photoacoustic equation would become

$$\nabla^2 P(r, \omega) + \frac{K_0}{K} k_0^2 P(r, \omega) = i \frac{k_0 \beta}{C_p} V_s \psi(r) \quad (4.3)$$

where k_0 is the wave number, V_s - sound speed, ψ is product of optical absorption coefficient and photon density ($\psi = \mu_a * \varphi$)

Wave number (k_0) is denoted by

$$k_0 = \frac{\omega}{V_s} \quad (4.4)$$

where ω is angular frequency. It is clear from this equation that sound speed and frequency are proportional. Since sound speed can depict the density and elasticity of the sample, changes in the mechano-biological

properties of the sample can significantly contribute to the photoacoustic waves. Therefore, spectral information of photoacoustic waves depicts the mechanobiological properties of the sample.

The following statements discuss the biological progress during the formation of clots from blood. In case of blood and blood clot there is a distinct change in elastic property. During injury or diseased condition, activated platelets convert prothrombin into thrombin. Subsequently, thrombin initiates the formation of fibrin strands that forms a mesh like solid structure for clot [12], [24]. This gradually increases the density of blood which leads to clot formation thereby increasing the sound speed compared to blood. The simulation study illustrated Chapter 3 (in Fig. 3.19) proves that enhancement in density and sound speed causes increase in dominant frequency; which correlates with experimental results and theoretical analysis. There is also an increase in spectral energy between blood and blood clots. The number of absorbers (red blood cells) within the illuminated region would have increased due to clot formation. Hence the PASR shows an increase in energy.

Section-4B

In this section, FFT based PASR technique is applied for detection of early stage Pneumonia. The experiments were performed on formalin fixed goat lungs in an in-vitro study. PA frequency spectral parameters obtained from different part of the goat lungs is analysed and compared with standard histopathology for correlation.

4.1B Motivation and hypothesis

Pneumonia is one of the most common diseases recorded worldwide and is more prevalent in developing countries [208]–[210]. Particularly, deaths caused due to pneumonia among children under the age of five are alarming [208], [211]. Non-invasive and early stage diagnosis of Pneumonia is pragmatic to control the mortality. The conventional non-invasive diagnostic tools available for Pneumonia

Chapter 4

diagnosis are X-Ray and CT scan. Among these techniques, X-Ray is used for primary detection whereas CT is considered as golden standard for Pneumonia diagnosis [212]. Despite extensive use of these techniques, it exhibits certain limitations which are detailed as follows [213]:

- The techniques suffer from ionisation radiation. Hence these are not applicable for young age group patients.
- These technique unable to provide early stage diagnosis.

The only possible way to detect pneumonia in early stages is to understand the etiology of the disease which is possible through histopathology [214]. Histopathology of a lung would provide information on the blood vessels in the alveoli which is an important factor for detection at the consolidation as well as red hepatisation level. However, histopathological results are available only after removal of tissues, invasively. That is not only inconvenient for the patients but also hinder continuous monitoring. However pathological information obtained from histology is very important for early stage diagnosis. Hence obtaining histopathological information of the lung in a noninvasive manner would lead to detection of pneumonia at an early stage. The solution for early detection of pneumonia would be to obtain pathological information preferably in a non-invasive manner and perform continuous monitoring.

Therefore, Photoacoustic spectral response is proposed as real-time, tissue elasticity based quantitative diagnostic tool for early stage Pneumonia detection. Since PA response contains elasticity information about sample, it is utilised for early detection of Pneumonia.

4.2B General introduction

4.2B.1 About Pneumonia

Pneumonia is inflammation and consolidation of lung tissues due to infection, inhalation of foreign particles or irradiation [215]. Pneumonia can be developed through different micro organism such as fungi, virus. However the primary reason of this disease is a particular species of bacteria, mainly Streptococcus and Mycoplasma. Based on the extent of the lesion, Pneumonia can be classified as the following types [216]:

- Lobular (a lobe segment is affected)
- Lobar (an entire lobe is affected)
- Bronchopneumonia (Affects bronchiole and adjacent alveoli)
- Interstitial (Primarily alveolar wall)

Development of Pneumonia usually occurs in four stages which are as follows [217]:

- *Congestion*: In the first stage (during 1-2 days) the affected lung parenchyma is consolidated i.e. alveoli is filled with inflammatory fluid. The alveolar lumen contains serous exudates, bacteria and rare leucocytes.
- *Red hepatisation*: This is the second stage of the disease that occurs after 2 to 3 days of congestion. During this stage, the lung shows resemblance with liver and become hyperaemic. The alveolar capillaries are engorged with blood. Subsequently the alveoli also flooded with fibrinous exudates. Microscopic analysis confirms presence of erythrocytes, neutrophils, desquamated epithelial cells etc. in the alveoli.
- *Grey hepatisation*: The third stage of Pneumonia i.e. grey hepatisation appears after 2 to 3 days of red hepatisation. This is avascular stage in which the lung filled with fibrinopurulent exudates, fibrinopurulent exudates,

Chapter 4

disintegration of red cells, and hemosiderin. The alveolar capillaries are compressed due to the pressure of the exudates. Migration of leucocytes into the congested alveoli is very common during this stage.

- *Resolution*: This stage is identified by the restoration of pulmonary architecture. The alveolar space is captured by a large number of macrophages that is followed by phagocytises of bacteria loaded leucocytes.

From the previous section, it is evident that blood vessels in the alveoli of the lung engorged with blood and other body fluid during progression of Pneumonia. This directly affects the density of that area, thereby changing the elasticity of the tissue. Elasticity changes in the tissue are highly reflected in the spectral information of the photoacoustic signal. Hence obtaining the spectral information through PASR technique would act as a signature of the tissue elastic property. The spectral information of the photoacoustic response and relate to elasticity of the tissue is investigated, thereby normal lung tissues from pneumonia was distinguished. Subsequently, PASR technique is applied onto formalin fixed goat lungs for early stage of Pneumonia i.e. red hepatisation diagnosis. Obtained PASR results from goat lungs were compared with standard histopathology.

4.3B Materials and methods

4.3B.1 Biological sample preparation

For this study, formalin fixed pneumonia affected goat lungs were cut into 1 cm × 1 cm pieces of lung tissues from two different animals was collected. Subsequently each of the samples was placed in the water tank after wrapping it with parafilm. PA time domain signals from four different locations of the sample (total eight locations from two different lung tissues) were obtained. The PA response obtained from the different sample positions were segregated into three groups, namely Group 1, Group 2 and control which is illustrated in Table 4.2. Group 1 contains oedematous fluid along with air Group2 is infected

with red hepatisation and the control part is normal lung tissue. PA responses were acquired from these three regions of the lungs. In order to obtain histological sections, 10 micrometer thin slices of the sample from the lung tissue were cut. Then the slices were stained with haematoxylin and eosin dye. Later microscopic images were taken by bright field microscope.

Table 4.2. Main compositions of different regions of goat lung

Sample name	Composition of alveoli	Tissue pathology
Group 1	Oedematous fluid along with air	Lung inflammation
Group 2	Excess of red blood cells	Red hepatisation
Control	Air	Normal lung

4.3B.2 PASR experiment

For this study, PASR experimental setup for solid sample was utilised as shown in Fig. 3.2. The sample was placed in a water tank which was irradiated with nano-second laser (Nd:YAG, 532nm, 5ns) with fluence of 10 mJ/cm². Generated PA response was acquired by an unfocused ultrasonic sensor with centre frequency 3.5 MHz. Since high frequency acoustic signals are more prone to attenuation in soft tissues, lower centre frequency (3.5 MHz) compared to blood (20 MHz) was used for the experiment. Acquired PA response was stored in computer after 200 time averaging.

4.3B.3 Frequency spectrum analysis of PA response

In order to extract quantitative pathological information of the sample, Fast Fourier Transform (FFT) of PA signal was performed. The key spectral features such as dominant frequency, total spectral energy and variance were obtained since these parameters depict the change in tissue elasticity i.e. density and sound speed. The dominant frequency

Chapter 4

was obtained from the PA frequency spectrum using custom built MATLAB program. Subsequently spectral energy and variance were calculated from Eq. 4.5. and Eq. 4.6. which are given as follows [218]

$$E = \sum_{n=-\infty}^{+\infty} [R(n)^2] \quad (4.5)$$

where, E is energy, R(n) is the frequency spectrum of PA signal

$$V = \left(\frac{1}{N-1}\right) \sum_{n=1}^N [R_n - \mu_m]^2 \quad (4.6)$$

$$\mu_m = \left(\frac{1}{N}\right) \sum_{n=1}^N (R_n) \quad (4.7)$$

where V is variance, R represents the frequency spectrum of PA signal, μ_m is mean of R , N is number of data in the set

4.3B.4 Histology of lung tissues

In order to obtain histological sections, 10 micrometer thin slices of the sample from the lung tissue were cut. Then the slices were stained with haematoxylin and eosin dye [219]. Later microscopic images were taken using bright field microscope. The protocol of histology is detailed in Appendix II.

4.4B Results

It is clear from Chapter 3, PA spectral information can reflect the density changes in the tissues. In this study, the diagnosis of early stage of pneumonia was investigated using PASR technique. Figure 4.6(a) and 4.6(b) show PA response and PASR spectrum of one of the results each from Group1, Group 2 and Control. The dominant frequency for Group 1 is 2.82 MHz whereas for Group 2 is 2.27 MHz and normal lung tissue exhibits dominant frequency around 1.55 MHz. Other parameters such as total spectral energy, variance etc. also show more than two fold increase in Group 1 compared to Group 2 as

illustrated in Table 4.3. In order to verify the pathology of the set two groups, histopathology of the tissue was performed and the image is shown in Fig. 4.7. The samples points of Group 1 are shown in the histopathology (encircled in green in Fig. 4.7) which clearly exhibit oedematous fluid along with air. In contrast, the portion belonging to Group 2 (encircled in yellow in Fig. 4.7) shows the presence of excess of inflammatory cells which is the stage of red hepatisation.

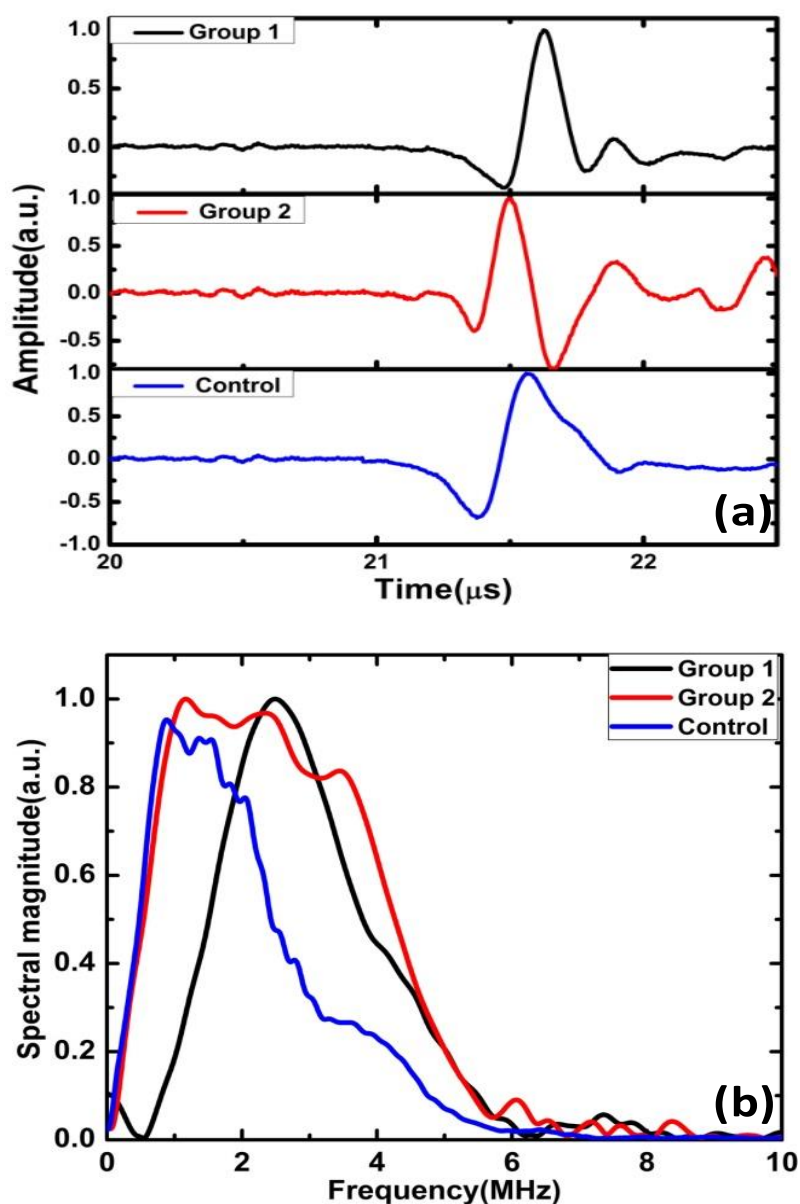


Fig. 4.6. (a) PA response and (b) Spectral information of control, Group 1 and Group 2 goat lungs

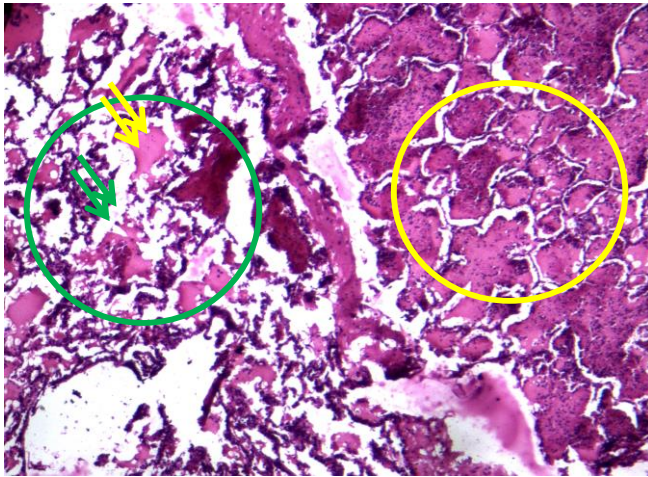


Fig. 4.7. Histopathology of Pneumonia affected goat lung in which green circle shows Group 1, yellow circle indicates Group 2, yellow arrows show the oedematous fluid and green arrows indicate the air

Table 4.3. PA frequency spectral parameters of goat lungs

Sample	Dominant frequency (MHz)	Energy (*10 ⁵)	Variance
Group 1	2.82±0.3	6.8±0.7	48.5±5.1
Group 2	2.27±0.09	3.01±0.3	22.2±2.7
Control	1.5±0.5	5.5±0.6	38±4.2

Therefore PASR technique is capable of differentiating red hepatisation from control in quantitative manner.

4.5B Discussion

The main motivation of this study is to detect early stage of pneumonia through pathological information of tissue as well as continuous monitoring. In order to understand tissue pathology, investigating tissue mechanobiological property i.e. elastic property is essential. It is well known from literature that tissue elastic property is related to density and sound speed of the sample as illustrated in Eq. 4.8. Since solid tissues are different from blood, the PA governing

equation is also includes approximations due to change in mechanical property.

Modelling the viscid point object irradiated by a laser pulse, the generation of photoacoustic wave followed by subsequent propagation of the same wave can be expressed as [220]

$$\frac{\partial^2}{\partial t^2} p(t) + a^2 \frac{\xi + \frac{4}{3}\eta_e}{d} \frac{\partial}{\partial t} p(r,t) + a^2 V_s^2 p(t) = \Gamma \frac{\partial H(t)}{\partial t} \quad (4.8)$$

where a is the propagation phase constant, d is the tissue density, ξ is the bulk viscosity, η_e is the shear viscosity and V_s is the acoustic velocity of the tissue. Γ is the Gruneisen constant expressed as $\Gamma = \frac{\beta V_s^2}{C_p}$ where β is the thermal expansion coefficient and C_p is constant pressure heat capacity per unit mass. $H(t)$ is the heating function of laser irradiation. The right hand side of Eq. 4.8 is the source term for the wave equation generated by the laser pulse heating and left side denotes the propagation term.

In all the conventional models, on delta heating, an initial pressure p_0 which is constant across the entire heated sphere is generated. This initial pressure is divided into equal parts of spherical wave. One wave moves outward and another move inward, thereby creating a "N" shaped PA wave generation. This signal is then propagated through the medium to reach the sensor. This model is sufficient to describe tomography applications as the amplitude of the PA wave is used for imaging applications. However, in real situations, the optical absorber behaves as an elastic body with damped oscillations, which is not accounted for conventional models. The PA damped oscillation, induced by the viscosity of the sample, is used to characterize the mechanical properties of the sample. A detailed analysis of the generation and subsequent propagation of PA wave is studied by Fei Gao et. al. [220], which is very apt to the experimental results obtained in this study. The following theoretical discussion

Chapter 4

would provide the relationship between PA wave generation, considering the absorber to be an elastic optical absorber. The PA equation is compared with a spring-mass damper system that can provide an intuitive perspective of the PA generation. The spring-mass damper system, shown in Fig. 4.8, can be expressed as [221]

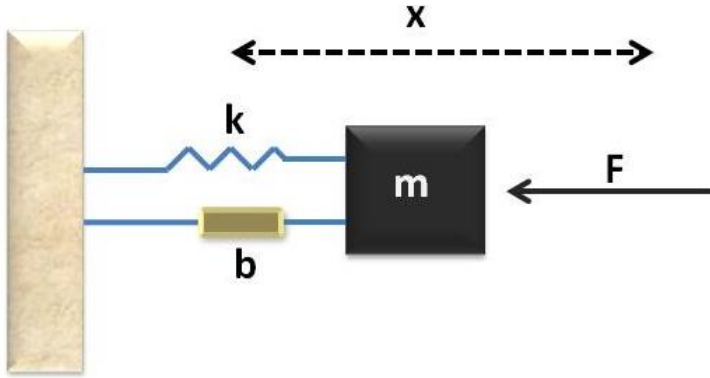


Fig. 4.8. Schematic of spring-mass damper system

$$\frac{\partial^2}{\partial t^2} x(t) + \frac{b}{m} \frac{\partial}{\partial t} x(t) + \frac{k}{m} x(t) = \frac{F(t)}{m} \quad (4.9)$$

where m , k and b are the mass, spring constant and damping coefficient respectively. The force acting on the mass is $F(t)$ which produces a displacement of $x(t)$. Since Eq. 4.9 is similar to Eq. 4.8, they can be compared and the PA wave parameters can be equated to m , k and b . While the laser pulse width is short enough to obey thermal and stress confinements [33],[57], the force term $F(t)$ can be simplified to be 0, and the spring-mass damper system would reduce to a typical second order system. Since the PA effect expands and contracts caused by transient laser-induced heating, the generated PA wave would normally follow an underdamped oscillating system with both positive and negative peaks. Solving Eq. 4.9 for an underdamped system and then substituting the parameters of PA wave from Eq. 4.8 would yield the generated PA oscillating signal as

$$p(t) = A_d e^{-\frac{1}{2}a^2 \frac{\xi + \frac{4}{3}\eta}{d} t} \cos \left(\sqrt{a^2 V_s^2 - \left(\frac{1}{2}a^2 \frac{\xi + \frac{4}{3}\eta}{d}\right)^2} t - \frac{\pi}{2} \right) \quad (4.10)$$

where the constant A_d is determined by the initial condition of the system (uniform optical illumination in the region of interest). Therefore, instead of having a constant pressure wave generation (p_0), the initial pressure would be a time-varying pressure source of Eq. 4.10 with the appropriate physical properties, thus reproducing the real experimental situation. The pressure wave generated would have two terms; a sinusoidal term and an exponential decaying term as shown in Fig. 4.9.

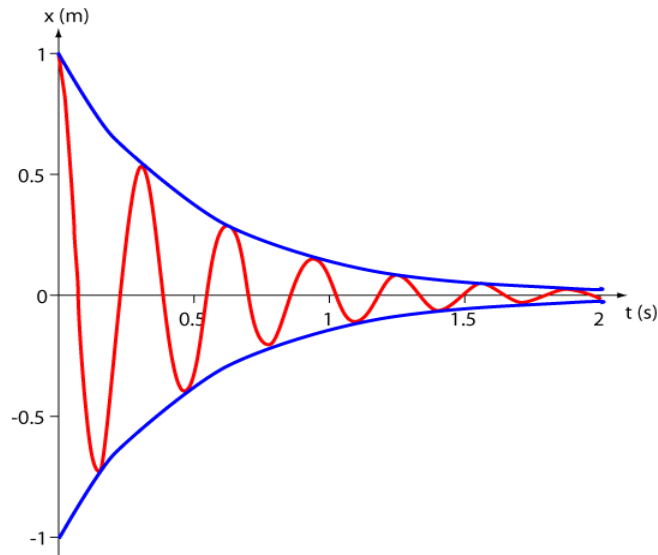


Fig. 4.9. Underdamped oscillatory behaviour

These two terms contain the parameters that are of the sample and hence the generated pressure wave would be a true signature of the sample. In order to quantitatively utilize this PA wave, the spectral information has been extracted from these time domain signals in our experiments. Eq. 4.10 can be simplified as follows:

$$p(t) = A_d e^{-\alpha t} \sin(\omega_0 t) u(t) \quad (4.11)$$

Chapter 4

$$\text{Where } \alpha = -\frac{1}{2}a^2 \frac{\xi + \frac{4}{3}\eta}{d} \text{ and } \omega_0 = \sqrt{a^2c^2 - \left(\frac{1}{2}a^2 \frac{\xi + \frac{4}{3}\eta}{d}\right)^2} \text{ and}$$

$u(t)$ is a unit step function. Applying Fourier transform to Eq. 4.11 would yield:

$$P(\omega) = A_d \frac{\omega_0}{\omega_0^2 + (\alpha + j\omega)^2} \quad (4.12)$$

It is clear from Eq. 4.12 that the frequency components of the generated PA wave are related to viscosity, density and other mechanical properties of the sample. Assuming a lossless medium with negligible impedance-mismatch, the transmission of this generated PA wave would take place as per the wave equation. The theoretical understanding was subsequently verified with experimental study on formalin fixed goat lung.

As described in Chapter 3, the tissue mimicking phantom study clearly delineates that increase in gelatine concentration enhances density, which in turn increases the sound speed in the sample. Since sound speed increases, it shifts the dominant frequency to higher value. The observation was further verified with simulation study performed using K-Wave toolbox in MATLAB as detailed in Chapter 3. Now to understand the reason behind the obtained results for goat lung study, the effect of spectral parameters on tissue pathology need to be investigated. Usually a normal lung contains enormous number of air pockets or alveoli which is responsible for gas exchange. Therefore normal lung contains high amount of air and the alveoli have fine blood vessels to perform gas exchange. But during Pneumonia, lung fills with fluids like blood, oedematous fluid etc. In case of red hepatisation, excess of blood fill up the affected area which consists of inflammatory cells to prevent the infection [222]. Due to increase in blood in alveoli blood vessels during red hepatisation, density increases in affected area. This is clearly reflected in PASR dominant

frequency increase from 1.5 MHz to 2.27 MHz. The results correlate well with tissue phantom study. Interestingly it is observed that dominant frequency of Group 1 is 2.8 MHz which is higher compared to Group 2. This may be due to the presence of heavy proteins like fibrinogen in oedematous fluid which enhances its density compared to blood [223]. In addition to dominant frequency, energy and variance also have a significant change between Group 2 and Group 1. Since Group 2 i.e. red hepatisation consists of high population of red blood cells, it increases scattering of acoustic signal thereby reduce the energy as well as variance [224]. Therefore it can be stated that PASR exhibits significant sensitivity towards tissue properties and hence could be one potential technique to relate the diagnosis of many diseases to pathology.

4.2 Summary

Subsequent to development of sample elasticity based PASR system, the applicability as a disease diagnostic tool was verified by applying the developed technique to differentiate normal and pathological samples. As a first step, solely frequency based signal processing tool FFT is employed to study blood and clot as well as early stage of Pneumonia.

FFT-PASR technique has been explored to understand the mechanism of formation of clots and also differentiate blood clots from blood. This study has shown that during the formation of clots (transition from blood), there is a significant increase in the spectral frequency, particularly the dominant frequency of the response shifting by 1.3 MHz during the middle of clot formation and subsequently by approximately 5 MHz after the complete formation of clots. Since shifting of frequency is related to elasticity of the clot, the proposed technique can monitor the mechano-biology of clot formation, a necessary study for many blood circulation related disorders.

Subsequently, the study has been extended to differentiate blood clots from blood through different parameters extracted from the

Chapter 4

PA spectral response. Significant changes in dominant frequency and spectral energy could clearly differentiate blood clots from blood. Since the focus was on spectral parameters rather than the amplitude of the PA signal, the accuracy of the technique in differentiating clots would hold good even in the presence of blood and other components. Therefore, a real-time, quantitative differentiation of blood clots has been achieved. This feature can be potentially applied in monitoring assays that could reveal biophysical understanding of blood clots and also continuous monitoring of clot formation during any treatments as well. For example, analyzing the mechanical properties of clots during any thrombi related disorders would be very important for effective treatment of patients and would find applications in deep vein thrombosis, myocardial infarction, ischemia etc.

The other application of FFT-PASR technique is detection of early stage of Pneumonia through quantitative assessment of pathological information. On applying FFT-PASR to different areas of Pneumonia affected goat lungs, it was obtained that oedematous fluid filled part (Group 1) as well as red hepatisation (Group 2) affected part exhibits higher dominant frequency compared to control. Therefore one can easily differentiate normal from pathological lung. In addition, the two pathological areas Group 1 and Group 2 show distinct change in spectral parameters and this helps to understand the pathology of the lung. The PASR results were compared with standard histopathology which also confirms presence of two pathological regions namely red hepatisation and heavy protein rich oedematous fluid in the tissue sample.

Therefore it is evident that PASR can provide high sensitivity in detection besides providing an understanding the pathology of the biological tissues. Hence, PASR technique has a good potential to find a wide applications in thrombotic disease diagnosis as well as early Pneumonia diagnosis in a non-invasive manner.

Chapter 5

Application of time-frequency based PASR technique for quantitative assessment of human breast masses.

*“Imagination is more important than knowledge. Knowledge is limited.
Imagination encircles the world”-Einstein*

5.1 Introduction

Chapter 4 details two major applications of FFT based PASR technique for blood and clot diagnosis and early stage Pneumonia detection. It focuses solely on the frequency based PASR technique that utilises spectral parameters such as dominant frequency and energy for quantitative differentiation of normal and pathological tissues. While moving onto complex tissues, depending solely frequency based technique such as FFT would face difficulty in providing the individual frequency components or mono-frequency components present in the signal due to spectral leakage [170]. The mono-frequency components act as the signature for differentiating complex tissues like breast masses [118], [225]. In addition, the individual frequency components are associated with tissue pathology which is useful for understanding stage/grade of the disease as well as early stage diagnosis . Therefore it is highly desirable to extract the individual frequency components. Hence advanced time-frequency based signal processing tools are employed for qualitative and quantitative differentiation of human breast masses which is the major content of this chapter.

A comparison with standard technique like histopathology would provide the efficiency of the technique. Since histopathology is the golden standard technique for breast cancer diagnosis through obtaining tissue pathological information [226], comparison of PASR and histopathology would be pragmatic to get additional information regarding tissue pathology. This would definitely help in better understanding of the disease mechanism thereby enhances chances of successful diagnosis.

The main objective of this chapter is to differentiate human breast masses into three main categories normal, benign and malignant masses in qualitative as well as quantitative manner and correlating with tissue pathology. In this regard, two time-frequency based signal

Chapter 5

processing tools namely Wigner-ville distribution (WVD) and Empirical Wavelet Transform (EWT) are employed. The WVD based PASR technique utilises individual frequency components and its energy density for qualitative differentiation. This is applied for real-time, non-invasive, qualitative differentiation of normal from malignant breast masses. Subsequently, for quantitative classification solid breast masses such as benign and malignant tumours, EWT based PASR is employed. This utilises time domain as well as frequency domain spectral features of mono-frequency components for classification. Besides, these features provide significant information regarding tissue pathology that would provide better insight of the disease. The obtained PASR results are compared with standard histopathology to verify the efficiency of the developed technique.

5.2 Motivation

Nowadays, breast cancer is a significant cause of morbidity and mortality for women worldwide [227], [228]. Defining breast cancer, it is uncontrolled proliferation of breast cells that forms malignant tumours. It has been observed that solid tumours detected prior to menopause are mostly benign. However rate of malignant breast tumour increases exponentially after menopause [229], [230]. There is also a probability of transformation of benign tumours into malignant. Hence, diagnosis of symptomatic breast masses is prevalent to control the mortality rate. Methods available clinically are as follows [231]:

- i. Clinical examination performed by the doctors to identify the tumour location, size and other characteristics.
- ii. Symptomatic breast masses are usually subjected to radio-imaging techniques such as X-ray mammography and ultrasonography. These techniques can identify the suspicious area in the breast
- iii. Based on these images and further investigations, the suspected cases need to undergo biopsy which is a golden standard for the detection of tumours

Depending upon results of biopsy, the breast masses are classified into three categories, namely normal, benign and malignant. Recently, conventional imaging techniques (X-Ray, US) are employed to detect breast malignancy. But these techniques either produce false negative result or lack in specificity [232]–[234], particularly if the breast is very dense, which is typical in humans. Thus there is no option for the clinicians to diagnose breast tumours other than biopsy. The primary problem of biopsy is it is an invasive technique. Although small percentage of the solid breast masses are identified as malignant, but the patient has to undergo the painful process of biopsy. With an increase in the number of patients with breast masses over the recent years, there is a necessity to look for diagnostic techniques that can non-invasively differentiate the breast masses at a high accuracy. This would help in reducing the number of patients undergoing biopsy.

As mentioned in earlier chapters, PASR technique is highly sensitive towards change in tissue elasticity. Since human breast masses exhibit significant change in elasticity, application of PASR technique would be pragmatic for breast masses classification. Since different frequency components serve as a signature of the tissue elastic property, it is very important to extract individual frequency components precisely for breast masses classification. The human breast masses are dense tissues which consist of different types of tissues as detailed in previous section. The population of these tissue types indicate tissue pathology. If the tissue is affected by a disease, the pathology of the tissues change and it becomes even more complicated. Differentiating these types of complicated tissues with solely frequency based technique FFT would be difficult due to following reasons [170], [171]:

- PA signals are non-stationary in nature. Applying FFT to non-stationary signals would provide spectral leakage i.e. presence of insignificant components in the frequency spectrum

Chapter 5

- FFT is a rigid technique which utilises predefined functions independent of processed signal. However solid breast masses are subjected to unpredictable changes in pathology. Hence utilising “rigid” techniques like FFT would not provide individual frequency components required for breast masses classification.

Due to these above mentioned reasons, advanced signal processing tools are required as they are capable of providing individual frequency components along with time information. In addition, adaptive signal processing techniques employs information of processed signals for development of the signal processing algorithm. Thus it can deal with the unpredictable changes in the signal [235], [236]. Due to this reason, utilising time-frequency based signal processing tools would be more efficient to classify complex breast masses as it can provide individual frequency components that would provide information regarding tissue pathology. Consequently adaptive technique would be more pragmatic to handle insignificant changes in solid breast masses.

5.3 Introduction to breast tumours

Breast cancer caused due to erratic growth and proliferation of breast cells (epithelial cells) that induce solid lump. Women with obesity, lack of physical exercise, alcohol consumption, exposure to ionising radiation, family history of breast cancer are prone to develop breast cancer [237]. Majority of breast lump detected before menopause is found to be benign or non-cancerous. However the rate of developing malignant lump is higher in post-menopausal period.

5.3.1 About human breasts

Breast is composed of three primary tissues namely fibrous (connective) tissues, fatty tissues and glandular tissues. The tissues are strongly connected by the muscles which serve as the base. The anatomical structure of breast is illustrated in Fig. 5.1.

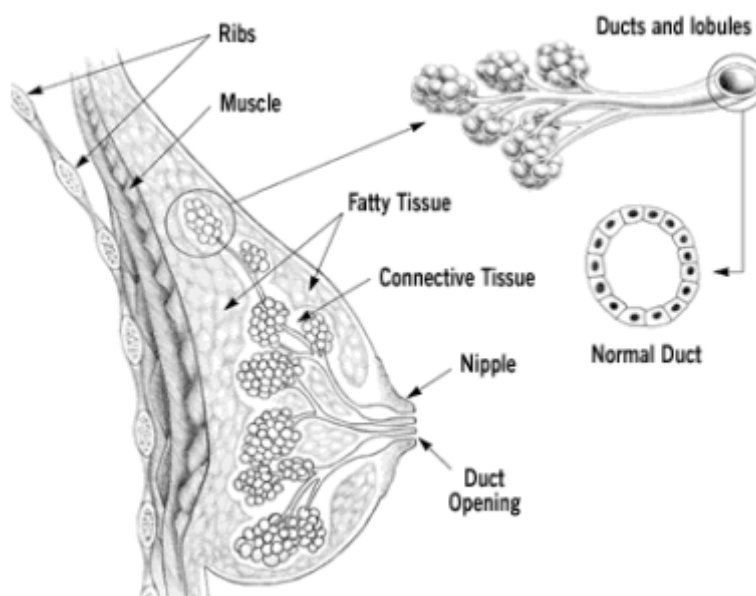


Fig. 5.1. Anatomical structure of human breast. The figure is taken from “http://www.breastcancertreatment.in/breast_anatomy.htm”

It can be clearly observed from Fig. 5.1, the main function of fibrous tissues are to support the fatty and glandular tissues. Fibrous tissues are mainly responsible for the shape of the breast. With aging, the fibrous tissues are replaced by the fatty tissues that cause change in shape and texture of breast. The fibrous tissues mostly consist of stromal cells and fibres.

The glandular tissues mostly consist of lobules. The main function of these lobules is to produce milk during pregnancy. These are connected to duct which has the opening in nipple. The globular tissues are subjected to hormonal change that often causes tender or lumpy breast.

In addition to mentioned tissues, breast consists of nerves, lymph vessels, lymph nodes and blood vessels. The lymph nodes and vessels, which are part of lymphatic system, are mainly responsible for body immune system. The clusters of lymph nodes are present throughout the body at particular location. The lymph vessels in breast are connected to the lymph nodes situated in armpit. The origin of the

Chapter 5

cancer is mostly in duct, lobe or in lobules which decides the type of the cancer. However the staging of cancer i.e. how far it has spread is decided by examining the lymph nodes. By examining the lymph nodes, progression of the disease is determined.

5.3.2 Type of breast masses

The solid breast tumours are classified into two groups such as benign or non-cancerous and malignant. The primary difference between benign and malignant tumours is malignant tumours are prone to spreading cells to other part of the body known as metastasis whereas benign tissues are self-confined and localised.

5.3.2.1 Benign breast tumours

The most common lesions of breast are represented by fibrocystic changes. In microscopic scale, the fibrocystic changes include epithelial metaplasia, hyperplasia of benign or usual type, adenosis, formation of cyst and fibrosis [238].

- (a) *Apocrine metaplasia*: This is very common in fibrocystic changes. The apocrine cells may form a cyst with clear serous fluid or it may contain blood also. This exhibits mostly mild to moderate and florid epithelial hyperplasia that may later lead to calcification.
- (b) *Sclerosing adenosis*: It is another form of breast proliferation in which a hard, irregular mass is attached to the adjacent structure. It exhibits distorted architecture due to proliferation in epithelial and myoepithelial cells in nearly ducts.
- (c) *Fibroadenoma*: The most common type of benign breast tumour is fibroadenoma that appears as painless, solitary and well defined nodules. Histologically, it exhibits combined proliferation of epithelial and stromal cells which develops pericanalicular and intracanalicular patterns. Some complex fibroadenomas with sclerosing adenosis, epithelial calcification or change in papillary apocrine exhibit 1.6 times higher risk for cancer development compared to normal fibroadenomas.

(d) *Phyllodes tumour*: This type of benign breast lesions is caused due to proliferation of periductal stromal cells of breast. It usually shows fleshy, well circumscribed, bulging masses along with curve structure like leaf or leaf buds. Phyllodes tumours consist of epithelial and stromal cellular components. The type of the tumour (benign or malignant) depends on microscopic features such as mitotic activity, tumour edge infiltration as well as stromal cellularity.

5.3.2.2 Types of malignant tumours

Malignant breast tumours are broadly classified into two types such as ductal breast cancer and lobular breast cancer [239]. These tumours may be in-situ or invasive.

- i. *In situ carcinoma*: This is the earlier stage of cancer which is remains in the developed area. However it has a risk to be converted into invasive carcinoma.
 - a) *Ductal carcinoma in situ (DCIS)*: It is the most common form of in-situ carcinoma that develops in the milk duct. Since it do not have the tendency to be spread in the surrounding tissues, it is not life threatening. However, this can enhance the chance of developing invasive cancer in later stage.
 - b) *Lobular carcinoma in-situ*: In this type, the cancer originates in the lobules, the milk producing glands. Similar to DCIS, it remains confined in the originated area.
- ii. *Invasive carcinoma*: In this type of breast cancer, malignant tissues spread into duct or lobular region of breast. Among all the invasive carcinoma, invasive ductal carcinoma is most common.
 - a) *Invasive ductal carcinoma (IDC)*: The invasive ductal carcinoma or infiltrating ductal carcinoma starts from

milk duct and invade into surrounding tissues. This is very dangerous since it can spread into different parts of the body through blood stream or lymphatic system. The IDC tumours have a distinct irregular border. It is also hard and firm compared to benign tumours. Histopathologically, these tumours exhibit dense population of epithelial cells compared to stromal cells that destroys the regular architecture of normal breast tissues.

- b) *Medullary carcinoma*: This is a rare case of carcinoma in which a distinct boundary is formed in between normal and malignant tissue.
- c) *Mucinous carcinoma*: Mucinous carcinoma is also known as colloid carcinoma. It is caused due to mucous producing malignant cells. The prognosis of mucinous carcinoma is better than common types of carcinoma.

Since fibroadenoma (benign tumour) and IDC (malignant tumour) are most common types of solid breast tumours, in this chapter an attempt is taken for differentiating them with developed PASR technique.

5.4 Qualitative differentiation of normal and malignant breast masses

As a first step toward breast masses differentiation, a time-frequency based signal processing technique Wigner-Ville Distribution (WVD) is applied to the PA response obtained from normal and malignant breast masses. This is a preliminary study to verify whether developed PASR technique is capable of differentiating human breast masses. In this regards, WVD was chosen as it is a time-frequency based technique. The main advantage of this technique is it can provide qualitative information about individual frequency components. Since the PA frequency components are the signature of tissue elasticity, obtaining the mono-frequency components would be pragmatic to differentiate normal to malignant tissues. In addition, WVD provide

the energy density of the frequency components which is related to tissue pathology. Hence WVD based PASR technique is applied to differentiate normal and malignant breast masses.

5.4.1 PASR experiments for normal and malignant tissue diagnosis

Excised breasts from patients are usually kept in buffered formalin which preserves the structural properties of tissues as it is [240]. This process is called tissue fixation and the fixed sample is generally considered as the standard for cancer diagnosis through histopathology [241]. Subsequently these fixed tissues were cut into 1 cm × 1 cm square pieces for PASR experiments. Total eight such samples (normal and malignant) from four different patients were collected with due approval. The samples were wrapped with parafilm before placing into PASR setup to avoid contamination. Since the breast masses are solid samples, PASR experimental setup illustrated in Fig. 3.2. is utilised for this set of experiment. PA response from the tissue samples were obtained by applying second harmonic laser pulses with fluence of 2 mJ/cm². As mentioned in previous chapter, due to high attenuation coefficient of soft tissues, low frequency ultrasound sensor (centre frequency, 3.5 MHz, bandwidth 3.8 MHz) is utilised for this study. In order to verify the consistency of the results, PA responses were acquired from different locations of each tissue sample. Prior to applying WVD on obtained PA responses, all the signals were normalised and background subtracted.

5.4.1.1 Wigner-Ville distribution

Wigner-Ville distribution is a time-frequency analysis technique which is based on the use of autocorrelation function to calculate the power spectrum. Generally to construct an auto correlation function r_{ss} , the signal $s(t)$ is compared with itself in all possible forms of delay and lag as illustrated in Eq. 5.1 [174], [175].

$$r_{ss} = \int s(t)s(t + \tau)dt \tag{5.1}$$

Chapter 5

where τ represents all shifts of the signal. In the standard autocorrelation, time is integrated out of result and r_{ss} is the only function of time lag τ . The difference between standard autocorrelation and WVD is the latter contains time function. Therefore WVD is known as instantaneous autocorrelation function.

$$R_{ss} = s\left(t + \frac{\tau}{2}\right)s^*(t - \tau) \quad (5.2)$$

Where τ is time lag and * represents the complex conjugate of the signal The WV distribution is defined in Eq.5.3

$$W_{ss}(t, \omega) = \frac{1}{2\pi} \int s\left(t + \frac{\tau}{2}\right)s^*(t - \tau)e^{-j\omega\tau} d\tau \quad (5.3)$$

Basically WVD provides time-frequency information of the signal by comparing the signal with its own information at other time and frequencies [175]. Now in order to understand the WVD, a typical PA signal is analysed. The sampling frequency is 200 MHz. After applying WVD to the PA response, time-frequency information of the PA signal is obtained which is shown in contour plot (Fig. 5.2). The frequency components of the signal appear as concentric circles. The colour of the circle represents the energy density of that particular frequency component. In this case there are two concentric circles which indicate presence of two frequency components in the signal. The lower frequency component (0.8 MHz) is highlighted with dotted circle and continuous circle represent the high frequency component (3 MHz). The colour of the circles indicate that the energy density of low frequency component (appears as red) is high compare to high frequency component (appears as yellow). Therefore WVD parameters such as frequency component and energy density can be used for qualitative discrimination of human breast masses.

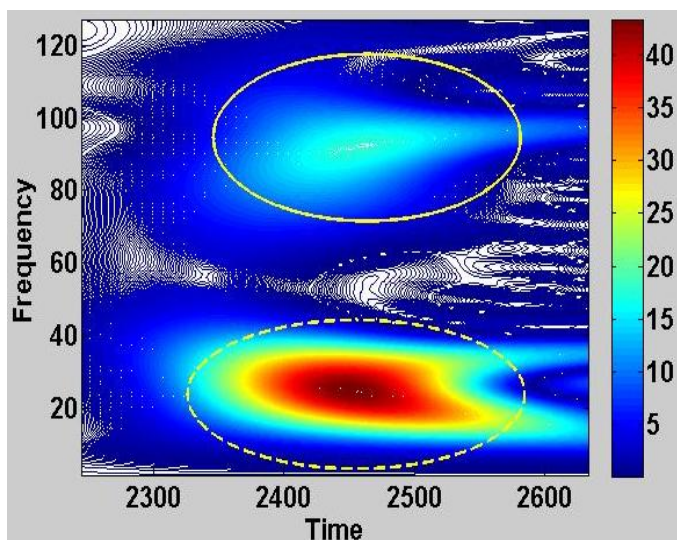


Fig. 5.2. Contour plot of typical PA time domain signal in which dotted circle represent the low frequency component and the other indicate the high frequency component. The conversion factor for Y-axis is $(\text{coordinate position} / 3000) * (F_s/2)$ and X-axis is $((\text{coordinate position} + 5000) / 3000) * (F_s/2)$. F_s is the sampling frequency (200 MHz). The unit of time and frequency is s and MHz respectively

5.4.1.2 Histology study

In order to obtain morphological information about the human breast masses, histopathology was performed. The samples were cut into 10 μm thin slices. Subsequently the slices were stained with haematoxylin-eosin dye. Then the microscopic slides are observed under microscope with 10x magnification.

5.4.2 Results and discussions

In this study, an attempt has been made to develop a tissue elasticity based screening tool for differentiating normal and malignant breast tissues. Hence time-frequency plot of PA response was obtained by applying WVD technique. Figure 5.3 illustrates WVD plots of normal and malignant breast tissues obtained from different patients. The contour plot clearly indicates that there are two major frequency components present in the signal. The low frequency component (~ 0.9 MHz) is evident in both the tissue types whereas a new frequency component i.e. the high frequency component (~ 3 MHz) appears for

Chapter 5

malignant tissue. The energy density of the high frequency component is very low (can be observed from colour bar) for normal tissue compared to malignant. This significant change in energy density of high frequency component clearly discriminates malignant from normal breast tissue. It is well known from literatures that malignant tissues are stiffer as compared to normal. The change in elasticity between normal and malignant tissue can be understood from histopathology. Figure 5.2 illustrates histopathology of normal and malignant breast tissue which clearly shows that normal breast tissue contains large amount of stromal cells which makes the normal breast tissue soft and elastic in nature whereas malignant tissue exhibits uncontrolled proliferation of epithelial cells which have an implicit property to bind together and form dense layer of cells. This enhances stiffness of the malignant breast tissues [242], [243].

Now to understand the PA time-frequency information, obtained from WVD technique the pathological understanding would play an important role. It is very well known from literature that biological tissues are viscoelastic. Therefore higher frequency components of acoustic signals get more attenuated in soft (more elastic) tissues. Thus in normal breast tissues the lower frequency component exhibits very high energy density whereas the high frequency component delineates very low energy density as observed from Fig 5.3. In the case of malignant tissues, enhanced stiffness causes shoot up in energy density of high frequency component [244]. As illustrated in Fig. 5.3 the results are consistent for four different patients of different age groups which prove the sensitivity of the developed technique. Thus it can be stated that WVD based PASR technique not only differentiate normal and malignant breast tissue but also provides information about tissue pathology.

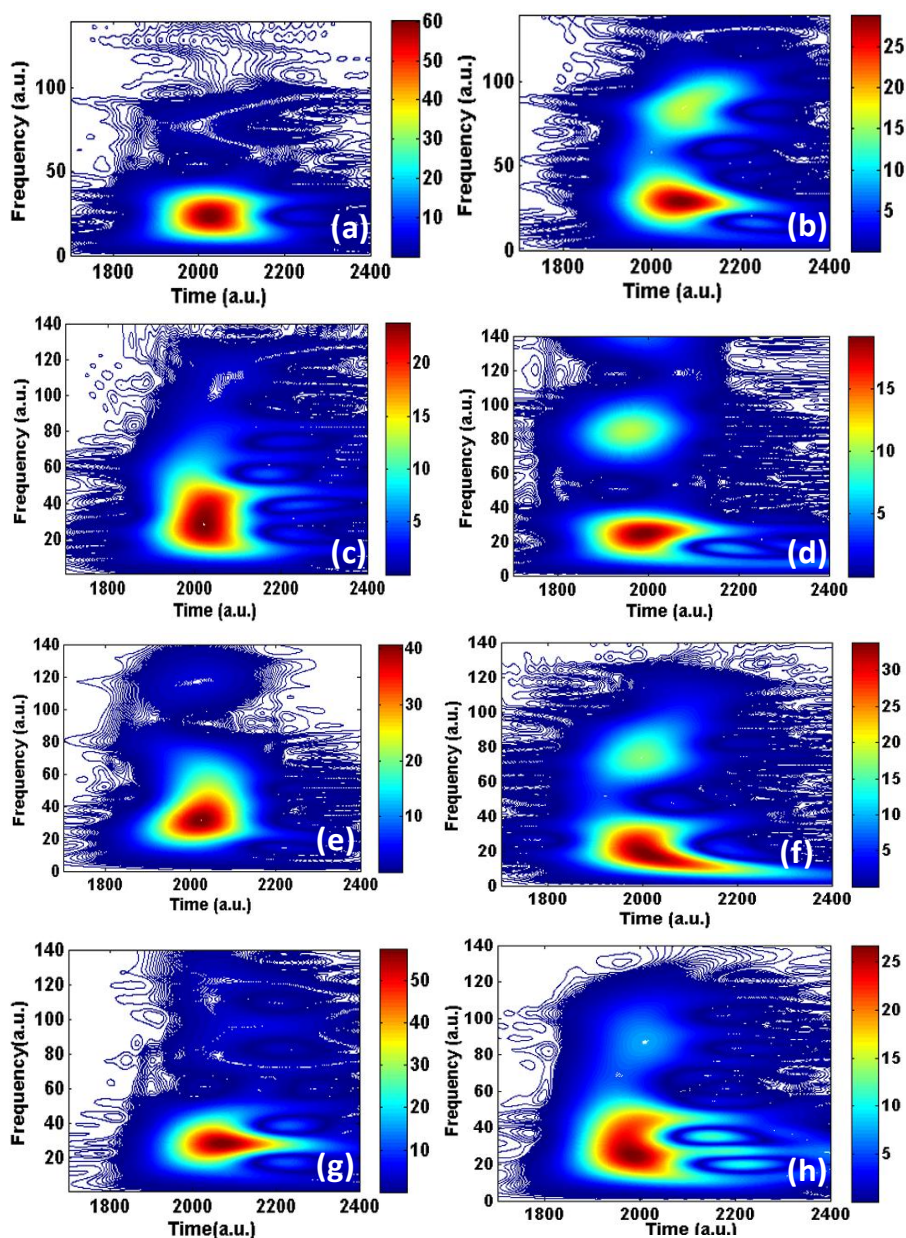


Fig. 5.3. WVD contour plot of human breast masses from different patient. Figures 4(a), (c), (e), (g) illustrate normal and figures 4(b),(d), (f), (h) illustrate malignant breast tissues. The conversion factor for Y-axis is $(\text{coordinate position} / 3000) * (F_s/2)$ and X-axis is $((\text{coordinate position} + 5000) / 3000) * (F_s/2)$. F_s is the sampling frequency (200 MHz). The unit of time and frequency is s and MHz respectively

5.5. Quantitative breast masses classification by EWT-PASR technique

Although WVD based PASR differentiates normal from malignant breast tissue, WVD could not distinguish benign and malignant tissue due to less significant change in biophysical property

between the two solid tumours [42]. Moreover this technique is qualitative. In order to perform quantitative classification of the breast masses, an advanced time-frequency technique EWT is employed. As mentioned earlier, individual frequency components serve as signature of tissue property [245]. Hence precise extraction of mono-frequency components is necessary to obtain tissue pathological information. Being an adaptive technique, EWT is capable of handling the variation in the spectrum. This is an added advantage over FFT as well as WVD. Let's take an example how EWT extracts mono-frequency components. Fig. 5.4(a) shows the Fourier spectrum of a typical PA signal with two different peaks. However, it becomes difficult to distinguish these two peaks (corresponds to different frequency components) from Fig. 5.4(a). In order to divide this spectral information into different frequency mono-components, an adaptive wavelet filter bank is required. Figure 5.4(b) shows the boundary segmented frequency components using a technique called EWT.

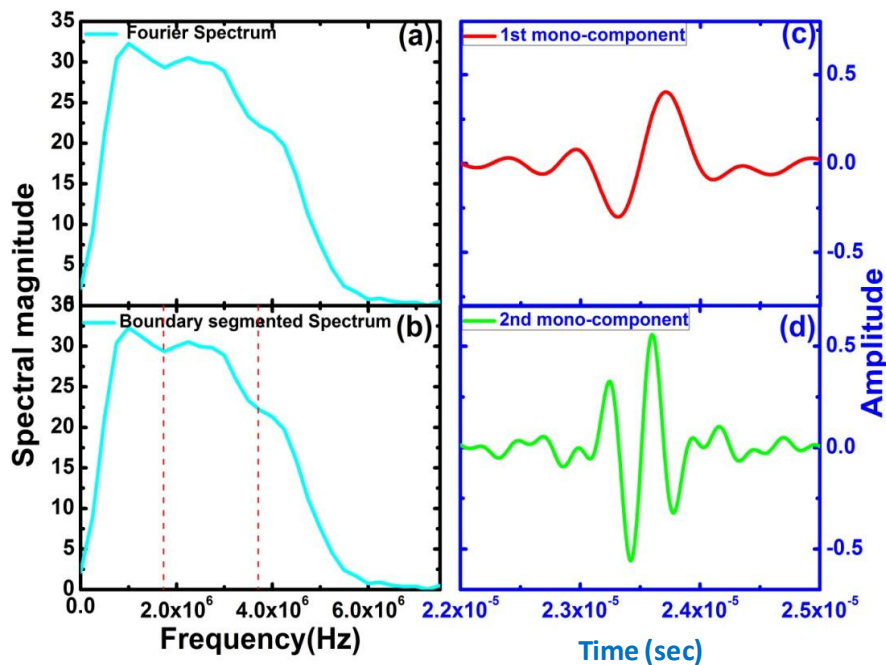


Fig. 5.4. (a) Fourier spectrum of a typical PA signal. (b) Boundary segmented Fourier spectrum (c) & (d) First and second mono-components of the PA signal obtained from Empirical Wavelet Transform

Figures 5.4(c) & 5.4(d) show the two mono-components (time domain representation of the individual frequency components of the PA signal) obtained from Fig. 5.4(b) that have frequencies such as 0.98 MHz and 2.35 MHz. Therefore, EWT based PASR is employed to the normal, benign and malignant breast masses.

5.5.1 Tissue sample preparation and EWT-PASR experiments

For this study, total 25 excised breast samples were collected from hospital. Out of these samples, ten samples were of invasive ductal carcinoma (IDC), seven were fibroadenoma and eight were normal tissues of patients aged between 40 and 80 years. The normal tissues were taken from the same mastectomy sample of duct carcinoma but from focus away from the tumour site. The basis of classification of these tissues was made based on the histopathology results. The tissues were cut into small square pieces of 1 cm size and wrapped with parafilm before placing in the photoacoustic experimental setup to perform the studies. The same experimental procedure detailed in section is followed for this study. Subsequent to PA response acquisition, EWT technique is applied.

5.5.2 Empirical wavelet transform

Empirical Wavelet Transform (EWT) was proposed by Jerome Gilles [170], [171] with an objective to extract different modes of non-stationary signals by building adaptive wavelets. This method works in the following three steps. i) Determine the frequency components of the applied signal using FFT. ii) Then different modes (frequency component) are extracted by obtaining proper segmentation of the Fourier spectrum and iii) Apply scaling and wavelet functions corresponding to each detected segment. Segmentation of the Fourier spectrum is the most important step that provides adaptability to this technique.

Let us consider a discrete signal $x(n)$ having sampling frequency of F_s . Firstly FFT is applied on $x(n)$ to obtain the Fourier spectra $X(\omega)$. Subsequently, a set of maxima $\chi = \chi_{i=1,2,\dots,N_f}$, and their

Chapter 5

corresponding frequency f_i in Fourier spectra were obtained from the magnitude and the frequency distance threshold. Here N_f corresponds to the number of frequency components obtained from FFT. The fundamental frequency was estimated. Next, the Fourier spectrum $[0, F_s/2]$ was segmented (N segments) by identifying boundaries to each segment using the estimated frequencies $f_i = 1, 2, \dots, N_f$. The global minima between two consecutive estimated frequencies i.e. f_i, f_{i+1} was considered to be a boundary Ω_i which satisfies the following condition [171]:

$$X(\Omega_i) \ll X(f_i) \quad \text{and}$$

$$X(\Omega_i) \ll X(f_{i+1}) \quad (5.4)$$

$$f_i < \Omega_i < f_{i+1} \quad \forall 1 \leq i \leq N - 1 \quad (5.5)$$

The estimated Fourier segments assuming the boundaries starts from $[0, F_s/2]$. Then a low-pass filter and (N_f-1) number of band pass filters corresponding to the scaling function ($\phi_1(\omega)$) and the empirical wavelet function ($\Psi_i(\omega)$) described in Eq. 5.6 and Eq. 5.7 [171]. These filters are built based on the frequency, its boundaries and a parameter (γ). The parameter is chosen such that very minimal overlap occurs between two consequent frequency components.

$$\phi_1(\omega) = \begin{cases} 1, & \text{if } |\omega| \leq (1 - \gamma)\Omega_1 \\ \cos\left(\frac{\pi}{2}\iota(\gamma, \omega, \Omega_1)\right), & \text{if } (1 - \gamma)\Omega_1 \leq |\omega| \leq (1 + \gamma)\Omega_1 \\ 0 & \end{cases} \quad (5.6)$$

$$\Psi_i(\omega) = \begin{cases} 1, & \text{if } (1 + \gamma)\Omega_i \leq |\omega| \leq (1 - \gamma)\Omega_{i+1} \\ \cos\left(\frac{\pi}{2}\iota(\gamma, \omega, \Omega_{i+1})\right), & \text{if } (1 - \gamma)\Omega_{i+1} \leq |\omega| \leq (1 + \gamma)\Omega_{i+1} \\ \sin\left(\frac{\pi}{2}\iota(\gamma, \omega, \Omega_i)\right), & \text{if } (1 - \gamma)\Omega_i \leq |\omega| \leq (1 + \gamma)\Omega_i \\ 0 & \end{cases} \quad (5.7)$$

$$\iota(\gamma, \omega, \Omega_i) = \iota\left(\frac{1}{2\gamma\Omega_i} (|\omega| - (1 - \gamma)\Omega_i)\right) \quad (5.8)$$

$$\iota(\gamma, \omega, \Omega) = \begin{cases} 0, & \text{if } \left(\frac{1}{2\gamma\Omega} (|\omega| - (1 - \gamma)\Omega)\right) \leq 0 \\ 1, & \text{if } \left(\frac{1}{2\gamma\Omega} (|\omega| - (1 - \gamma)\Omega)\right) \geq 1 \\ \iota(\gamma, \omega, \Omega) + \iota(1 - \gamma, \omega, \Omega) = 1, & \text{if } \left(\frac{1}{2\gamma\Omega} (|\omega| - (1 - \gamma)\Omega)\right) \in [0,1] \end{cases} \quad (5.9)$$

In order to obtain approximation coefficient, inner product of signal x and empirical scaling function is performed as given as follows [171]

$$W_x(1, n) = \langle x, \Phi_1 \rangle = IFFT(X(\omega)\Phi_1(\omega)) \quad (5.10)$$

The detailed coefficients are obtained utilising empirical wavelet illustrated as [171]

$$W_x(i, n) = \langle x, \psi_i \rangle = IFFT(X(\omega)\Psi_i(\omega)) \quad (5.11)$$

To reconstruct the complete signal, following equation is used [171]

$$W_x(n) = IFFT(W_x(1, \omega)\Phi_1(\omega) + \sum_{i=2}^N W_x(i, \omega) \Psi_i(\omega)) \quad (5.12)$$

Where,

$$W_x(i, \omega) = FFT(W_x(i, n)) \quad (5.13)$$

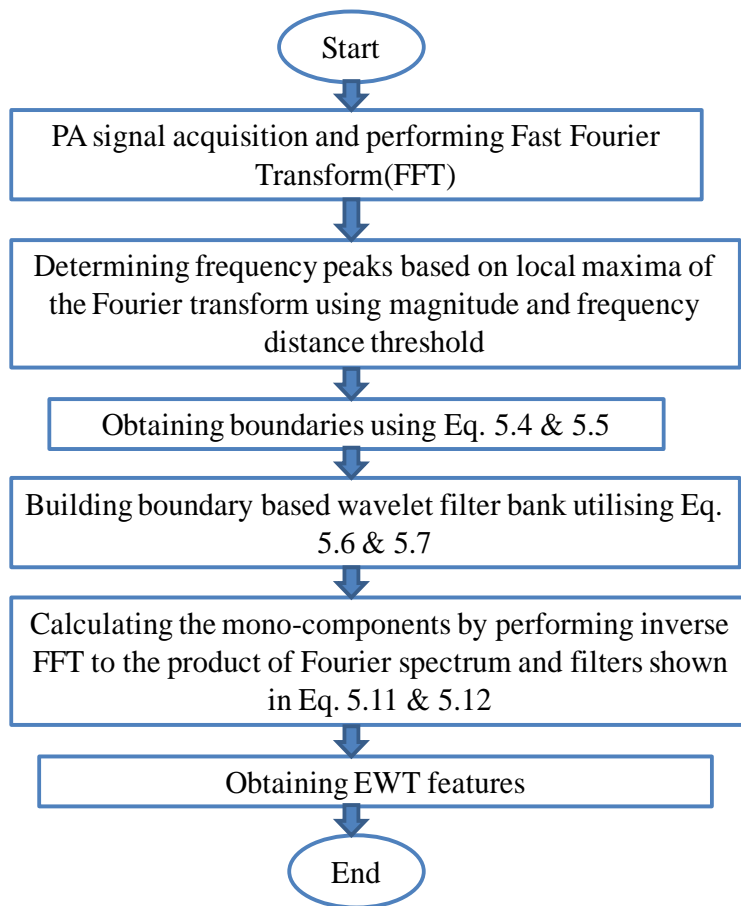


Fig. 5.5. Flow chart of EWT technique. The equations mentioned in flow chart are detailed in Section 5.5.2

Now let us consider applying this EWT technique onto a typical PA response. Fourier spectrum of a time domain PA signal is obtained, with a sampling rate of 200 MS/s as shown in Fig. 5.6(a). The fundamental frequency (highest frequency peak) is obtained from the spectrum. Further, EWT performs magnitude thresholding (3% of fundamental frequency) and frequency distance thresholding (2 MHz) to obtain the different peaks of the spectrum and avoiding fake frequencies. In Fig. 5.6(a), the fundamental frequency corresponds to the second peak of 3.28 MHz. Giving a span of 2 MHz as the frequency distance and calculating peaks of 3% of this magnitude would provide the first and third peak at 0.99 MHz and 11.2 MHz. Following this, the frequency boundaries are obtained by determining the global minima between two consecutive frequency peaks.

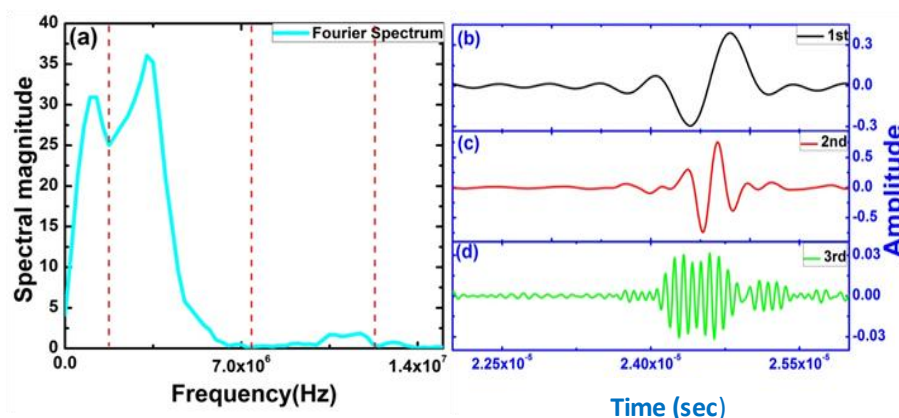


Fig. 5.6. EWT analysis of PA signal (a) Boundary segmented Fourier spectrum (b) First mono-component (frequency 0.99 MHz) (c) Second mono-component (frequency 3.3 MHz) (d) Third mono-component (frequency 11.2 MHz)

For example, the global minima between 0.99 MHz and 3.28 MHz lies at 1.7 MHz. The other obtained are at 1.7 MHz, 7.8 MHz and 12.3 MHz with the frequency peaks at 0.99 MHz, 3.28 MHz and 11.2 MHz respectively. These boundaries are shown in Fig 5.6(a) using red dotted lines. Subsequently, the different mono-components of the signal were obtained by filter bank and adaptive wavelets as detailed in the previous section. Figures 5.6(b-d) shows the three mono-components obtained from EWT. Different features of the mono-components such as amplitude, energy can be utilized for tissue characterization. The EWT algorithm is detailed in flow chart (Fig. 5.5).

5.5.3 Results

5.5.3.1 Frequency spectrum analysis of photoacoustic signals of human breast masses

At the outset, a qualitative analysis has been performed to understand the differences in the three types of tissues. PA response for Normal, Fibroadenoma and Malignant tissues were acquired and shown in Fig. 5.7. Subsequently, EWT technique was applied onto the signals to obtain the frequency spectra of the tissues along with the boundaries as shown in Fig. 5.8. It can be observed from Fig. 5.8 that

Chapter 5

two major frequency components (0.9 ± 0.04 MHz and 2.5 ± 0.5 MHz) are present in all the three frequency spectra of the tissues. At the first instant, analyzing the magnitudes of these spectral components would distinguish normal and malignant tissues from fibroadenoma samples.

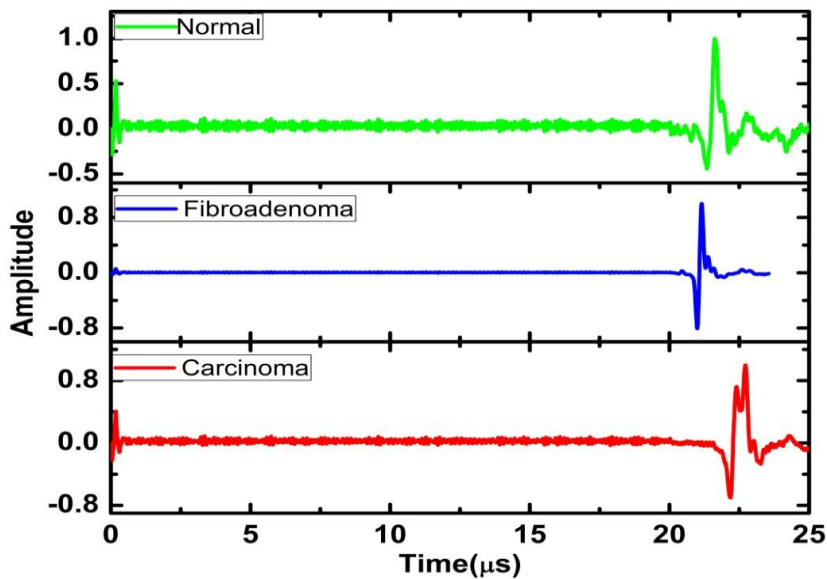


Fig. 5.7. PA response of Normal tissue, Fibroadenoma and Malignant breast tissues

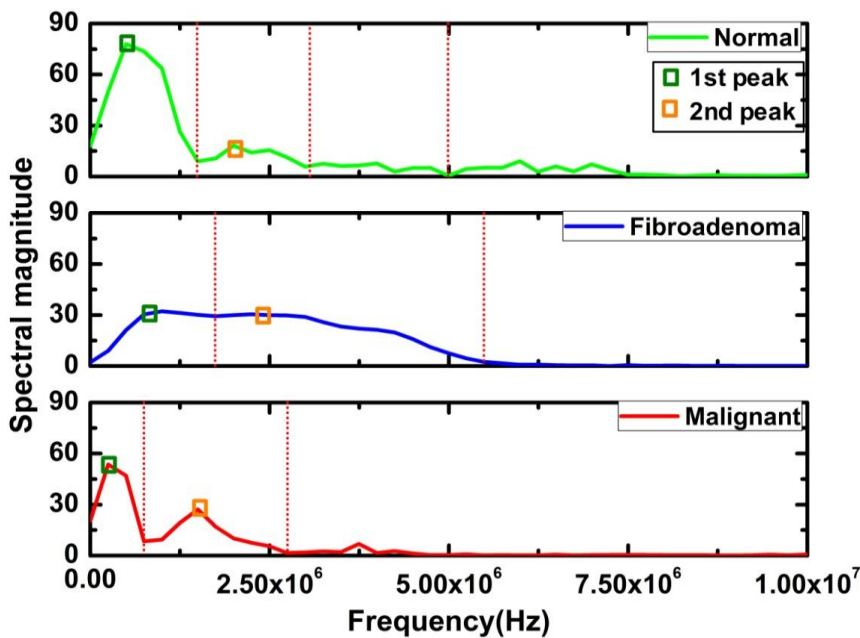


Fig. 5.8. Boundary segmented Fourier spectrum of Normal tissue, Fibroadenoma and Malignant breast tissues

It can be observed from Table 5.1 that there is a two fold increase in spectral magnitude of second frequency component for

malignant (29.01) compared to normal tissue (13.8) whereas fibroadenoma exhibits almost equal spectral magnitude (35.8 and 37.1) for both the frequency components. The same experiments were repeated on all the tissues and a statistical analysis tabulated also confirms the consistency of the results. Hence from this preliminary study, it is evident that frequency spectral magnitude can be one important parameter to distinguish between human breast masses through mechano-biological information.

Table 5.1. Spectral magnitude along with error of different breast masses (FC: Frequency component)

Sample	1st FC	2nd FC
Normal	58.01 ± 2.7	13.8 ± 1.5
Fibroadenoma	35.8 ± 2.01	37.1 ± 3.18
Malignant	54.5 ± 2.75	29.01 ± 1.14

5.5.3.2 EWT extracted mono-component analysis of breast masses

Empirical Wavelet Transform (EWT) is a time-frequency analysis tool. In the previous section, the magnitude of the frequency component has been analysed. In this section, the time component analysis has been performed quantitatively by calculating the energy of the mono-components. Mono-components of two major frequencies were derived using EWT technique from Eq. 5.10 & 5.11. Figures 5.9(a) & 5.9(b) show the two major frequency mono-components obtained from normal tissue, fibroadenoma and malignant tumours respectively. It can be clearly seen from Fig. 5.9(b) that the second mono-component of the normal tissue exhibits approximately 50% reduction in amplitude compared to malignant one. In order to understand the result in a more quantitative manner, we calculate the energy of the mono-components. Energy (E) from these mono-components can be derived by Eq. 4.5. The energy obtained for the

Chapter 5

two mono-components (E1 and E2) for all the three tissue types are shown in Fig. 5.10. It is evident that the energy of the first mono-component decreases for fibroadenoma and malignant samples as compared to the normal tissue. On the contrary, the energy of the second mono-component (corresponding to ~ 2.5 MHz) increases when we move from normal tissue to fibroadenoma tumour. It is also worthwhile to note that the energy of both the mono-components for the fibroadenoma is approximately similar. This study has also been consistent for 40 PA signals taken altogether from the tissues and illustrated in Fig. 5.10 (error bars). Quantitative analysis through energy calculation performed in this study using EWT provides both time domain information as well as spectral information.

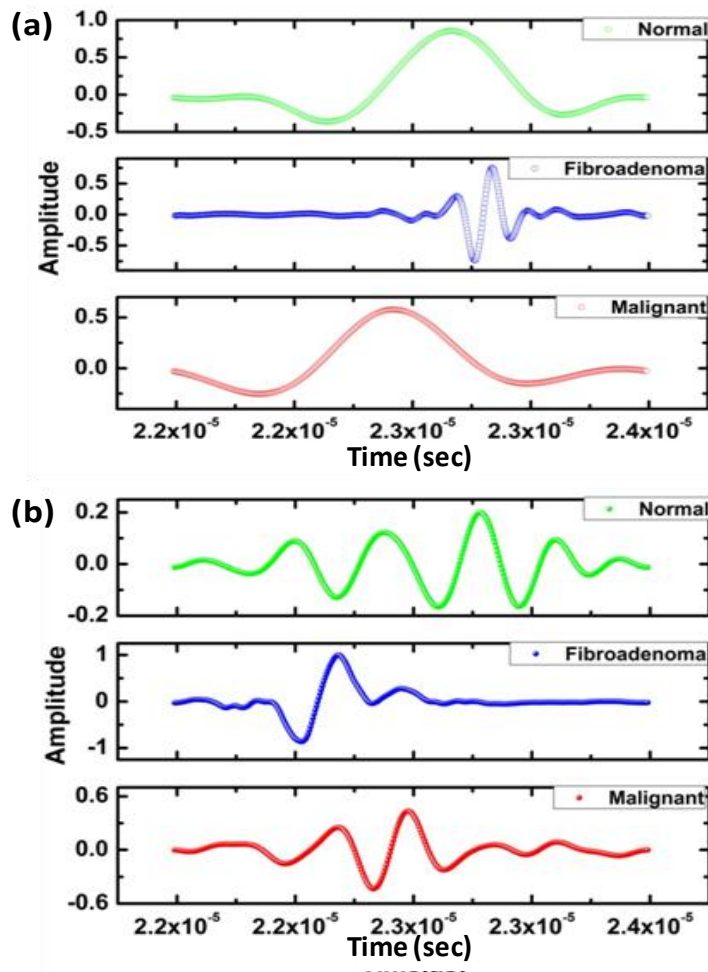


Fig. 5.9. EWT extracted mono-components of benign tissue, fibroadenoma and malignant tumour (a) First mono-component (b) Second mono-component

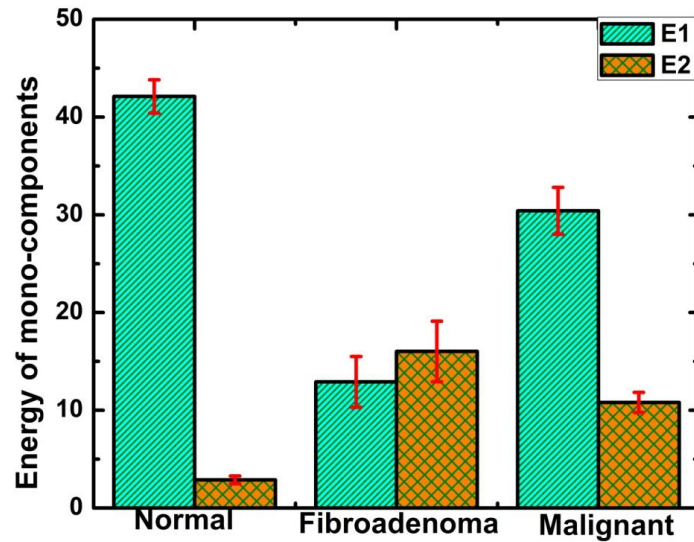


Fig. 5.10. Energy of mono-components (E1 and E2) of Normal, fibroadenoma and malignant tissues

5.5.3.3 Feature based differentiation of breast masses

After obtaining quantitatively, the spectral magnitude and time domain energy of the mono-components, features from EWT can be applied onto these signals to classify the signals into three different tissue types. This would provide a combination of both the time domain information as well as frequency domain information in a quantitative manner. The following are the features extracted from the EWT analysis. The first feature F_1 , which is a ratio of the energy of the mono-components involves solely time domain parameters.

$$F_1 = \frac{E_2}{E_1} \quad (5.14)$$

The second feature F_2 , which is a combination of the spectral magnitudes and the energy of the mono-components is given by Eq. 5.15. This feature provides the quantitative analysis of both the time domain as well as the frequency domain information

$$F_2 = \frac{A_2 E_2}{A_1 E_1} \quad (5.15)$$

Chapter 5

The third feature F3, is given by ratio of the spectral magnitudes of the two dominant frequency mono-components.

$$F_3 = \frac{A_1}{A_1 + A_2} \quad (5.16)$$

The feature values obtained for the three tissue types are provided as a box plot in Fig. 5.11. The entire range of values clearly helps us differentiate the tissue types into normal, fibroadenoma and malignant. The results correspond to the feature values of 40 PA signals with the mean evidently different for the three tissue types. The technique could differentiate fibroadenoma from malignant tissue with 97.5% efficiency with one of the signals overlapping in the region of malignant tissues. The ways to improve this efficiency is provided in the discussion section.

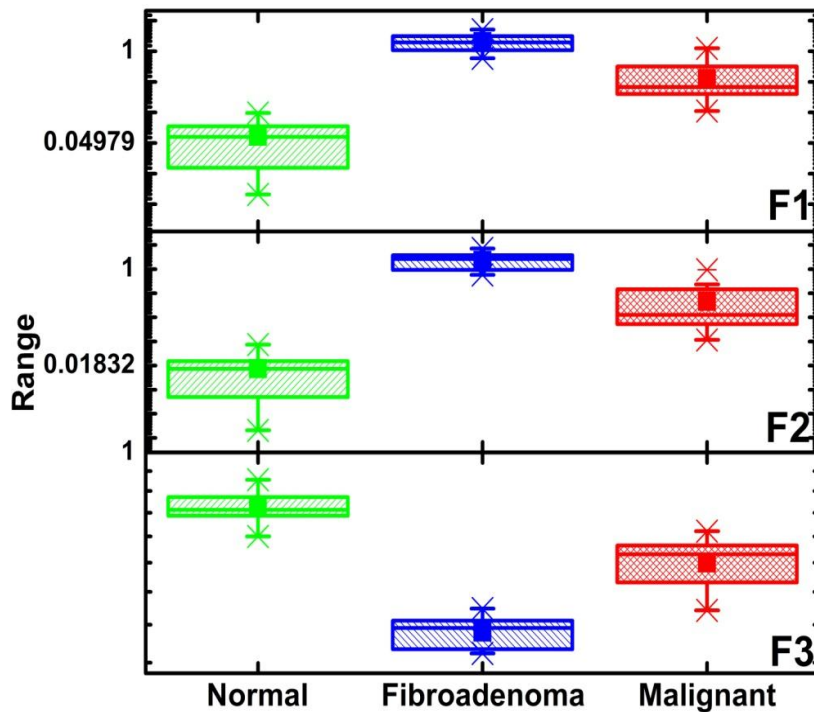


Fig. 5.11. Box Plot of EWT based features of normal, benign and malignant breast masses. The Y-axis is shown in log scale. The shaded box represent 25 - 75 % of the data set. The line in the box is the median and mean value is shown as solid box. The whiskers (cross sign) show the maximum and minimum of data set

5.5.3.4 Histopathology of human breast masses

Standard histopathology was performed for normal, fibroadenoma and malignant tumours to confirm structural changes in tissues. Since structural changes (e.g. density) are related to tissue elasticity, histopathology becomes very important. Figure 5.12 illustrates histopathological images of all three types of breast masses (normal, fibroadenoma and malignant). It is clear from Fig. 5.12, the normal tissue has more of stromal cells (represented in pink) compared to epithelial cells (appears as blue). Another significant observation is that normal breast tissues have a regular architecture whereas malignant tissue exhibits an overpopulation of epithelial cells. It destroys the regular architecture of normal breast tissue. However, equal amount of epithelial cells and stromal cells are present in fibroadenoma. The epithelial cells and stromal cells are highlighted using circles and arrows in Fig. 5.12 respectively.

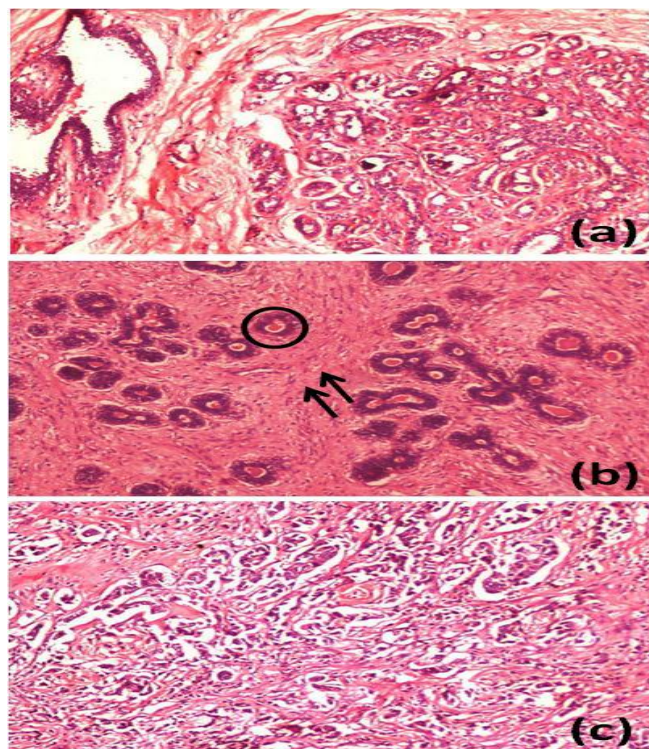


Fig. 5.12. Microscopic images of histopathology of (a) Normal, (b) Fibroadenoma and (c) Malignant tissue; The cells encircled are epithelial cells and the stromal population are pointed with arrows

Chapter 5

5.5.4 Discussions

Quantitatively, time, frequency and time-frequency analysis have been performed and the proposed EWT technique on photoacoustic has yielded 97.5% efficiency in classifying the three types of breast masses. The results were also compared with histopathology to corroborate our results and they are in agreement. In this section, the main reasons for the change in the features are elucidated to have a better understanding of the technique.

5.5.4.1 Spectral magnitude of frequency components

Figure 5.8 shows the decrease in spectral magnitude when we move from normal to malignant tissues. It is known that malignant tissues have uncontrolled proliferation of epithelial cells which not only drastically reduce the amount of stromal tissue but also disturb the regular architecture of normal breast tissues [246]. These epithelial cells have an inherent tendency to bind together and form thick sheet like structure, thereby exhibiting increase in density of the tumour [243]. The stiffer the tissue is, lesser is the attenuation for the higher frequency component and vice versa [244]. This explains the two fold increase in the second frequency component (high frequency) spectral magnitude. Also, since the spectral magnitude of second frequency component (A2) is higher for the malignant tissue, this would give a lower F3 value according to equation (Eq. 5.16) as compared to the normal tissue. Hence it can be confirmed that density plays a role in the results obtained which is correlating to the medical understanding of the tissues.

5.5.4.2 Energy analysis of mono-components

Based on the histopathology results shown in Fig. 5.12, the population of stromal and epithelial cells are provided in Table 5.2 to provide a better understanding [246]. In general, stromal tissues contain elastin, collagen and fibers that makes the tissue more elastic [244], [247]. Since malignant tissue contains more of epithelial cells (that of stromal cells) and epithelial cells exhibit lower attenuation of

higher frequency components, E2 increases when we move from normal to malignant tissue. Interestingly, since stromal cells and epithelial cells are more or less of equal population in fibroadenoma, the two frequency components exhibit almost equal energy. The same reasons would apply to the features derived later as they are related to the spectral magnitude and energy of the PA signals. Therefore, quantitatively assessing the mechano-biological properties of the tissues through energy and features of EWT have proved to provide 97.5% diagnosis. The results were also repeatable for 40 PA signals which show the consistency of the results.

Table 5.2. Cell population in different breast masses

Sample	Normal	Malignant
Stromal cells	↑	↓
Epithelial cells	↓	↑

In the proposed technique, PASR was focussed on blood as a target. In order to improve the efficiency, the technique can be extended to targeting other components of the tissues such as water content. For example, extracellular water content of fibroadenoma has been reported to be very high compared to malignant tumours [248]. This could improve the efficiency of the technique and would provide a way to use this technique for pre-clinical diagnosis to reduce the number of patients undergoing biopsy.

5.6 Summary

Time-frequency based PASR technique is employed for qualitative and quantitative differentiation of formalin fixed human breast masses in in-vitro study. Qualitative discrimination of normal and malignant masses was successfully accomplished with WVD-PASR technique by obtaining the frequency components and energy density of PA response. Appearance of distinct high frequency

Chapter 5

component with enhanced energy density for malignant masses was the significant observation of the study.

EWT-PASR technique was explored for quantitative differentiation of normal, benign and malignant breast masses through time domain and frequency domain derived features. Distinct disparity in spectral amplitude (frequency domain) and mono-frequency components energy (time domain) of the two frequency components are the primary features for differentiation that provide 97.5% discrimination accuracy for forty breast samples. In addition, EWT derived spectral amplitude and energy of mono-frequency components substantiates correlation with tissue pathology (population of epithelial and stromal cells). The results of this work illustrate high resemblance with standard histopathology.

Based on the results of this study it can be stated that time-frequency based PASR technique would be a potential pre-clinical tool for breast cancer diagnosis as it saves time and provide quantitative results. This would enable in quick screening of patients for breast tumour diagnosis and would also aid in reducing the number of cases to undergo biopsy.

Chapter 6

PASR technique for therapeutic application: differentiating normal and thermally coagulated tissues

“Science is the poetry of reality”-Richard Dawkins

6.1 Introduction and motivation

It is clearly demonstrated in the previous two chapters that developed PASR technique can differentiate normal and pathological tissues based on PA spectral parameters (e.g. spectral magnitude, dominant frequency, energy) in qualitative and quantitative manner. Different diseases like identification of blood clot, early stage Pneumonia diagnosis, differentiating normal, benign and malignant breast masses are the major studies performed by developed PASR technique. It is also evident that all the applications of developed PASR technique are focused solely on different diseases diagnosis. But medical science is not only restricted to mere diagnosis, it also includes therapy. Monitoring the progress of treatment also plays a very important role in addition to diagnosis.

For example, solid tumours (benign and malignant) can be discriminated utilising PASR technique (detailed in Chapter 5). In addition to diagnosis, treating the tumour is highly essential to cure the disease [249]. The most common way of treating cancer is removing the suspicious tissue through surgery [250]. However surgery fails to cure the disease of advanced stage patients. In addition, surgery has inherent risk of rapid growth of cancer. Hence other non-invasive or minimally invasive therapeutic techniques such as chemotherapy, radiation therapy, thermotherapy, cryotherapy are gaining interest [251]–[254]. Among these therapeutic techniques, chemotherapy and radiation therapy are very often used by the clinicians. However, these techniques cause harmful side effects to the patients as these techniques are not capable of targeted applications [255], [256]. On contrary, thermotherapy employs targeted therapy that prevents the side effects of chemo and radiation therapy. This technique involves heating of the pathological tissue that causes increase in temperature (50°C to 80°C) followed by coagulated necrosis [191], [257], [258]. As mentioned earlier, monitoring the response to the therapy is important

Chapter 6

to observe the treated area as well as the surrounding tissues. In this aspect, non-invasive monitoring techniques are highly desirable.

6.2 Conventional non-invasive monitoring techniques

There are several techniques such as MRI, ultrasound imaging, optical tomography available for detecting coagulated tissues non-invasively [259]–[261]. Although the mentioned techniques have its own merits for monitoring thermal therapy, these techniques exhibit certain limitations as well. The disadvantages are given as follows [262]:

- a) MRI suffers from high diagnostic cost and long acquisition time. In addition, it is only effective for restricted body parts.
- b) Ultrasound is limited to providing adequate contrast between normal and coagulated tissue due to insignificant change in acoustic impedance between these tissue types
- c) Optical tomography techniques are restricted by the depth of penetration.

6.3 Applying PASR to monitor therapeutic process

It is evident from the previous sections that differentiating normal from coagulated tissue is highly essential to monitor the response of thermal therapy treated solid tumours and the conventional techniques are limited by certain drawbacks that hinder differentiation of normal and coagulated tissues. Hence, this chapter attempts to solve the above mentioned drawbacks of the conventional techniques and facilitate normal and coagulated tissue discrimination by developed PASR technique for non-invasive, highly sensitive and quick diagnosis. Many literatures state that normal and coagulated tissues elucidate significant change in elasticity. Developed PASR technique is proposed to differentiate normal and coagulated tissues as it is very sensitive towards change in elasticity. Since thermal therapy causes damage to the surrounding tissues, this chapter will also focus on application of external absorbers to minimize the damage of surrounding tissue as well as aiding targeted coagulation.

In order to prove the hypothesis, FFT based PASR technique is applied on to in-vitro study performed on excised chicken liver and muscle tissue. Dominant frequency of PA frequency spectrum is utilised as the primary parameter for normal and coagulated tissue differentiation. Gold nanoparticles are employed as external absorbers to reduce the energy of the thermal treatment and minimise the damage of surrounding tissues.

6.4 Basics of tissue coagulation

When laser light is irradiated on a tissue surface, various phenomenon can occur depending upon tissue properties as well as laser parameters. Upon radiation of laser pulses onto the tissues, energy of laser is converted into heat due to absorption by the tissue chromophores. Based on degree of heating, stepwise tissue alteration can be observed as mentioned below [262]:

- At 37°C temperature, there are no conformational changes observed in biological tissues since it is the body temperature.
- By increasing the temperature to 42°C to 50°C, the tissue undergoes hyperthermia. Conformational changes in molecules are attributed to thermal effect on tissue. Therefore during hyperthermia, bond destruction and cellular membrane alteration is observed. Sustention of hyperthermia stage for several minutes would cause necrosis or cell death.
- Tissue coagulation starts at 60°C which provide macroscopic response by visible change in colour of tissue. In this step of thermal interaction, denaturisation of proteins and collagen occurs.
- At 80°C, the permeability of cell membrane increases drastically that disrupt the chemical equilibrium of the cell
- Further increase in temperature around 100°C causes vaporisation of water in cells. Gas bubbles are formed during

Chapter 6

phase transition that leads to mechanical rupture and thermal decomposition of tissue fragments.

- Carbonisation of tissues occurs when the temperature increased beyond 150°C. During this stage colour of the tissue turns in to black and smoke is also observed.

Since tissue coagulation is gaining interest for treating malignant tumours, this chapter focuses on differentiating normal and coagulated tissues.

6.5 Sample preparation for coagulation study

For this study, five chicken livers and five chicken muscles were collected from slaughter house. Subsequently, tissues were cut into 2 cm × 2 cm pieces. For thermal therapy of the tissues, samples were exposed to nano second pulsed laser with energy of 150 mJ for 1 min. The liver tissues were irradiated with second harmonic wavelength whereas muscle tissues were exposed to fundamental wavelength of identical energy. The reason is liver tissue has plenty of blood but muscle contains more of water. Therefore the absorption of liver tissue is high for second harmonic wavelength [263]. By contrast, muscle tissue exhibits higher absorption in infrared region [264].

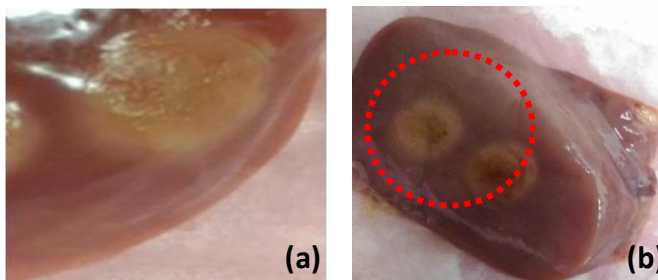


Fig. 6.1. Photograph of chicken tissues (a) muscle (b) liver. Discoloured part indicates the coagulated regions

Figure 6.1 shows the picture of coagulated liver and muscle tissues. Then the samples were coated with thin layer of ultrasound gel and wrapped with parafilm avoiding bubble formation. Thereafter, the samples were stuck to the bottom of the water tank (of PASR setup) to avoid movement.

6.6 Differentiation of normal and coagulated tissues using PASR technique

The primary objective of this study is to differentiate normal from coagulated tissue based on elastic property of the samples. Hence FFT based PASR technique is applied onto chicken liver and muscle tissue to obtain PA frequency spectral parameter such as dominant frequency. This would serve as the finger print for normal and coagulated tissues. For this purpose, PA responses were acquired from three different regions of normal and coagulated part of each sample by applying the developed PASR setup as described in Chapter 3. Since the samples are solid tissues, PASR experimental setup for solid samples were employed. The samples were irradiated with pulsed laser (1 mJ, 5 ns, 532 nm) which causes generation of PA responses. Subsequently, a water immersion ultrasonic sensor (3.5 MHz centre frequency) was employed for PA response acquisition. Later, FFT is applied to the acquired PA responses for quantitative differentiation of normal and coagulated samples.

Figure 6.2(a) illustrates PA responses acquired from normal and coagulated chicken muscle that certainly shows distinct change in PA response. The normal tissue exhibits significant change in relaxation time and also less oscillation compared to coagulated muscles. The change in PA response is clearly reflected in PA frequency spectrum as shown in Fig. 6.2(b). The coagulated muscle elucidates two fold enhancement in dominant frequency compared to normal. To verify the obtained result, the same experiment was repeated with another four muscle tissues. The box plot illustrated in Fig. 6.3 clearly shows that the dominant frequency of normal muscle tissue lies between 1.3 to 1.7 MHz whereas coagulated tissues exhibits range of 2.8 to 3.3 MHz.

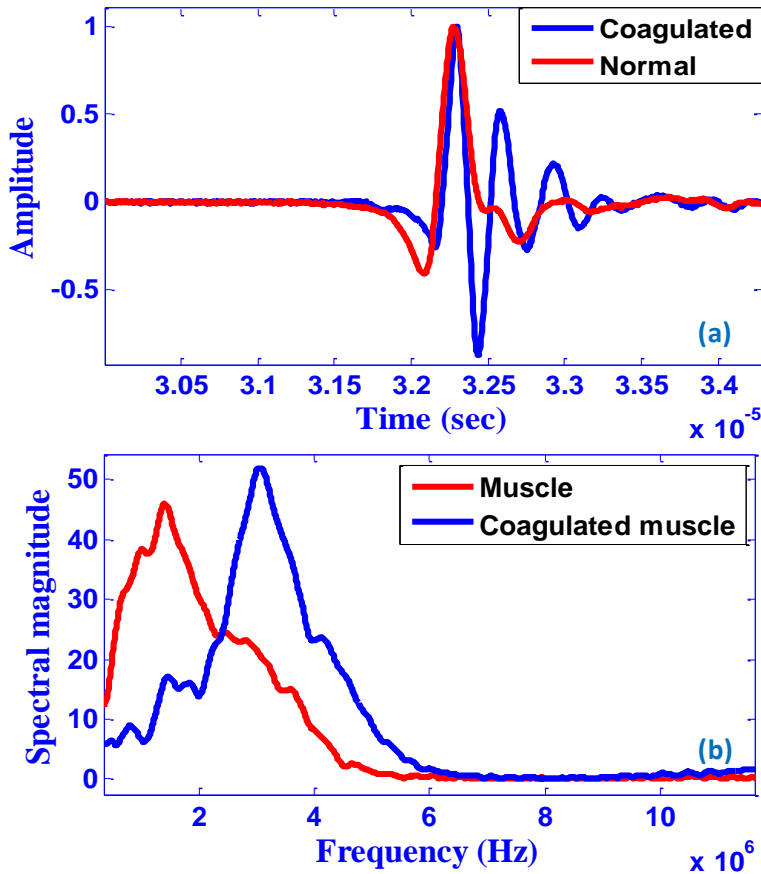


Fig. 6.2. Chicken muscle tissue normal and coagulated (a) PA response (b) PA frequency spectrum

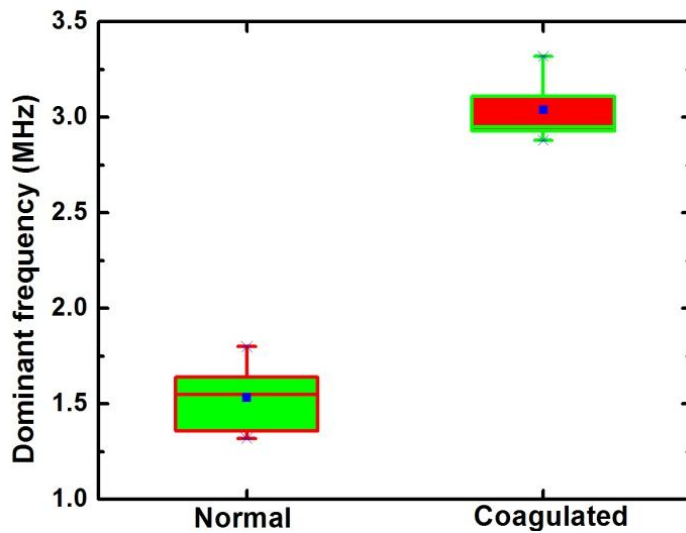


Fig. 6.3. Box plot of normal and coagulated muscle. The Y-axis illustrates dominant frequency in MHz. The shaded box represent 25 - 75 % of the data set. The line in the box is the median and mean value is shown as solid box. The whiskers (cross sign) show the maximum and minimum of data set

Consequently, normal and coagulated chicken liver tissues were also experimented with PASR technique to verify the applicability of the technique for different tissue types. PA responses obtained from normal and coagulated liver is illustrated in Fig. 6.4(a) that shows significant disparity in relaxation time and oscillation between the two samples. Hence, PA frequency spectrum as shown in fig. 6.4(b) also illustrates ~ 1 MHz increase in dominant frequency of coagulated liver compared to normal.

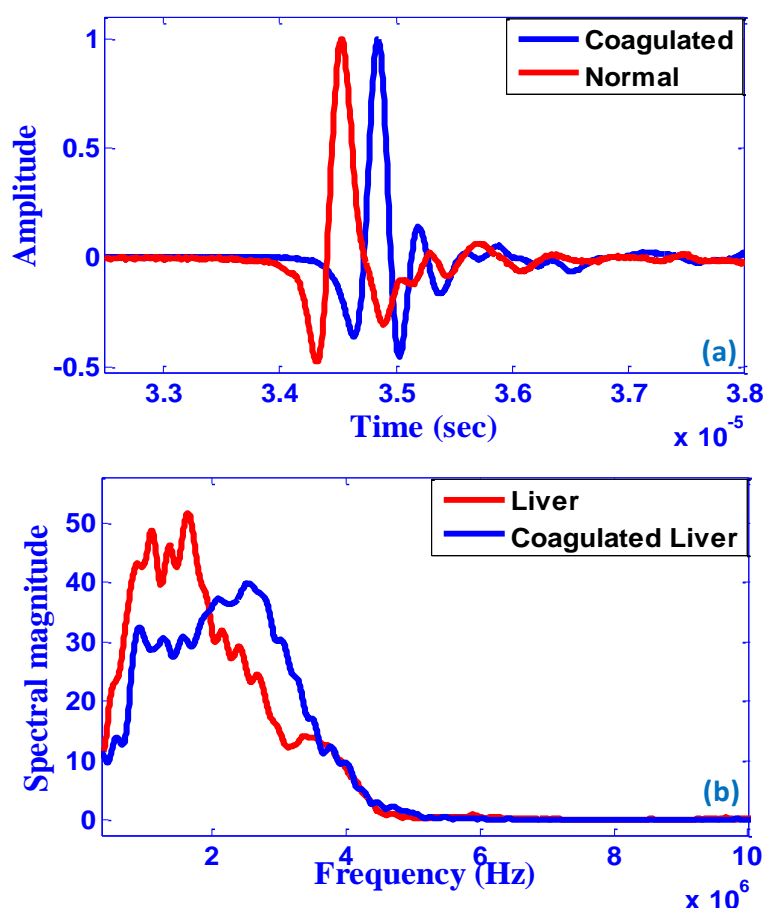


Fig. 6.4. Chicken liver tissue normal and coagulated (a) PA response (b) PA frequency spectrum

For statistical analysis, PASR experiments were performed on four other liver tissues as shown in Fig. 6.5 This clearly exhibits dominant frequency of normal liver lies between 1.5 to 2.2 MHz whereas coagulated liver delineates dominant frequency between 2.9 to 3.6 MHz. Since dominant frequency is related to sample's elastic property, distinct change is observed for normal and coagulated

Chapter 6

tissues. In addition, obtained results are consistent for different tissue types (liver and muscle) as well which would lead PASR technique for to clinical application for monitoring thermal therapy.

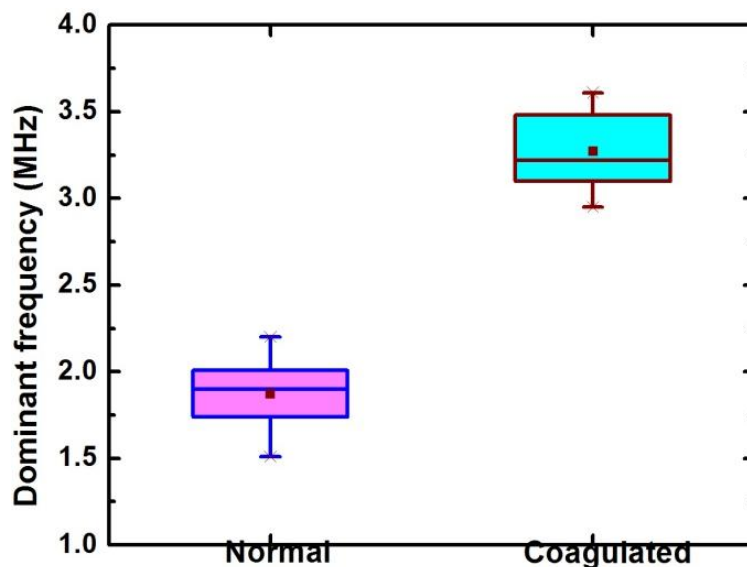


Fig. 6.5. Box plot of normal and coagulated liver. The Y-axis illustrates dominant frequency in MHz. The shaded box represent 25 - 75 % of the data set. The line in the box is the median and mean value is shown as solid box. The whiskers (cross sign) show the maximum and minimum of data set

As discussed in Chapter 4, PA frequency spectral parameter such as dominant frequency is related to sample's elasticity. This chapter also provide detailed theoretical explanation about how density and dominant frequency are related. During thermal therapy, the cellular protein collagen undergoes denaturisation process. During denaturisation, the fibril fibres shrink to maintain the organisation of micro fibril [265]. Thus the density of the coagulated tissue significantly increases compared to normal tissue. This shrinkage of fibril fibres causes oscillation in the PA response of coagulated tissues and increase in density cause shifting of dominant frequency to higher value. The obtained results highly correlates with simulation and experimental studies described in earlier chapters.

6.7 Coagulation with external absorber

Subsequent to successful discrimination of normal and coagulated tissue, now the focus is to utilise external absorbers to minimize the energy of thermal therapy as well as targeted coagulation. Reducing the energy of thermal therapy is imperative to curtail the damage of surrounding normal tissues caused by thermal therapy [266]. In this context, black ink is primarily used as an external absorber for thermal therapy. The reason behind choosing black ink as external absorber is it exhibits high absorbance in a broad optical absorption spectrum as illustrated in Fig. 6.6. Hence using black ink as an external absorber would be pragmatic to reduce the energy of thermal therapy. This will definitely minimise the damage of the surrounding tissue.

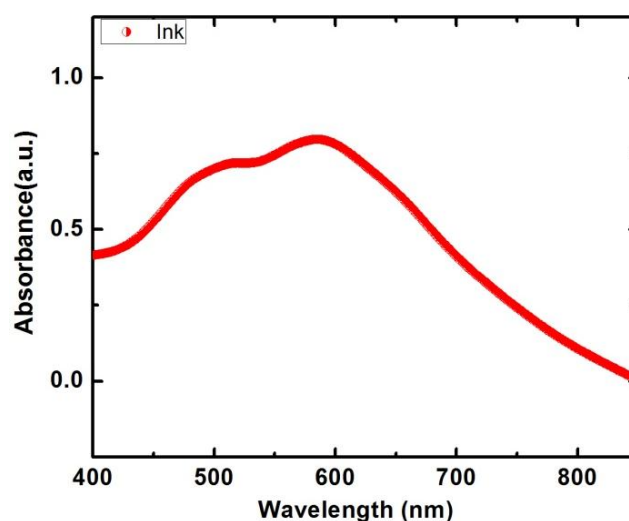


Fig. 6.6. Absorption spectra of black ink

6.7.1 Sample preparation

For this study, excised chicken liver tissues were taken. After cutting the tissues in $2\text{ cm} \times 2\text{ cm}$ square pieces, 0.2 ml black ink was injected into the tissue sample. Thereafter, the tissue sample with ink and without ink was exposed to laser pulses with 75 mJ energy. Since ink exhibits high absorbance in 532 nm wavelength, liver with ink illustrated coagulation whereas only liver tissue did not exhibit any coagulation. As detailed in section, chicken liver coagulates at 150 mJ

Chapter 6

energy without any external absorber. Therefore it is evident that utilising black ink has reduced the energy of thermal therapy by half (150 mJ to 75 mJ). Since the energy of thermal therapy is remarkably reduced, it would certainly cause minimise the damage of surrounding tissues. Subsequent to thermal therapy, the tissues were wrapped in parafilm and placed in the water tank.

6.7.2 PASR experiments with chicken liver and black ink

After confirming that use of external absorber (black ink) significantly reduces the thermal energy for therapy, FFT-PASR technique is applied to the liver samples with and without ink. This is very important to ensure that presence of black ink do not change the sample's elasticity. Therefore prior to coagulation, PA response was acquired from the liver tissue with black ink and without ink region. Then FFT is applied to obtain the PA frequency spectrum as illustrated in Fig. 6.7. From the figure it can be clearly observe that there is only ~ 0.05 MHz change in the dominant frequency between with and without ink region of liver tissue. This is certainly negligible compared to the change in dominant frequency (1 MHz) observed for normal and coagulated liver tissue (detailed in section 6.6). Thus it can be stated that presence of black ink induces negligible change in tissue property.

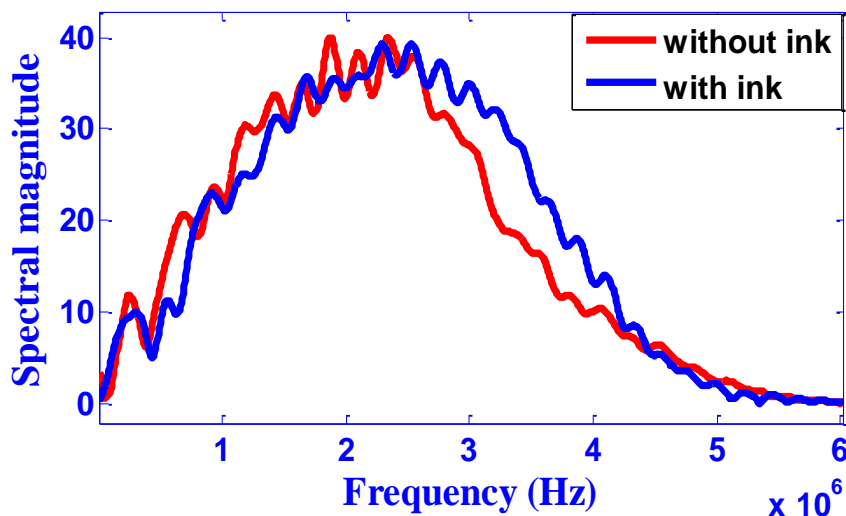


Fig. 6.7. PA frequency spectrum of liver tissue with and without ink

Subsequently, FFT-PASR technique is applied to the normal (without black ink) and coagulated (with black ink) liver tissues. Figure 6.8 illustrates PA frequency spectrum of normal and coagulated liver with ink. This clearly exhibits PA frequency spectrum of the normal and coagulated liver with ink delineates significant change in terms of frequency components, dominant frequency and spectral magnitude. Coagulated liver exhibits two distinct frequency components (~ 0.3 MHz and ~ 2 MHz) whereas normal liver shows one frequency component (~ 1.5 MHz). In addition, the spectral magnitude of coagulated tissue is almost two times higher compared to normal. A significant increase in dominant frequency (~ 0.8 MHz) can also be observed for coagulated tissue compared to normal. Now comparing coagulated tissues with and without ink as shown in Fig. 6.8 clearly exhibits coagulation with ink illustrates significant changes compared to without ink coagulation. Therefore utilising external absorber will not only reduce the thermal energy but also provide prominent changes in PA spectral parameter that would increase the detection accuracy of the PASR system.

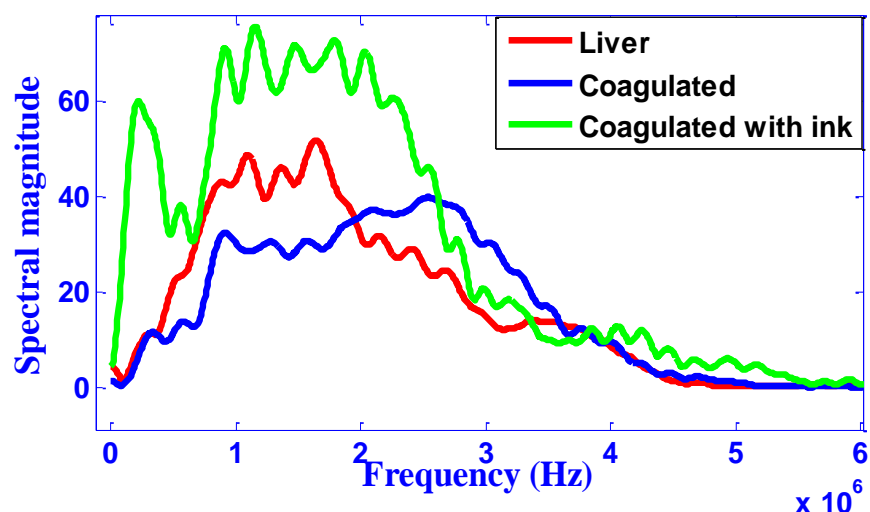


Fig. 6.8. PA frequency spectrum of liver tissue obtained from normal, coagulated and coagulated with ink region

However this study has proved the potential of black ink as an external absorber for coagulation, but there are certain limitation for

Chapter 6

utilising black ink for in-vivo study. The drawbacks are listed as follows:

- Black ink is not bio-compatible
- Black ink cannot be used for targeted application since it cannot be easily functionalised

For the above mentioned problems, black ink cannot be utilised for thermal therapy monitoring for in-vivo applications.

6.7.3 Alternative external absorber for targeted thermal therapy and monitoring

From the previous section, it is very evident that for in-vivo applications a bio-compatible and functional absorber is imperative. In this context, gold nanoparticles (GNPs) can be utilised as external absorber. It is well known from literatures that GNPs are highly bio-compatible [267], [268]. In addition, the GNPs can be functionalised with antibodies for targeted applications [269], [270]. Therefore it has been explored in various applications including genomics, biosensors, immunoassay, laser phototherapy, drug delivery, optical bio imaging etc. [271]–[273].

For this study, GNPs are suitable as it complements the limitation of black ink. Thus GNPs were purchased from Sigma Aldrich for performing PASR experiments. Since the optical property of the GNP depends upon its size, characterisation is very essential.

6.7.3.1 Gold nanoparticle characterisation

6.7.3.1.1 Field emission scanning electron microscopy (FESEM) study

In order to confirm the size of the GNPs, FESEM study is performed using Supra T M 55, Carl Zeiss. It can be observed SEM image as illustrated in Fig. 6.9, the size of the GNPs are ~20 nm. However the GNPs are aggregated that forms big clusters.

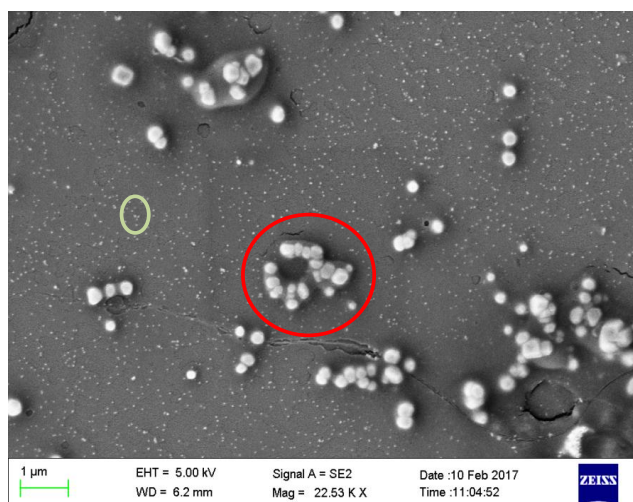


Fig. 6.9. SEM micrograph of GNPs. The clustered nanoparticles are shown in red circle and the single nano particles are shown in green circle

6.7.3.1.2 UV-Visible spectroscopy

UV-Visible spectroscopy was carried out to obtain the optical absorption spectrum of the GNPs as illustrated in Fig 6.10. This clearly indicates presence of a distinct peak around 530 nm. Since for PASR studies utilises 532 nm for irradiation of samples, high absorbance of GNPs at this wavelength would be helpful for enhancing the absorption thereby reducing the energy of thermal therapy.

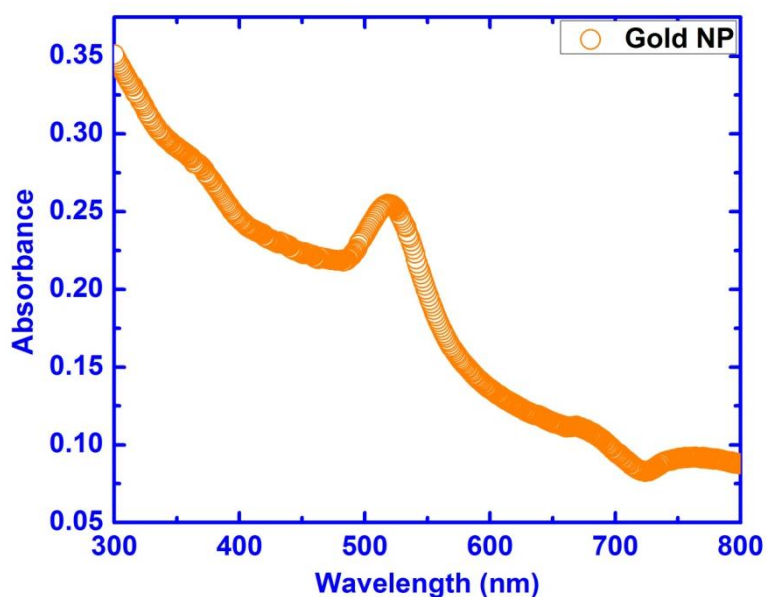


Fig.6.10. Absorption spectra of GNPs

Chapter 6

6.7.3.2 PASR experiments of gold nanoparticles

In order to obtain the PA response from GNPs, the sample is poured in silicone tube container. Thereafter PASR setup for liquid sample was employed for PA response acquisition. The sample was irradiated by laser pulses with 2 mJ energy and 532 nm wavelength. Generated PA responses were acquired by an unfocused ultrasound sensor (centre frequency 3.5 MHz and bandwidth 3.8 MHz). Figure 6.11 illustrates PA response obtained from GNPs.

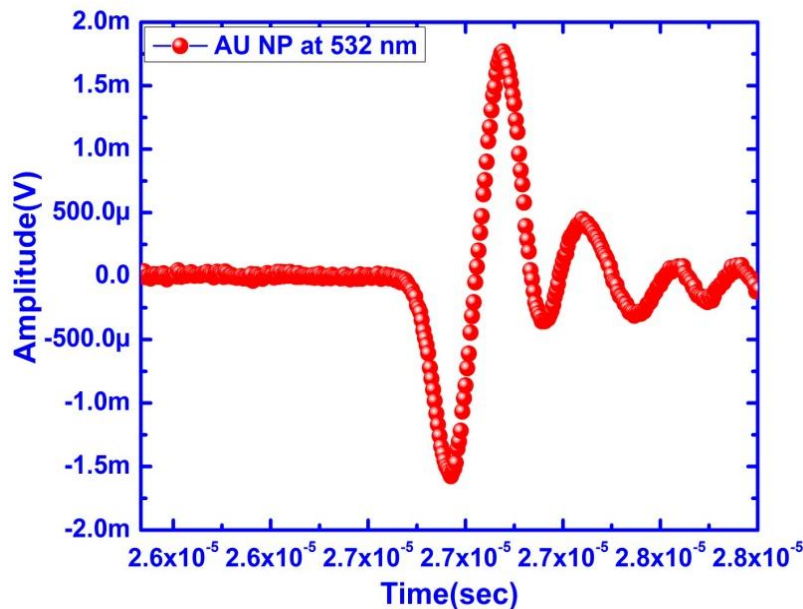


Fig. 6.11. PA response obtained from GNPs

It can be clearly obtained from the figure that the amplitude of the PA response is 1.9 mV. For comparison, PA response was acquired from blood sample with similar energy and experimental setup as shown in Fig. 6.12. By comparing the amplitudes of the PA responses from GNP and blood, it is evident that GNP (~2 mV) exhibits approximately tenfold higher amplitude compared to blood (~0.25 mV). Since PA response amplitude is related to sample's optical absorption, GNP delineates ten times higher absorption compared to blood which is the primary absorber in any biological tissues. Therefore utilising GNP as external absorber would definitely inhibit the laser energy for thermal therapy. In addition, by functionalising the GNPs with particular antibody would pave the way for targeted therapy as well as

monitoring. Thermal coagulation as well as target therapy using GNPs is the future work of this thesis which is discussed in Chapter 7.

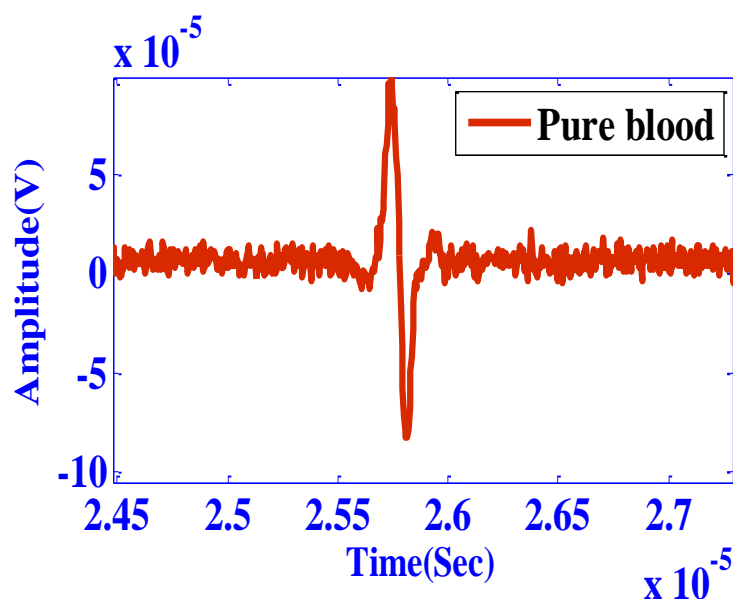


Fig. 6.12. PA response obtained from pure blood

6.8 Summary

Developed PASR technique is employed to differentiate normal and coagulated tissue chicken liver and muscle tissue in in-vitro study. Since normal and coagulated tissue delineates significant change in elasticity, dominant frequency of PA frequency spectrum is utilised for differentiation of these tissue types. Two fold increase in dominant frequency is observed in coagulated muscle tissues compared to normal. Further, coagulated liver tissue elucidated ~ 1 MHz enhancement in dominant frequency compare to normal. Obtained results are consistent for a group of tissues (ten tissue samples). Thus it can be stated that developed PASR technique would be able to identify normal and coagulated tissue which would lead PASR for a new application for monitoring thermal therapy in non-invasive and instantaneous manner.

Thereafter, external absorbers are explored to optimise the energy of thermal therapy and targeted application. In this context, black ink was utilised primarily as external absorber that reduces the

Chapter 6

thermal energy from 150 mJ to 75 mJ and provide distinct change in PA spectral parameters for normal and coagulated tissues.

Subsequently, a highly bio-compatible external absorber, gold nanoparticles was experimented with developed PASR technique. This exhibits ten times higher PA response amplitude compared to blood. Therefore using GNPs as external absorber would definitely inhibit the energy of thermal therapy and pave the way for targeted therapy.

Chapter 7

Conclusions and future work

“Some pretty words were followed by some pretty words”-Anonymous

7.1 Conclusion

In this thesis, tissue elasticity based PASR technique for various biomedical applications is reported. Quantitative differentiation of normal and pathological tissues is performed by obtaining PA frequency spectral parameters by applying different signal processing tools such as FFT, WVD, EWT to PA time domain signal regarded as PA response. As a first step, custom built PASR system was developed in house that consists of LABVIEW based user interface for real time monitoring. Subsequently, the developed system is tested with tissue mimicking phantom as well as biological samples. Then, the obtained PA response from experiments was compared with simulation study. On applying PASR technique to blood, significant change in PA response amplitude was observed due to change in RBC concentration and shape. This correlates well with theoretical understanding of the relation between PA response amplitude and sample's optical absorption. After successful testing of developed PASR system, it was applied to gelatine samples with various concentrations that depict change in elastic property. Dominant frequency of PA frequency spectrum was obtained by applying FFT to PA response. Increase in concentration of gelatine illustrated enhancement in dominant frequency as it relates to sample's elasticity. By applying PASR technique onto biological samples such as chicken liver and muscle that exhibits contrast in elasticity, elucidated distinct change in dominant frequency and spectral amplitude. The results illustrates that developed PASR technique is sensitive towards change in sample's elasticity that can quantitatively differentiate tissue samples (normal and pathological) with disparity in elasticity.

Subsequent to successful experiments on tissue mimicking phantoms and biological samples, PASR technique was extended to differentiation of blood and clot as well as studying blood clotting mechanism through quantitative assessment of PA frequency spectral

Chapter 7

parameters. Differentiating clot immersed in blood and studying blood clotting mechanism of blood is investigated by in-vitro study in which citrated human blood samples were artificially clotted by adding CaCl_2 at 37°C temperature. By applying FFT-PASR technique to blood, during clot formation and clot, 1.3 MHz increase in dominant frequency was observed middle of clot formation whereas 5 MHz enhancement is observed after formation of solid clot compared to blood. For statistical analysis, FFT-PASR technique was applied to group of 20 blood and clot samples collected from different age group donor. Dominant frequency of blood remained between 4.5 to 6 MHz whereas clot exhibited range from 7.5 to 12 MHz.

Another application of developed PASR technique was explored in early stage Pneumonia diagnosis by quantitative assessment of pathological information. Pneumonia affected goat lung tissue with three distinct regions such as oedematous fluid filled region, red hepatisation affected region and normal part was investigated by FFT-PASR technique in an in-vitro study. Approximately two fold increase in dominant frequency was observed for oedematous fluid filled region compared to normal whereas red hepatisation affected region delineated significant increase (~ 1 MHz) in dominant frequency compared to normal. Moreover total spectral energy and variance has also shown distinct disparity among the three regions of lung tissue. Comparison of PASR results with standard histopathology confirmed presence of the mentioned three regions that confirmed change in PA spectral parameters is due to change in tissue pathology of lung.

Qualitative and quantitative classification of formalin fixed human breast masses were performed by developed PASR technique that utilises advanced signal processing tools such as WVD and EWT for extraction of time domain and frequency domain parameters. Qualitative differentiation of normal and malignant breast masses was performed by WVD-PASR. Individual frequency components and its energy density were obtained from WVD contour plots. Presence of

two distinct frequency component for malignant compared to one frequency component for normal was observed that qualitatively differentiate these two breast masses.

Quantitative classification of solid breast tumours such as fibroadenoma (benign) and IDC (malignant) was explored for first time with EWT-PASR technique. Time domain parameters (energy of mono frequency components) and frequency domain parameters (spectral magnitude) were extracted by applying EWT technique on PA responses for defining features for classification. Forty samples (normal, benign and malignant) were classified with 97.5% accuracy by EWT-PASR. By comparing the EWT-PASR results with standard histopathology, high correlation with tissue pathology was obtained.

Consequently, PASR technique was delved for monitoring response from tissues after thermal therapy. Normal and coagulated chicken liver and muscle tissues were investigated with developed PASR technique. Two fold enhancement in dominant frequency was obtained for coagulated tissue compared to normal due to increase in density. External absorber such as black ink and gold nano particles were explored for minimising energy of thermal therapy. Application of black ink reduced the laser energy for thermal therapy by half. Gold nanoparticles delineated ten times higher PA response amplitude compared to blood which proves the potential of GNPs as external absorber.

7.2 Future prospects of PASR technique

- i. Compact instrument for hospitals: In this thesis, PASR technique is developed using pulsed laser excitation and ultrasound sensor as detectors. The PA response acquired by ultrasound sensor is connected to a digitizer that converts the analog signal into digital signal and transfers data into computer memory. Since the primary objective of this thesis is to build an instrument that can be used at patient bed side, but existing system consists of many bulky and costly components that complicate the use of PASR technique for clinical applications. Therefore replacing the digitizer as well as computer with custom build ADCs and FPGA based acquisition system would definitely reduce the cost of the instrument as well as become more compact that can be easily taken up to patient sight.
- ii. PASR study of normal and diseased RBCs: Another direction of studying RBC shape through PA frequency spectrum. Investigation reported in this thesis is limited to solely PA response amplitude to normal, swollen and shrunken RBCs. Differentiating normal and diseases RBCs such as sickle cell anaemia, thalassaemia, malaria through PA frequency spectral parameters would be pragmatic to diagnoses these diseases in its early stage non-invasively.
- iii. In-vivo study of blood coagulation and clot diagnosis: This thesis reports blood clotting mechanism by artificially clotting citrated blood in in-vitro study. Exploring PASR technique to animal model for differentiating normal and haematological diseased blood would provide a better understanding of the disease and pave the way for early

stage diagnosis haematological diseases by non-invasively.

- iv. Staging of breast cancer: In this thesis, human breast masses were classified using developed PASR technique. Qualitative and quantitative differentiation of breast masses is illustrated in this study which also provides pathological information about the tissue. This pathological information would be very helpful to perform staging of malignant tumours which has significant importance in clinical side. Since developed PASR technique is non-invasive and provide real time diagnosis, staging of tumour would be a potential application of PASR technique.
- v. PASR for targeted therapy monitoring: As detailed in this thesis, PASR technique is able to discriminate normal from coagulated tissue; it can be used for monitoring response from thermally treated tissues. Application of GNP as external absorber would reduce the laser energy for thermal therapy that would inhibit the damage of surrounding tissues. Since GNP can be functionalised with antibodies, it would enable targeted therapy as well tracking and monitoring targets during and after therapy.

Appendix I

Acoustic properties of different biological tissues [1], [2]

	Density (kg/m ³)	Sound speed(m/s)	Acoustic impedance (kg/m ² s)	Acoustic attenuation coefficient (dB/cm)
Air	1.2	344	0.00043	11.9
Lung	400	650	0.26	
Fat	920	1467	1.33	0.6
Water	1000	1520	1.48	0.00022
Brain	1030	1504-1612	1.55-1.66	0.85
Kidney	1040	1558	1.62	0.78
Liver	1566	1566	1.66	0.96
Myocardium	1070	1561-1626	1.67-1.74	1.3-3.2
Skull Bone	1380- 1810	2717-4077	3.75-7.38	11.3-20

References

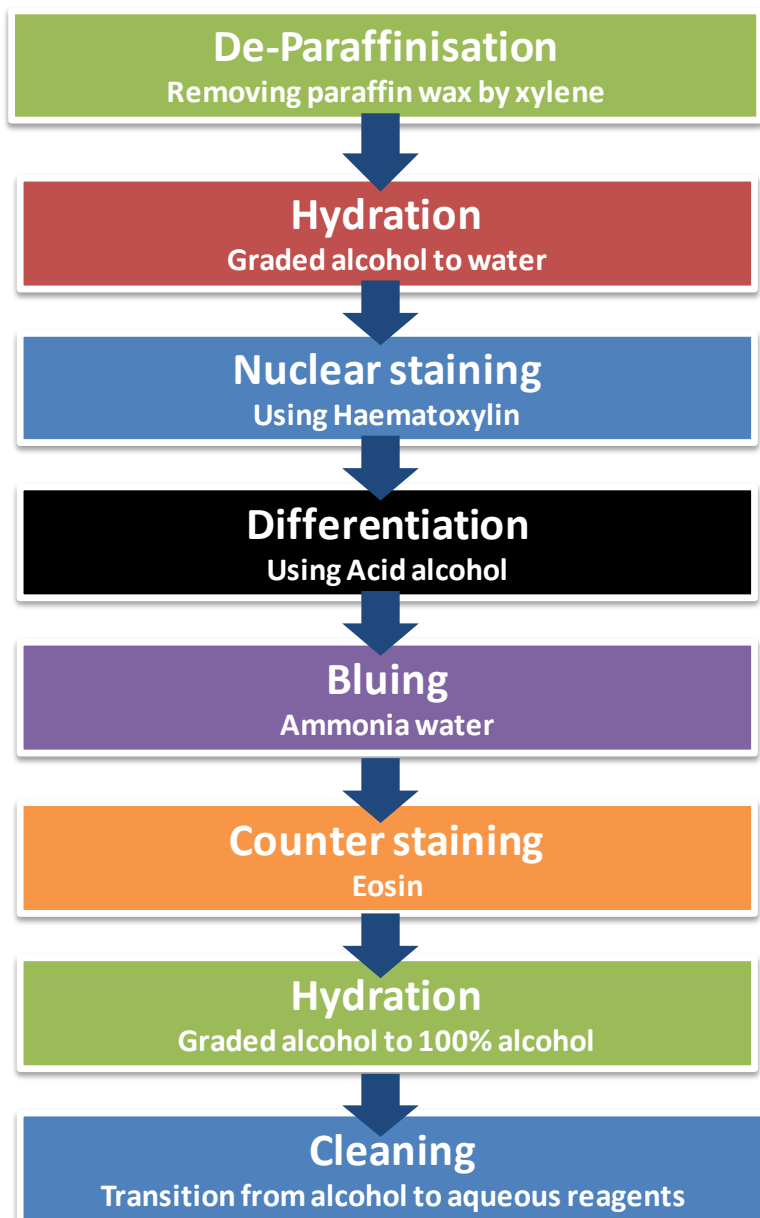
- [1] J. Brnjac-Kraljevic *et al.*, "Physical Bases of Medical Ultrasound," *Donald Sch. Basic Textb. Ultrasound Obstet. Gynecol.*, vol. 400, no. 650, p. 1, 2014.
- [2] H. Azhari, "Ultrasound: medical imaging and beyond (an invited review)," *Curr. Pharm. Biotechnol.*, vol. 13, no. 11, pp. 2104–2116, Sep. 2012.

Appendix I

Appendix II

H&E staining

The primary stains employed in histology are Haematoxylin and eosin. These are widely used by the pathologist for medical diagnosis and considered as golden standard for looking into tissue pathology. This is also referred as H&E staining. The standard procedure of H&E staining is given in the flow chart as follows [1], [2]:



Appendix II

References

- [1] P. Deprez, "Textbook of Chemical Peels," *Superf. Medium Deep Peels Cosmet. Pract. Inf. UK Lond.*, 2007.
- [2] D. Groelz, L. Sobin, P. Branton, C. Compton, R. Wyrich, and L. Rainen, "Non-formalin fixative versus formalin-fixed tissue: A comparison of histology and RNA quality," *Exp. Mol. Pathol.*, vol. 94, no. 1, pp. 188–194, Feb. 2013.

References

- [1] H.-J. Gabius, R. Engelhardt, S. Rehm, and F. Cramer, "Biochemical characterization of endogenous carbohydrate-binding proteins from spontaneous murine rhabdomyosarcoma, mammary adenocarcinoma, and ovarian teratoma," *J. Natl. Cancer Inst.*, vol. 73, no. 6, pp. 1349–1357, 1984.
- [2] A. A. Tzika *et al.*, "Biochemical characterization of pediatric brain tumors by using in vivo and ex vivo magnetic resonance spectroscopy," *J. Neurosurg.*, vol. 96, no. 6, pp. 1023–1031, 2002.
- [3] D. V. Becker *et al.*, "Optimal use of blood tests for assessment of thyroid function," *JAMA*, vol. 269, no. 21, pp. 2736–2737, 1993.
- [4] H. Melbye, B. Straume, U. Aasebø, and J. Brox, "The diagnosis of adult pneumonia in general practice: the diagnostic value of history, physical examination and some blood tests," *Scand. J. Prim. Health Care*, vol. 6, no. 2, pp. 111–117, 1988.
- [5] N. F. Maclagan, "Liver Function Tests in Jaundice," *Br. Med. J.*, vol. 2, no. 4518, p. 197, 1947.
- [6] P. H. Sönksen, S. L. Judd, and C. Lowy, "Home monitoring of blood-glucose: method for improving diabetic control," *The Lancet*, vol. 311, no. 8067, pp. 729–732, 1978.
- [7] S. Walford, E. A. M. Gale, S. P. Allison, and R. B. Tattersall, "Self-monitoring of blood-glucose: improvement of diabetic control," *The Lancet*, vol. 311, no. 8067, pp. 732–735, 1978.
- [8] M. Hoheisel, "Review of medical imaging with emphasis on X-ray detectors," *Nucl. Instrum. Methods Phys. Res. Sect. Accel. Spectrometers Detect. Assoc. Equip.*, vol. 563, no. 1, pp. 215–224, Jul. 2006.
- [9] D. Moratal, "Biomedical Imaging: Principles and Applications [Book Review]," *IEEE Pulse*, vol. 6, no. 3, pp. 61–62, May 2015.
- [10] H. Azhari, "Ultrasound: medical imaging and beyond (an invited review)," *Curr. Pharm. Biotechnol.*, vol. 13, no. 11, pp. 2104–2116, Sep. 2012.
- [11] M. A. Balafar, A. R. Ramli, M. I. Saripan, and S. Mashohor, "Review of brain MRI image segmentation methods," *Artif. Intell. Rev.*, vol. 33, no. 3, pp. 261–274, 2010.
- [12] A. Webb and G. C. Kagadis, "Introduction to biomedical imaging," *Med. Phys.*, vol. 30, no. 8, pp. 2267–2267, 2003.
- [13] D. Pewsner, P. Jüni, M. Egger, M. Battaglia, J. Sundström, and L. M. Bachmann, "Accuracy of electrocardiography in diagnosis of left ventricular hypertrophy in arterial hypertension: systematic review," *Bmj*, vol. 335, no. 7622, p. 711, 2007.

References

- [14] J. S. Windsor, G. W. Rodway, and H. E. Montgomery, "A review of electrocardiography in the high altitude environment," *High Alt. Med. Biol.*, vol. 11, no. 1, pp. 51–60, 2010.
- [15] T. Sand, "Electroencephalography in migraine: a review with focus on quantitative electroencephalography and the migraine vs. epilepsy relationship," *Cephalalgia*, vol. 23, no. s1, pp. 5–11, 2003.
- [16] B. E. Wallace, A. K. Wagner, E. P. Wagner, and J. T. McDevitt, "A history and review of quantitative electroencephalography in traumatic brain injury," *J. Head Trauma Rehabil.*, vol. 16, no. 2, pp. 165–190, 2001.
- [17] R. Aston, *Principles of biomedical instrumentation and measurement*. Prentice Hall, 1990.
- [18] R. Khandpur, *Biomedical instrumentation: Technology and applications*. McGraw-Hill Prof Med/Tech, 2004.
- [19] S. Venkataramanan, P. Prabhat, S. R. Choudhury, H. B. Nemade, and J. S. Sahambi, "Biomedical instrumentation based on electrooculogram (EOG) signal processing and application to a hospital alarm system," in *Intelligent Sensing and Information Processing, 2005. Proceedings of 2005 International Conference on*, 2005, pp. 535–540.
- [20] J. G. Fujimoto *et al.*, "Optical biopsy and imaging using optical coherence tomography," *Nat. Med.*, vol. 1, no. 9, pp. 970–972, 1995.
- [21] M. R. Hee *et al.*, "Optical coherence tomography of the human retina," *Arch. Ophthalmol.*, vol. 113, no. 3, pp. 325–332, 1995.
- [22] A. Diaspro, "Confocal and two-photon microscopy: foundations, applications and advances," *Confocal Two-Photon Microsc. Found. Appl. Adv. Alberto Diaspro Ed. Pp 576 ISBN 0-471-40920-0 Wiley-VCH Novemb. 2001*, p. 576, 2001.
- [23] S. González and Z. Tannous, "Real-time, in vivo confocal reflectance microscopy of basal cell carcinoma," *J. Am. Acad. Dermatol.*, vol. 47, no. 6, pp. 869–874, 2002.
- [24] R. H. Webb, "Confocal optical microscopy," *Rep. Prog. Phys.*, vol. 59, no. 3, p. 427, 1996.
- [25] L. V. Wang and S. Hu, "Photoacoustic tomography: in vivo imaging from organelles to organs," *Science*, vol. 335, no. 6075, pp. 1458–1462, 2012.
- [26] A. B. Karpouk *et al.*, "Combined ultrasound and photoacoustic imaging to detect and stage deep vein thrombosis: phantom and ex vivo studies," *J. Biomed. Opt.*, vol. 13, no. 5, p. 54061, Oct. 2008.

-
- [27] F. J. Harren, J. Mandon, and S. M. Cristescu, "Photoacoustic spectroscopy in trace gas monitoring," *Encycl. Anal. Chem.*, 2000.
- [28] V. Koskinen, J. Fonsen, J. Kauppinen, and I. Kauppinen, "Extremely sensitive trace gas analysis with modern photoacoustic spectroscopy," *Vib. Spectrosc.*, vol. 42, no. 2, pp. 239–242, 2006.
- [29] A. Miklós, P. Hess, and Z. Bozóki, "Application of acoustic resonators in photoacoustic trace gas analysis and metrology," *Rev. Sci. Instrum.*, vol. 72, no. 4, pp. 1937–1955, 2001.
- [30] A. Rosencwaig, *Photoacoustics and photoacoustic spectroscopy*. Wiley, 1980.
- [31] T. Schmid, "Photoacoustic spectroscopy for process analysis," *Anal. Bioanal. Chem.*, vol. 384, no. 5, pp. 1071–1086, 2006.
- [32] M. Xu and L. V. Wang, "Photoacoustic imaging in biomedicine," *Rev. Sci. Instrum.*, vol. 77, no. 4, p. 41101, 2006.
- [33] P. Beard, "Biomedical photoacoustic imaging," *Interface Focus*, p. rsfs20110028, Jun. 2011.
- [34] K. H. Michaelian, *Photoacoustic IR spectroscopy: instrumentation, applications and data analysis*. John Wiley & Sons, 2010.
- [35] S. Manohar and D. Razansky, "Photoacoustics: a historical review," *Adv. Opt. Photonics*, vol. 8, no. 4, pp. 586–617, 2016.
- [36] A. Mandelis, "Photoacoustic, Photothermal, and Diffusion-Wave Sciences in the Twenty-First Century: Triumphs of the Past Set the Trends for the Future," *Int. J. Thermophys.*, vol. 33, no. 10–11, pp. 1776–1777, 2012.
- [37] M. Xu and L. V. Wang, "Universal back-projection algorithm for photoacoustic computed tomography," *Phys. Rev. E*, vol. 71, no. 1, p. 16706, 2005.
- [38] X. Wang, X. Xie, G. Ku, L. V. Wang, and G. Stoica, "Noninvasive imaging of hemoglobin concentration and oxygenation in the rat brain using high-resolution photoacoustic tomography," *J. Biomed. Opt.*, vol. 11, no. 2, pp. 24015–24015, 2006.
- [39] L. V. Wang, "Multiscale photoacoustic microscopy and computed tomography," *Nat. Photonics*, vol. 3, no. 9, pp. 503–509, 2009.
- [40] R. Fainchtein, B. J. Stoyanov, J. C. Murphy, D. A. Wilson, and D. F. Hanley, "Local determination of hemoglobin concentration and degree of oxygenation in tissue by pulsed photoacoustic spectroscopy," in *BiOS 2000 The International Symposium on Biomedical Optics*, 2000, pp. 19–33.
- [41] T. J. Allen, A. Hall, A. P. Dhillon, J. S. Owen, and P. C. Beard, "Spectroscopic photoacoustic imaging of lipid-rich plaques in the

References

- human aorta in the 740 to 1400 nm wavelength range,” *J. Biomed. Opt.*, vol. 17, no. 6, pp. 0612091–06120910, 2012.
- [42] M. Heijblom *et al.*, “Visualizing breast cancer using the Twente photoacoustic mammoscope: what do we learn from twelve new patient measurements?,” *Opt. Express*, vol. 20, no. 11, pp. 11582–11597, 2012.
- [43] G. Xi *et al.*, “Role of blood clot formation on early edema development after experimental intracerebral hemorrhage,” *Stroke*, vol. 29, no. 12, pp. 2580–2586, 1998.
- [44] J. Ketolainen, M. Oksanen, J. Rantala, J. Stor-Pellinen, M. Luukkala, and P. Paronen, “Photoacoustic evaluation of elasticity and integrity of pharmaceutical tablets,” *Int. J. Pharm.*, vol. 125, no. 1, pp. 45–53, 1995.
- [45] N. Nakamura *et al.*, “Study of elastic anisotropy of Cu thin films by resonant-ultrasound spectroscopy coupled with laser-Doppler interferometry and pump-probe photoacoustics,” *Jpn. J. Appl. Phys.*, vol. 45, no. 5S, p. 4580, 2006.
- [46] R. M. Burbelo, A. L. Gulyaev, L. I. Robur, M. K. Zhabitenko, B. A. Atamanenko, and Y. A. Kryl, “Photoacoustic visualization of residual stress in ceramic material,” *J. Phys. IV*, vol. 4, no. C7, pp. C7–311, 1994.
- [47] M. S. Singh and H. Jiang, “Elastic property attributes to photoacoustic signals: an experimental phantom study,” *Opt. Lett.*, vol. 39, no. 13, pp. 3970–3973, 2014.
- [48] L. Fass, “Imaging and cancer: a review,” *Mol. Oncol.*, vol. 2, no. 2, pp. 115–152, 2008.
- [49] T. Franquet, “Imaging of pneumonia: trends and algorithms,” *Eur. Respir. J.*, vol. 18, no. 1, pp. 196–208, 2001.
- [50] O. Gehmacher, G. Mathis, A. Kopf, and M. Scheier, “Ultrasound imaging of pneumonia,” *Ultrasound Med. Biol.*, vol. 21, no. 9, pp. 1119–1122, 1995.
- [51] D. Sandler *et al.*, “Diagnosis of deep-vein thrombosis: comparison of clinical evaluation, ultrasound, plethysmography, and venoscan with X-ray venogram,” *The Lancet*, vol. 324, no. 8405, pp. 716–719, 1984.
- [52] E. Spuentrup *et al.*, “Molecular magnetic resonance imaging of coronary thrombosis and pulmonary emboli with a novel fibrin-targeted contrast agent,” *Circulation*, vol. 111, no. 11, pp. 1377–1382, 2005.
- [53] R. A. Robb, *Biomedical imaging, visualization, and analysis*. John Wiley & Sons, Inc., 1999.
- [54] “Optical Imaging Techniques in Cell Biology, Second Edition,” *CRC Press*.

- [55] I. V. Meglinski and S. J. Matcher, “Quantitative assessment of skin layers absorption and skin reflectance spectra simulation in the visible and near-infrared spectral regions,” *Physiol. Meas.*, vol. 23, no. 4, p. 741, 2002.
- [56] T. Gambichler *et al.*, “Characterization of benign and malignant melanocytic skin lesions using optical coherence tomography in vivo,” *J. Am. Acad. Dermatol.*, vol. 57, no. 4, pp. 629–637, 2007.
- [57] L. V. Wang and H. Wu, *Biomedical optics: principles and imaging*. John Wiley & Sons, 2012.
- [58] W. G. Bradley, “History of medical imaging,” *Proc. Am. Philos. Soc.*, vol. 152, no. 3, pp. 349–361, Sep. 2008.
- [59] J. H. Scatliff and P. J. Morris, “From Roentgen to magnetic resonance imaging: the history of medical imaging,” *N. C. Med. J.*, vol. 75, no. 2, pp. 111–113, Apr. 2014.
- [60] A. Goddi, M. Bonardi, and S. Alessi, “Breast elastography: a literature review,” *J. Ultrasound*, vol. 15, no. 3, pp. 192–198, 2012.
- [61] J. A. Seibert, “One hundred years of medical diagnostic imaging technology,” *Health Phys.*, vol. 69, no. 5, pp. 695–720, Nov. 1995.
- [62] C. Zhang and Y. Wang, “Comparison of Various Imaging Modes for Photoacoustic Tomography,” in *13th International Conference on Biomedical Engineering*, Springer, Berlin, Heidelberg, 2009, pp. 121–124.
- [63] K. S. Valluru, B. K. Chinni, N. A. Rao, S. Bhatt, and V. S. Dogra, “Basics and clinical applications of photoacoustic imaging,” *Ultrasound Clin.*, vol. 4, no. 3, pp. 403–429, 2009.
- [64] M. Haltmeier, O. Scherzer, and G. Zangerl, “A reconstruction algorithm for photoacoustic imaging based on the nonuniform FFT,” *IEEE Trans. Med. Imaging*, vol. 28, no. 11, pp. 1727–1735, 2009.
- [65] B. E. Treeby and B. T. Cox, “k-Wave: MATLAB toolbox for the simulation and reconstruction of photoacoustic wave fields,” *J. Biomed. Opt.*, vol. 15, no. 2, pp. 21314–21314–12, 2010.
- [66] E. M. Strohm, E. S. Berndl, and M. C. Kolios, “High frequency label-free photoacoustic microscopy of single cells,” *Photoacoustics*, vol. 1, no. 3, pp. 49–53, 2013.
- [67] E. M. Strohm, M. J. Moore, and M. C. Kolios, “Single cell photoacoustic microscopy: a review,” *IEEE J. Sel. Top. Quantum Electron.*, vol. 22, no. 3, pp. 137–151, 2016.
- [68] A. G. Bell, “On the production and reproduction of sound by light,” *Am. J. Sci.*, vol. Series 3 Vol. 20, no. 118, pp. 305–324, Oct. 1880.

References

- [69] E. De Montigny, “Photoacoustic tomography: principles and applications,” *Dep. Phys. Eng. Polytech. Sch. Montr.*, 2011.
- [70] G. J. Diebold, T. Sun, and M. I. Khan, “Photoacoustic monopole radiation in one, two, and three dimensions,” *Phys. Rev. Lett.*, vol. 67, no. 24, p. 3384, 1991.
- [71] G. J. Diebold and T. Sun, “Properties of photoacoustic waves in one, two, and three dimensions,” *Acta Acust. United Acust.*, vol. 80, no. 4, pp. 339–351, 1994.
- [72] B. E. Treeby and B. T. Cox, “Fast tissue-realistic models of photoacoustic wave propagation for homogeneous attenuating media,” in *SPIE BiOS: Biomedical Optics*, 2009, pp. 717716–717716.
- [73] M. A. Breazeale and O. Leroy, *Physical Acoustics: Fundamentals and Applications*. Springer Science & Business Media, 2012.
- [74] B. E. Treeby, “Acoustic attenuation compensation in photoacoustic tomography using time-variant filtering,” *J. Biomed. Opt.*, vol. 18, no. 3, pp. 36008–36008, 2013.
- [75] A. Marion, J. Boutet, M. Debourdeau, J.-M. Dinten, and D. Vray, “A quantitative study to design an experimental setup for photoacoustic imaging,” in *Engineering in Medicine and Biology Society, EMBC, 2011 Annual International Conference of the IEEE*, 2011, pp. 7211–7214.
- [76] C. Guittet, F. Ossant, L. Vaillant, and M. Berson, “In vivo high-frequency ultrasonic characterization of human dermis,” *IEEE Trans. Biomed. Eng.*, vol. 46, no. 6, pp. 740–746, Jun. 1999.
- [77] C. Li and L. V. Wang, “Photoacoustic tomography and sensing in biomedicine,” *Phys. Med. Biol.*, vol. 54, no. 19, p. R59, 2009.
- [78] W. Jackson and N. M. Amer, “Piezoelectric photoacoustic detection: theory and experiment,” *J. Appl. Phys.*, vol. 51, no. 6, pp. 3343–3353, 1980.
- [79] H. Wang and L. Z. Xiang, “Scanning Photoacoustic Tomography of Biological Tissues with a Piezoelectricity Double-Ring Sensor,” in *Key Engineering Materials*, 2008, vol. 364, pp. 1105–1110.
- [80] A. A. Vives, *Piezoelectric Transducers and Applications*. Springer Science & Business Media, 2013.
- [81] J. Tichý, J. Erhart, E. Kittinger, and J. Prívratká, *Fundamentals of Piezoelectric Sensorics: Mechanical, Dielectric, and Thermodynamical Properties of Piezoelectric Materials*. Springer Science & Business Media, 2010.
- [82] C. G. A. Hoelen and F. F. M. De Mul, “A new theoretical approach to photoacoustic signal generation,” *J. Acoust. Soc. Am.*, vol. 106, no. 2, pp. 695–706, 1999.

- [83] D. Biswas, A. Gorey, G. C. Chen, N. Sharma, and S. Vasudevan, "Investigation of diseases through red blood cells' shape using photoacoustic response technique," presented at the SPIE BiOS, 2015, p. 93220K–93220K–5.
- [84] C. Hoelen, F. De Mul, R. Pongers, and A. Dekker, "Three-dimensional photoacoustic imaging of blood vessels in tissue," *Opt. Lett.*, vol. 23, no. 8, pp. 648–650, 1998.
- [85] M. Heijblom, W. Steenbergen, and S. Manohar, "Clinical photoacoustic breast imaging: the Twente experience," *IEEE Pulse*, vol. 6, no. 3, pp. 42–46, 2015.
- [86] S. H. Holan and J. A. Viator, "Automated wavelet denoising of photoacoustic signals for circulating melanoma cell detection and burn image reconstruction," *Phys. Med. Biol.*, vol. 53, no. 12, p. N227, 2008.
- [87] Z. Ren, G. Liu, and Z. Xiong, "Photoacoustic signals denosing of the glucose aqueous solutions using an improved wavelet threshold method," 2016, vol. 10153, p. 101530A–101530A–9.
- [88] S. A. Telenkov, R. Alwi, and A. Mandelis, "Photoacoustic correlation signal-to-noise ratio enhancement by coherent averaging and optical waveform optimization," *Rev. Sci. Instrum.*, vol. 84, no. 10, p. 104907, Oct. 2013.
- [89] V. Moock *et al.*, "Signal processing for photoacoustic tomography," in *2012 5th International Congress on Image and Signal Processing*, 2012, pp. 957–961.
- [90] J. Yao and L. V. Wang, "Sensitivity of photoacoustic microscopy," *Photoacoustics*, vol. 2, no. 2, pp. 87–101, Jun. 2014.
- [91] L. Chmelka and J. Kozumplik, "Wavelet-based wiener filter for electrocardiogram signal denoising," in *Computers in Cardiology, 2005*, 2005, pp. 771–774.
- [92] A. B. Wiltschko, G. J. Gage, and J. D. Berke, "Wavelet filtering before spike detection preserves waveform shape and enhances single-unit discrimination," *J. Neurosci. Methods*, vol. 173, no. 1, pp. 34–40, 2008.
- [93] L. Zeng, D. Xing, H. Gu, D. Yang, S. Yang, and L. Xiang, "High antinoise photoacoustic tomography based on a modified filtered backprojection algorithm with combination wavelet," *Med. Phys.*, vol. 34, no. 2, pp. 556–563, 2007.
- [94] A. A. Oraevsky, R. O. Esenaliev, and A. A. Karabutov, "Laser optoacoustic tomography of layered tissues: signal processing," in *BiOS'97, Part of Photonics West*, 1997, pp. 59–70.
- [95] J. Gamelin *et al.*, "Curved array photoacoustic tomographic system for small animal imaging," *J. Biomed. Opt.*, vol. 13, no. 2, p. 24007, 2008.

References

- [96] G. T. Herman, *Fundamentals of Computerized Tomography: Image Reconstruction from Projections*. Springer Science & Business Media, 2009.
- [97] J. D. Bronzino, *Biomedical Engineering Handbook*. CRC Press, 1999.
- [98] B. E. Treeby, E. Z. Zhang, and B. T. Cox, “Photoacoustic tomography in absorbing acoustic media using time reversal,” *Inverse Probl.*, vol. 26, no. 11, p. 115003, 2010.
- [99] Y. Hristova, P. Kuchment, and L. Nguyen, “Reconstruction and time reversal in thermoacoustic tomography in acoustically homogeneous and inhomogeneous media,” *Inverse Probl.*, vol. 24, no. 5, p. 55006, 2008.
- [100] K. Firouzi, B. T. Cox, B. E. Treeby, and N. Saffari, “A first-order k-space model for elastic wave propagation in heterogeneous media,” *J. Acoust. Soc. Am.*, vol. 132, no. 3, pp. 1271–1283, 2012.
- [101] Y. Jing, T. Wang, and G. T. Clement, “A k-space method for moderately nonlinear wave propagation,” *IEEE Trans. Ultrason. Ferroelectr. Freq. Control*, vol. 59, no. 8, pp. 1664–1673, 2012.
- [102] O. Oralkan *et al.*, “Capacitive micromachined ultrasonic transducers: Next-generation arrays for acoustic imaging?,” *IEEE Trans. Ultrason. Ferroelectr. Freq. Control*, vol. 49, no. 11, pp. 1596–1610, 2002.
- [103] Y. Zeng, D. Xing, Y. Wang, B. Yin, and Q. Chen, “Photoacoustic and ultrasonic coimage with a linear transducer array,” *Opt. Lett.*, vol. 29, no. 15, pp. 1760–1762, 2004.
- [104] Y. Xu, M. Xu, and L. V. Wang, “Exact frequency-domain reconstruction for thermoacoustic tomography. II. Cylindrical geometry,” *IEEE Trans. Med. Imaging*, vol. 21, no. 7, pp. 829–833, 2002.
- [105] E. Zhang, J. Laufer, and P. Beard, “Backward-mode multiwavelength photoacoustic scanner using a planar Fabry-Perot polymer film ultrasound sensor for high-resolution three-dimensional imaging of biological tissues,” *Appl. Opt.*, vol. 47, no. 4, pp. 561–577, 2008.
- [106] H. F. Zhang, K. Maslov, G. Stoica, and L. V. Wang, “Functional photoacoustic microscopy for high-resolution and noninvasive in vivo imaging,” *Nat. Biotechnol.*, vol. 24, no. 7, pp. 848–851, Jul. 2006.
- [107] K. Maslov, G. Stoica, and L. V. Wang, “In vivo dark-field reflection-mode photoacoustic microscopy,” *Opt. Lett.*, vol. 30, no. 6, pp. 625–627, 2005.
- [108] M. R. Chatni, J. Yao, A. Danielli, C. P. Favazza, K. I. Maslov, and L. V. Wang, “Functional photoacoustic microscopy of pH,” *J. Biomed. Opt.*, vol. 16, no. 10, pp. 100503-100503–3, 2011.

- [109] C. Hoelen and F. De Mul, “A new theoretical approach to photoacoustic signal generation,” *J. Acoust. Soc. Am.*, vol. 106, no. 2, pp. 695–706, 1999.
- [110] S.-H. Tseng, P. Bargo, A. Durkin, and N. Kollias, “Chromophore concentrations, absorption and scattering properties of human skin in-vivo,” *Opt. Express*, vol. 17, no. 17, pp. 14599–14617, Aug. 2009.
- [111] J. R. Rajian, P. L. Carson, and X. Wang, “Quantitative photoacoustic measurement of tissue optical absorption spectrum aided by an optical contrast agent,” *Opt. Express*, vol. 17, no. 6, pp. 4879–4889, Mar. 2009.
- [112] R. O. Esenaliev, M. Motamedi, D. S. Prough, and A. A. Oraevsky, *Optoacoustic monitoring of blood oxygenation*. Google Patents, 2002.
- [113] J. Laufer, D. Delpy, C. Elwell, and P. Beard, “Quantitative spatially resolved measurement of tissue chromophore concentrations using photoacoustic spectroscopy: application to the measurement of blood oxygenation and haemoglobin concentration,” *Phys. Med. Biol.*, vol. 52, no. 1, p. 141, 2006.
- [114] G. Xu, I. A. Dar, C. Tao, X. Liu, C. X. Deng, and X. Wang, “Photoacoustic spectrum analysis for microstructure characterization in biological tissue: A feasibility study,” *Appl. Phys. Lett.*, vol. 101, no. 22, p. 221102, 2012.
- [115] Y. Yang, S. Wang, C. Tao, X. Wang, and X. Liu, “Photoacoustic tomography of tissue subwavelength microstructure with a narrowband and low frequency system,” *Appl. Phys. Lett.*, vol. 101, no. 3, p. 34105, 2012.
- [116] R. E. Kumon, C. X. Deng, and X. Wang, “Frequency-domain analysis of photoacoustic imaging data from prostate adenocarcinoma tumors in a murine model,” *Ultrasound Med. Biol.*, vol. 37, no. 5, pp. 834–839, 2011.
- [117] G. Xu, J. B. Fowlkes, C. Tao, X. Liu, and X. Wang, “Photoacoustic spectrum analysis for microstructure characterization in biological tissue: Analytical model,” *Ultrasound Med. Biol.*, vol. 41, no. 5, pp. 1473–1480, 2015.
- [118] S. D. Kamath, S. Ray, and K. K. Mahato, “Photoacoustic spectroscopy of ovarian normal, benign, and malignant tissues: a pilot study,” *J. Biomed. Opt.*, vol. 16, no. 6, pp. 67001–67001, 2011.
- [119] M. Priya, B. S. S. Rao, S. Ray, and K. K. Mahato, “Photoacoustic spectroscopy in the monitoring of breast tumor development: A pre-clinical study,” in *SPIE BiOS*, 2014, pp. 894347–894347.
- [120] M. Priya, B. S. S. Rao, S. Chandra, A. Datta, S. G. Nayak, and K. K. Mahato, “Monitoring breast tumor progression by

References

- photoacoustic measurements: a xenograft mice model study,” *J. Biomed. Opt.*, vol. 20, no. 10, pp. 105002–105002, 2015.
- [121] M. Priya, B. S. Rao, S. Ray, and K. K. Mahato, “Prediction of absorption coefficients by pulsed laser induced photoacoustic measurements,” *Spectrochim. Acta. A. Mol. Biomol. Spectrosc.*, vol. 127, pp. 85–90, 2014.
- [122] S. D. Kamath, V. B. Kartha, and K. K. Mahato, “Dynamics of L-tryptophan in aqueous solution by simultaneous laser induced fluorescence (LIF) and photoacoustic spectroscopy (PAS),” *Spectrochim. Acta. A. Mol. Biomol. Spectrosc.*, vol. 70, no. 1, pp. 187–194, 2008.
- [123] S. Hu, K. Maslov, V. Tsytarev, and L. V. Wang, “Functional transcranial brain imaging by optical-resolution photoacoustic microscopy,” *J. Biomed. Opt.*, vol. 14, no. 4, pp. 40503–40503, 2009.
- [124] J. Yao and L. V. Wang, “Photoacoustic brain imaging: from microscopic to macroscopic scales,” *Neurophotonics*, vol. 1, no. 1, pp. 11003–11003, 2014.
- [125] X. Wang, Y. Pang, G. Ku, X. Xie, G. Stoica, and L. V. Wang, “Noninvasive laser-induced photoacoustic tomography for structural and functional in vivo imaging of the brain,” *Nat. Biotechnol.*, vol. 21, no. 7, pp. 803–806, 2003.
- [126] G. Ku, X. Wang, X. Xie, G. Stoica, and L. V. Wang, “Imaging of tumor angiogenesis in rat brains in vivo by photoacoustic tomography,” *Appl. Opt.*, vol. 44, no. 5, pp. 770–775, 2005.
- [127] X. Wang, X. Xie, G. Ku, L. V. Wang, and G. Stoica, “Noninvasive imaging of hemoglobin concentration and oxygenation in the rat brain using high-resolution photoacoustic tomography,” *J. Biomed. Opt.*, vol. 11, no. 2, pp. 24015–24015, 2006.
- [128] X. Wang, D. L. Chamberland, and D. A. Jamadar, “Noninvasive photoacoustic tomography of human peripheral joints toward diagnosis of inflammatory arthritis,” *Opt. Lett.*, vol. 32, no. 20, pp. 3002–3004, 2007.
- [129] E. Falk, P. K. Shah, and V. Fuster, “Coronary plaque disruption,” *Circulation*, vol. 92, no. 3, pp. 657–671, 1995.
- [130] A. Farb *et al.*, “Coronary plaque erosion without rupture into a lipid core,” *Circulation*, vol. 93, no. 7, pp. 1354–1363, 1996.
- [131] A. H. Association, *Heart and stroke facts*. The Association, 1993.
- [132] M. J. Davies, “A macro and micro view of coronary vascular insult in ischemic heart disease,” *Circulation*, vol. 82, no. 3 Suppl, p. II38–46, 1990.

- [133] T. J. Allen, A. Hall, A. P. Dhillon, J. S. Owen, and P. C. Beard, “Spectroscopic photoacoustic imaging of lipid-rich plaques in the human aorta in the 740 to 1400 nm wavelength range,” *J. Biomed. Opt.*, vol. 17, no. 6, pp. 612091–6120910, 2012.
- [134] J. Zhang, S. Yang, X. Ji, Q. Zhou, and D. Xing, “Characterization of lipid-rich aortic plaques by intravascular photoacoustic tomography,” *J. Am. Coll. Cardiol.*, vol. 64, no. 4, pp. 385–390, 2014.
- [135] B. Wang *et al.*, “Plasmonic intravascular photoacoustic imaging for detection of macrophages in atherosclerotic plaques,” *Nano Lett.*, vol. 9, no. 6, pp. 2212–2217, 2008.
- [136] T. Quillard and P. Libby, “Molecular imaging of atherosclerosis for improving diagnostic and therapeutic development,” *Circ. Res.*, vol. 111, no. 2, pp. 231–244, 2012.
- [137] M. O’Donnell *et al.*, “Multimodality cardiovascular molecular imaging technology,” *J. Nucl. Med.*, vol. 51, no. Supplement 1, p. 38S–50S, 2010.
- [138] Y. Lao, D. Xing, S. Yang, and L. Xiang, “Noninvasive photoacoustic imaging of the developing vasculature during early tumor growth,” *Phys. Med. Biol.*, vol. 53, no. 15, p. 4203, 2008.
- [139] R. I. Siphanto *et al.*, “Serial noninvasive photoacoustic imaging of neovascularization in tumor angiogenesis,” *Opt. Express*, vol. 13, no. 1, pp. 89–95, 2005.
- [140] X. Liang-Zhong *et al.*, “In vivo monitoring of neovascularization in tumour angiogenesis by photoacoustic tomography,” *Chin. Phys. Lett.*, vol. 24, no. 3, p. 751, 2007.
- [141] E. I. Galanzha and V. P. Zharov, “Photoacoustic flow cytometry,” *Methods*, vol. 57, no. 3, pp. 280–296, 2012.
- [142] E. I. Galanzha, M. Sarimollaoglu, D. A. Nedosekin, S. G. Keyrouz, J. L. Mehta, and V. P. Zharov, “In vivo flow cytometry of circulating clots using negative photothermal and photoacoustic contrasts,” *Cytometry A*, vol. 79, no. 10, pp. 814–824, 2011.
- [143] E. Hysi, R. K. Saha, M. Rui, and M. C. Kolios, “Detection and characterization of red blood cell (RBC) aggregation with photoacoustics,” in *SPIE BiOS*, 2012, p. 82233E–82233E.
- [144] R. K. Saha and M. C. Kolios, “A simulation study on photoacoustic signals from red blood cells,” *J. Acoust. Soc. Am.*, vol. 129, no. 5, pp. 2935–2943, 2011.
- [145] J. J. Cronan, G. S. Dorfman, F. H. Scola, B. Schepps, and J. Alexander, “Deep venous thrombosis: US assessment using vein compression,” *Radiology*, vol. 162, no. 1, pp. 191–194, 1987.

References

- [146] E. Hysi, R. K. Saha, and M. C. Kolios, "On the use of photoacoustics to detect red blood cell aggregation," *Biomed. Opt. Express*, vol. 3, no. 9, pp. 2326–2338, 2012.
- [147] E. M. Strohm, E. S. Berndl, and M. C. Kolios, "Probing red blood cell morphology using high-frequency photoacoustics," *Biophys. J.*, vol. 105, no. 1, pp. 59–67, 2013.
- [148] J.-T. Oh, M.-L. Li, H. F. Zhang, K. Maslov, G. Stoica, and L. V. Wang, "Three-dimensional imaging of skin melanoma in vivo by dual-wavelength photoacoustic microscopy," *J. Biomed. Opt.*, vol. 11, no. 3, pp. 34032–34032, 2006.
- [149] M. Gerling *et al.*, "Real-time assessment of tissue hypoxia in vivo with combined photoacoustics and high-frequency ultrasound," *Theranostics*, vol. 4, no. 6, p. 604, 2014.
- [150] M.-L. Li *et al.*, "Simultaneous molecular and hypoxia imaging of brain tumors in vivo using spectroscopic photoacoustic tomography," *Proc. IEEE*, vol. 96, no. 3, pp. 481–489, 2008.
- [151] Q. Shao, E. Morgounova, C. Jiang, J. Choi, J. Bischof, and S. Ashkenazi, "In vivo photoacoustic lifetime imaging of tumor hypoxia in small animals," *J. Biomed. Opt.*, vol. 18, no. 7, pp. 76019–76019, 2013.
- [152] K. Pantel and C. Alix-Panabières, "Circulating tumour cells in cancer patients: challenges and perspectives," *Trends Mol. Med.*, vol. 16, no. 9, pp. 398–406, 2010.
- [153] E. I. Galanzha, E. V. Shashkov, P. M. Spring, J. Y. Suen, and V. P. Zharov, "In vivo, noninvasive, label-free detection and eradication of circulating metastatic melanoma cells using two-color photoacoustic flow cytometry with a diode laser," *Cancer Res.*, vol. 69, no. 20, pp. 7926–7934, 2009.
- [154] E. I. Galanzha and V. P. Zharov, "Photoacoustic flow cytometry," *Methods*, vol. 57, no. 3, pp. 280–296, 2012.
- [155] V. P. Zharov, E. I. Galanzha, E. V. Shashkov, N. G. Khlebtsov, and V. V. Tuchin, "In vivo photoacoustic flow cytometry for monitoring of circulating single cancer cells and contrast agents," *Opt. Lett.*, vol. 31, no. 24, pp. 3623–3625, 2006.
- [156] D. Wu, L. Huang, M. S. Jiang, and H. Jiang, "Contrast agents for photoacoustic and thermoacoustic imaging: a review," *Int. J. Mol. Sci.*, vol. 15, no. 12, pp. 23616–23639, 2014.
- [157] S. Bhattacharyya, S. Wang, D. Reinecke, W. Kiser Jr, R. A. Kruger, and T. R. DeGrado, "Synthesis and evaluation of near-infrared (NIR) dye- herceptin conjugates as photoacoustic computed tomography (PCT) probes for HER2 expression in breast cancer," *Bioconjug. Chem.*, vol. 19, no. 6, pp. 1186–1193, 2008.

-
- [158] P.-C. Li *et al.*, “Photoacoustic imaging of multiple targets using gold nanorods,” *IEEE Trans. Ultrason. Ferroelectr. Freq. Control*, vol. 54, no. 8, pp. 1642–1647, 2007.
- [159] K. Homan *et al.*, “Combined ultrasound and photoacoustic imaging of pancreatic cancer using nanocage contrast agents,” in *SPIE BiOS: Biomedical Optics*, 2009, p. 71771M–71771M.
- [160] X. Yang, S. E. Skrabalak, Z.-Y. Li, Y. Xia, and L. V. Wang, “Photoacoustic tomography of a rat cerebral cortex in vivo with Au nanocages as an optical contrast agent,” *Nano Lett.*, vol. 7, no. 12, pp. 3798–3802, 2007.
- [161] Y. Wang *et al.*, “Photoacoustic tomography of a nanoshell contrast agent in the in vivo rat brain,” *Nano Lett.*, vol. 4, no. 9, pp. 1689–1692, 2004.
- [162] S. Mallidi, G. P. Luke, and S. Emelianov, “Photoacoustic imaging in cancer detection, diagnosis, and treatment guidance,” *Trends Biotechnol.*, vol. 29, no. 5, pp. 213–221, 2011.
- [163] L. V. Wang, “Tutorial on photoacoustic microscopy and computed tomography,” *IEEE J. Sel. Top. Quantum Electron.*, vol. 14, no. 1, pp. 171–179, 2008.
- [164] W. G. Zijlstra, A. Buursma, and W. P. Meeuwssen-Van der Roest, “Absorption spectra of human fetal and adult oxyhemoglobin, de-oxyhemoglobin, carboxyhemoglobin, and methemoglobin,” *Clin. Chem.*, vol. 37, no. 9, pp. 1633–1638, 1991.
- [165] K. H. Song and L. V. Wang, “Deep reflection-mode photoacoustic imaging of biological tissue,” *J. Biomed. Opt.*, vol. 12, no. 6, pp. 60503–60503, 2007.
- [166] M. Weik, *Communications Standard Dictionary*. Springer Science & Business Media, 2012.
- [167] J. Beutel, H. L. Kundel, and R. L. V. Metter, *Handbook of Medical Imaging: Physics and psychophysics*. SPIE Press, 2000.
- [168] W. J. Tompkins, *Biomedical Digital Signal Processing: C-language Examples and Laboratory Experiments for the IBM PC*. Prentice-Hall Of India Pvt. Limited, 2006.
- [169] J. G. Proakis and D. G. Manolakis, *Digital Signal Processing*. Pearson Prentice Hall, 2007.
- [170] K. Thirumala, A. C. Umarikar, and T. Jain, “Estimation of single-phase and three-phase power-quality indices using empirical wavelet transform,” *IEEE Trans. Power Deliv.*, vol. 30, no. 1, pp. 445–454, 2015.
- [171] J. Gilles, “Empirical wavelet transform,” *IEEE Trans. Signal Process.*, vol. 61, no. 16, pp. 3999–4010, 2013.
- [172] G. Rutkowski, K. Patan, and P. Leśniak, “Comparison of Time-Frequency Feature Extraction Methods for EEG Signals

References

- Classification,” in *Artificial Intelligence and Soft Computing*, 2013, pp. 320–329.
- [173] M. Unser and A. Aldroubi, “A review of wavelets in biomedical applications,” *Proc. IEEE*, vol. 84, no. 4, pp. 626–638, 1996.
- [174] B. Boashash, *Time-frequency signal analysis and processing: a comprehensive reference*. Academic Press, 2015.
- [175] W. J. Staszewski, K. Worden, and G. R. Tomlinson, “Time–frequency analysis in gearbox fault detection using the Wigner–Ville distribution and pattern recognition,” *Mech. Syst. Signal Process.*, vol. 11, no. 5, pp. 673–692, 1997.
- [176] P. S. Wright, “Short-time Fourier transforms and Wigner-Ville distributions applied to the calibration of power frequency harmonic analyzers,” *IEEE Trans. Instrum. Meas.*, vol. 48, no. 2, pp. 475–478, 1999.
- [177] Q. Shen, T. Sato, M. Hashimoto, C. Chen, and T. Toyoda, “Photoacoustic and photoelectrochemical characterization of CdSe-sensitized TiO₂ electrodes composed of nanotubes and nanowires,” *Thin Solid Films*, vol. 499, no. 1, pp. 299–305, 2006.
- [178] C. G. Hoelen, R. Pongers, G. Hamhuis, F. F. de Mul, and J. Greve, “Photoacoustic blood cell detection and imaging of blood vessels in phantom tissue,” in *BiOS Europe ’97*, 1998, pp. 142–153.
- [179] J. M. Diamond, “The mechanism of isotonic water transport,” *J. Gen. Physiol.*, vol. 48, no. 1, p. 15, 1964.
- [180] S. M. Huber, N. Gamper, and F. Lang, “Chloride conductance and volume-regulatory nonselective cation conductance in human red blood cell ghosts,” *Pflüg. Arch. Eur. J. Physiol.*, vol. 441, no. 4, pp. 551–558, 2001.
- [181] R. Glaser, “The shape of red blood cells as a function of membrane potential and temperature,” *J. Membr. Biol.*, vol. 51, no. 3–4, pp. 217–228, 1979.
- [182] H. Masugata *et al.*, “Physical properties of the mitral valve tissue assessed by tissue sound speed in cardiac amyloidosis: relationship to the severity of mitral regurgitation,” *Ultrasound Med. Biol.*, vol. 26, no. 7, pp. 1191–1198, 2000.
- [183] B. E. Treeby, J. Jaros, D. Rohrbach, and B. T. Cox, “Modelling elastic wave propagation using the k-Wave MATLAB Toolbox,” in *2014 IEEE International Ultrasonics Symposium*, 2014, pp. 146–149.
- [184] B. T. Cox, J. G. Laufer, K. P. Kostli, and P. C. Beard, “Experimental validation of photoacoustic k-Space propagation models,” 2004, p. 238.

- [185] J. R. Cook, R. R. Bouchard, and S. Y. Emelianov, “Tissue-mimicking phantoms for photoacoustic and ultrasonic imaging,” *Biomed. Opt. Express*, vol. 2, no. 11, pp. 3193–3206, 2011.
- [186] K. M. Quan, G. B. Christison, H. A. MacKenzie, and P. Hodgson, “Glucose determination by a pulsed photoacoustic technique: an experimental study using a gelatin-based tissue phantom,” *Phys. Med. Biol.*, vol. 38, no. 12, p. 1911, 1993.
- [187] K. Zell, J. I. Sperl, M. W. Vogel, R. Niessner, and C. Haisch, “Acoustical properties of selected tissue phantom materials for ultrasound imaging,” *Phys. Med. Biol.*, vol. 52, no. 20, p. N475, 2007.
- [188] J. J. Hawkes, M. J. Long, W. T. Coakley, and M. B. McDonnell, “Ultrasonic deposition of cells on a surface,” *Biosens. Bioelectron.*, vol. 19, no. 9, pp. 1021–1028, 2004.
- [189] X. M. Zhang, M. Fatemi, R. R. Kinnick, and J. F. Greenleaf, “Noncontact ultrasound stimulated optical vibrometry study of coupled vibration of arterial tubes in fluids,” *J. Acoust. Soc. Am.*, vol. 113, no. 3, pp. 1249–1257, 2003.
- [190] D. W. Rickey, P. A. Picot, D. A. Christopher, and A. Fenster, “A wall-less vessel phantom for Doppler ultrasound studies,” *Ultrasound Med. Biol.*, vol. 21, no. 9, pp. 1163–1176, 1995.
- [191] A. Vogel and V. Venugopalan, “Mechanisms of pulsed laser ablation of biological tissues,” *Chem. Rev.*, vol. 103, no. 2, pp. 577–644, 2003.
- [192] B. Dahlbäck, “Blood coagulation,” *The Lancet*, vol. 355, no. 9215, pp. 1627–1632, 2000.
- [193] H. Li, D. Han, G. Pauletti, and A. Steckl, “Blood coagulation screening using a paper-based microfluidic lateral flow device,” *Lab. Chip*, vol. 14, no. 20, pp. 4035–4041, 2014.
- [194] D. J. Kuter and R. D. Rosenberg, “Hemorrhagic disorders III. Disorders of hemostasis,” *Hematology*, pp. 577–598, 1991. [195] K. E. Brummel, “Thrombin functions during tissue factor-induced blood coagulation,” *Blood*, vol. 100, no. 1, pp. 148–152, Jun. 2002.
- [196] D. Gailani and G. J. Broze, “Factor XI activation in a revised model of blood coagulation,” *Science*, vol. 253, no. 5022, pp. 909–912, Aug. 1991.
- [197] J. W. Weisel, “The mechanical properties of fibrin for basic scientists and clinicians,” *Biophys. Chem.*, vol. 112, no. 2–3, pp. 267–276, Dec. 2004.
- [198] J. F. Greenleaf, M. Fatemi, and M. Insana, “Selected methods for imaging elastic properties of biological tissues,” *Annu. Rev. Biomed. Eng.*, vol. 5, no. 1, pp. 57–78, 2003.

References

- [199] Y. Saijo *et al.*, “Ultrasonic tissue characterization of atherosclerosis by a speed-of-sound microscanning system,” *IEEE Trans. Ultrason. Ferroelectr. Freq. CONTROL*, vol. 54, no. 8, p. 1571, 2007.
- [200] J. E. Hall, *Guyton and Hall Textbook of Medical Physiology E-Book*. Elsevier Health Sciences, 2015.
- [201] E. W. Davie and K. Fujikawa, “Basic mechanisms in blood coagulation,” *Annu. Rev. Biochem.*, vol. 44, no. 1, pp. 799–829, 1975.
- [202] D. M. Adcock, D. C. Kressin, and R. A. Marlar, “Minimum specimen volume requirements for routine coagulation testing: dependence on citrate concentration,” *Am. J. Clin. Pathol.*, vol. 109, no. 5, pp. 595–599, 1998.
- [203] Y. Liu and Z. Yuan, “Multi-spectral photoacoustic elasticity tomography,” *Biomed. Opt. Express*, vol. 7, no. 9, p. 3323, Sep. 2016.
- [204] H.-P. Brecht, R. Su, M. Fronheiser, S. A. Ermilov, A. Conjusteau, and A. A. Oraevsky, “Whole-body three-dimensional optoacoustic tomography system for small animals,” *J. Biomed. Opt.*, vol. 14, no. 6, pp. 64007–64007–8, 2009.
- [205] M. Ishihara, M. Sato, S. Sato, T. Kikuchi, K. Fujikawa, and M. Kikuchi, “Viscoelastic characterization of biological tissue by photoacoustic measurement,” *Jpn. J. Appl. Phys.*, vol. 42, no. 5B, p. L556, 2003.
- [206] M. Ishihara, M. Sato, S. Sato, T. Kikuchi, K. Fujikawa, and M. Kikuchi, “Biomechanical characterization of tissue-engineered cartilages by photoacoustic measurement,” in *Biomedical Optics 2003*, 2003, pp. 221–225.
- [207] B. Furie and B. C. Furie, “The molecular basis of blood coagulation,” *Cell*, vol. 53, no. 4, pp. 505–518, 1988.
- [208] S. Sazawal and R. E. Black, “Effect of pneumonia case management on mortality in neonates, infants, and preschool children: a meta-analysis of community-based trials,” *Lancet Infect. Dis.*, vol. 3, no. 9, pp. 547–556, Sep. 2003.
- [209] O. Ruuskanen, E. Lahti, L. C. Jennings, and D. R. Murdoch, “Viral pneumonia,” *Lancet Lond. Engl.*, vol. 377, no. 9773, pp. 1264–1275, Apr. 2011.
- [210] L. Liu *et al.*, “Global, regional, and national causes of child mortality in 2000–13, with projections to inform post-2015 priorities: an updated systematic analysis,” *Lancet Lond. Engl.*, vol. 385, no. 9966, pp. 430–440, Jan. 2015.
- [211] J. Bryce, C. Boschi-Pinto, K. Shibuya, R. E. Black, W. C. H. E. R. Group, and others, “WHO estimates of the causes of death in children,” *The Lancet*, vol. 365, no. 9465, pp. 1147–1152, 2005.

- [212] M. Fiszman, W. W. Chapman, D. Aronsky, R. S. Evans, and P. J. Haug, “Automatic detection of acute bacterial pneumonia from chest X-ray reports,” *J. Am. Med. Inform. Assoc.*, vol. 7, no. 6, pp. 593–604, 2000.
- [213] R. Smith-Bindman *et al.*, “Radiation dose associated with common computed tomography examinations and the associated lifetime attributable risk of cancer,” *Arch. Intern. Med.*, vol. 169, no. 22, pp. 2078–2086, 2009.
- [214] P. Moine, J.-B. Vercken, S. Chevret, C. Chastang, and P. Gajdos, “Severe community-acquired pneumonia: etiology, epidemiology, and prognosis factors,” *Chest*, vol. 105, no. 5, pp. 1487–1495, 1994.
- [215] L. A. Mandell *et al.*, “Infectious Diseases Society of America/American Thoracic Society consensus guidelines on the management of community-acquired pneumonia in adults,” *Clin. Infect. Dis.*, vol. 44, no. Supplement 2, pp. S27–S72, 2007.
- [216] A. P. the U. of S. M. H. M. L. Story and L. Story, *Pathophysiology*. Jones & Bartlett Publishers, 2011.
- [217] J. F. Tomashefski, *Dail and Hammar’s Pulmonary Pathology: Volume I: Nonneoplastic Lung Disease*. Springer Science & Business Media, 2009.
- [218] W. Navidi, *Statistics for Engineers and Scientists*. McGraw-Hill Education, 2014.
- [219] A. H. Fischer, K. A. Jacobson, J. Rose, and R. Zeller, “Hematoxylin and eosin staining of tissue and cell sections,” *Cold Spring Harb. Protoc.*, vol. 2008, no. 5, p. pdb–prot4986, 2008.
- [220] F. Gao, X. Feng, and Y. Zheng, “Photoacoustic elastic oscillation and characterization,” *Opt. Express*, vol. 23, no. 16, pp. 20617–20628, 2015.
- [221] K. Ogata, *Modern Control Engineering*. Prentice Hall, 2010.
- [222] J. Lorenz, D. Sheth, and J. Patel, “Bronchial Artery Embolization,” *Semin. Interv. Radiol.*, vol. 29, no. 3, pp. 155–160, Sep. 2012.
- [223] H. A. McCordock and R. S. Muckenfuss, “The similarity of virus pneumonia in animals to epidemic influenza and interstitial bronchopneumonia in man,” *Am. J. Pathol.*, vol. 9, no. 2, p. 221, 1933.
- [224] K. K. Shung, “On the ultrasound scattering from blood as a function of hematocrit,” *IEEE Trans. Sonics Ultrason.*, vol. 29, no. 6, pp. 327–330, 1982.
- [225] G. Xu, Z. Meng, J. Lin, P. Carson, and X. Wang, “Functional pitch of a liver: fatty liver disease diagnosis with photoacoustic spectrum analysis,” 2014, vol. 8943, p. 89431G–89431G–9.

References

- [226] F. Sardanelli *et al.*, “Sensitivity of MRI versus mammography for detecting foci of multifocal, multicentric breast cancer in fatty and dense breasts using the whole-breast pathologic examination as a gold standard,” *Am. J. Roentgenol.*, vol. 183, no. 4, pp. 1149–1157, 2004.
- [227] C. DeSantis, J. Ma, L. Bryan, and A. Jemal, “Breast cancer statistics, 2013,” *CA. Cancer J. Clin.*, vol. 64, no. 1, pp. 52–62, Feb. 2014.
- [228] A. Jemal *et al.*, “Cancer Statistics, 2008,” *CA. Cancer J. Clin.*, vol. 58, no. 2, pp. 71–96, Mar. 2008.
- [229] D. Trichopoulos, B. MacMahon, and P. Cole, “Menopause and breast cancer risk,” *J. Natl. Cancer Inst.*, vol. 48, no. 3, pp. 605–613, 1972.
- [230] E. H. B. C. C. Group and others, “Body mass index, serum sex hormones, and breast cancer risk in postmenopausal women,” *J. Natl. Cancer Inst.*, vol. 95, no. 16, pp. 1218–1226, 2003.
- [231] V. Singh, C. Saunders, L. Wylie, and A. Bourke, “New diagnostic techniques for breast cancer detection,” *Future Oncol. Lond. Engl.*, vol. 4, no. 4, pp. 501–513, Aug. 2008.
- [232] I. Saarenmaa *et al.*, “The effect of age and density of the breast on the sensitivity of breast cancer diagnostic by mammography and ultrasonography,” *Breast Cancer Res. Treat.*, vol. 67, no. 2, pp. 117–123, May 2001.
- [233] R. E. Bird, T. W. Wallace, and B. C. Yankaskas, “Analysis of cancers missed at screening mammography,” *Radiology*, vol. 184, no. 3, pp. 613–617, Sep. 1992.
- [234] K. N. Anderson, R. B. Schwab, and M. E. Martinez, “Reproductive risk factors and breast cancer subtypes: a review of the literature,” *Breast Cancer Res. Treat.*, vol. 144, no. 1, pp. 1–10, Feb. 2014.
- [235] Z. Gao, J. Lin, X. Wang, and X. Xu, “Bearing Fault Detection Based on Empirical Wavelet Transform and Correlated Kurtosis by Acoustic Emission,” *Materials*, vol. 10, no. 6, p. 571, May 2017.
- [236] J. P. Amezcquita-Sanchez and H. Adeli, “A New Music-empirical Wavelet Transform Methodology for Time-frequency Analysis of Noisy Nonlinear and Non-stationary Signals,” *Digit Signal Process*, vol. 45, no. C, pp. 55–68, Oct. 2015.
- [237] N. F. Boyd, L. J. Martin, M. Bronskill, M. J. Yaffe, N. Duric, and S. Minkin, “Breast tissue composition and susceptibility to breast cancer,” *J. Natl. Cancer Inst.*, vol. 102, no. 16, pp. 1224–1237, Aug. 2010.
- [238] D. G. Tse, D. P. H. Tan, and P. D. F. Schmitt, “Basic Histopathology of Breast Lesions,” in *Fine Needle Aspiration*

-
- Cytology of the Breast*, Springer Berlin Heidelberg, 2013, pp. 7–29.
- [239] T. Tot, *Breast Cancer: A Lobar Disease*. Springer Science & Business Media, 2010.
- [240] D. Groelz, L. Sobin, P. Branton, C. Compton, R. Wyrich, and L. Rainen, “Non-formalin fixative versus formalin-fixed tissue: A comparison of histology and RNA quality,” *Exp. Mol. Pathol.*, vol. 94, no. 1, pp. 188–194, Feb. 2013.
- [241] I. Eltoun, J. Fredenburgh, R. B. Myers, and W. E. Grizzle, “Introduction to the theory and practice of fixation of tissues,” *J. Histotechnol.*, vol. 24, no. 3, pp. 173–190, 2001.
- [242] R. Farhadifar, J.-C. Röper, B. Aigouy, S. Eaton, and F. Jülicher, “The influence of cell mechanics, cell-cell interactions, and proliferation on epithelial packing,” *Curr. Biol. CB*, vol. 17, no. 24, pp. 2095–2104, Dec. 2007.
- [243] P. N. T. Wells and H.-D. Liang, “Medical ultrasound: imaging of soft tissue strain and elasticity,” *J. R. Soc. Interface*, vol. 8, no. 64, pp. 1521–1549, Nov. 2011.
- [244] O. Rouvière *et al.*, “MR elastography of the liver: preliminary results,” *Radiology*, vol. 240, no. 2, pp. 440–448, Aug. 2006.
- [245] C. H. Liu *et al.*, “Human breast tissues studied by IR Fourier-transform Raman spectroscopy,” in *Conference on Lasers and Electro-Optics*, 1991, p. CWF51.
- [246] B. Elenbaas *et al.*, “Human breast cancer cells generated by oncogenic transformation of primary mammary epithelial cells,” *Genes Dev.*, vol. 15, no. 1, pp. 50–65, Jan. 2001.
- [247] M. Guray and A. A. Sahin, “Benign Breast Diseases: Classification, Diagnosis, and Management,” *The Oncologist*, vol. 11, no. 5, pp. 435–449, May 2006.
- [248] Y. Guo *et al.*, “Differentiation of clinically benign and malignant breast lesions using diffusion-weighted imaging,” *J. Magn. Reson. Imaging JMRI*, vol. 16, no. 2, pp. 172–178, Aug. 2002.
- [249] I. M. Ariel and J. B. Clearly, “Breast cancer: Diagnosis and treatment,” 1987.
- [250] T. M. Tuttle, E. B. Habermann, E. H. Grund, T. J. Morris, and B. A. Virnig, “Increasing use of contralateral prophylactic mastectomy for breast cancer patients: a trend toward more aggressive surgical treatment,” *J. Clin. Oncol.*, vol. 25, no. 33, pp. 5203–5209, 2007.
- [251] E. B. C. T. C. Group and others, “Effects of chemotherapy and hormonal therapy for early breast cancer on recurrence and 15-year survival: an overview of the randomised trials,” *The Lancet*, vol. 365, no. 9472, pp. 1687–1717, 2005.

References

- [252] D. E. Dolmans, D. Fukumura, and R. K. Jain, "Photodynamic therapy for cancer," *Nat. Rev. Cancer*, vol. 3, no. 5, pp. 380–387, 2003.
- [253] S. Rossi *et al.*, "Percutaneous RF interstitial thermal ablation in the treatment of hepatic cancer.," *AJR Am. J. Roentgenol.*, vol. 167, no. 3, pp. 759–768, 1996.
- [254] S. O. Pfliederer, M. G. Freesmeyer, C. Marx, R. Kühne-Heid, A. Schneider, and W. A. Kaiser, "Cryotherapy of breast cancer under ultrasound guidance: initial results and limitations," *Eur. Radiol.*, vol. 12, no. 12, pp. 3009–3014, 2002.
- [255] H. J. Burstein, "Side effects of chemotherapy," *J. Clin. Oncol.*, vol. 18, no. 3, pp. 693–693, 2000.
- [256] H. Birgisson, L. Pålman, U. Gunnarsson, and B. Glimelius, "Adverse effects of preoperative radiation therapy for rectal cancer: long-term follow-up of the Swedish Rectal Cancer Trial," *J. Clin. Oncol.*, vol. 23, no. 34, pp. 8697–8705, 2005.
- [257] I. H. El-Sayed, X. Huang, and M. A. El-Sayed, "Selective laser photo-thermal therapy of epithelial carcinoma using anti-EGFR antibody conjugated gold nanoparticles," *Cancer Lett.*, vol. 239, no. 1, pp. 129–135, 2006.
- [258] S. N. Goldberg, G. S. Gazelle, and P. R. Mueller, "Thermal ablation therapy for focal malignancy: a unified approach to underlying principles, techniques, and diagnostic imaging guidance," *Am. J. Roentgenol.*, vol. 174, no. 2, pp. 323–331, 2000.
- [259] T. Wu, J. P. Felmlee, J. F. Greenleaf, S. J. Riederer, and R. L. Ehman, "Assessment of thermal tissue ablation with MR elastography," *Magn. Reson. Med.*, vol. 45, no. 1, pp. 80–87, 2001.
- [260] S. Fife, C. D. Andereck, and S. Rahal, "Ultrasound thermometry in transparent and opaque fluids," *Exp. Fluids*, vol. 35, no. 2, pp. 152–158, 2003.
- [261] B. C. Wilson, I. A. Vitkin, W. M. Whelan, and L.-L. Chin, "Radiance-based monitoring of the extent of tissue coagulation during laser interstitial thermal therapy," *Opt. Lett. Publ. Opt. Soc. Am.*, no. 9, pp. 959–961, 2004.
- [262] M. H. Niemz, *Laser-Tissue Interactions: Fundamentals and Applications*. Springer Science & Business Media, 2013.
- [263] C. T. Germer *et al.*, "Optical properties of native and coagulated human liver tissue and liver metastases in the near infrared range," *Lasers Surg. Med.*, vol. 23, no. 4, pp. 194–203, 1998.
- [264] S. Grabtchak, L. G. Montgomery, and W. M. Whelan, "Optical absorption and scattering properties of bulk porcine muscle phantoms from interstitial radiance measurements in 650-900 nm

- range,” *Phys. Med. Biol.*, vol. 59, no. 10, pp. 2431–2444, May 2014.
- [265] L. J. Gathercole, M. J. Miles, T. J. McMaster, and D. F. Holmes, “Scanning probe microscopy of collagen I and pN-collagen I assemblies and the relevance to scanning tunnelling microscopy contrast generation in proteins,” *J. Chem. Soc. Faraday Trans.*, vol. 89, no. 15, pp. 2589–2594, Jan. 1993.
- [266] M. Ahn, N. T. Hau, N. Van Phuc, J. Oh, and H. W. Kang, “Photoactive dye-enhanced tissue ablation for endoscopic laser prostatectomy,” *Lasers Surg. Med.*, vol. 46, no. 9, pp. 703–711, Nov. 2014.
- [267] R. Shukla, V. Bansal, M. Chaudhary, A. Basu, R. R. Bhonde, and M. Sastry, “Biocompatibility of gold nanoparticles and their endocytotic fate inside the cellular compartment: a microscopic overview,” *Langmuir*, vol. 21, no. 23, pp. 10644–10654, 2005.
- [268] T. R. Tshikhudo, Z. Wang, and M. Brust, “Biocompatible gold nanoparticles,” *Mater. Sci. Technol.*, vol. 20, no. 8, pp. 980–984, 2004.
- [269] P. M. Tiwari, K. Vig, V. A. Dennis, and S. R. Singh, “Functionalized gold nanoparticles and their biomedical applications,” *Nanomaterials*, vol. 1, no. 1, pp. 31–63, 2011.
- [270] S. Rana, A. Bajaj, R. Mout, and V. M. Rotello, “Monolayer coated gold nanoparticles for delivery applications,” *Adv. Drug Deliv. Rev.*, vol. 64, no. 2, pp. 200–216, 2012.
- [271] X. Huang, P. K. Jain, I. H. El-Sayed, and M. A. El-Sayed, “Gold nanoparticles: interesting optical properties and recent applications in cancer diagnostics and therapy,” *Nanomed.*, vol. 2, no. 5, pp. 681–693, 2007.
- [272] L. Dykman and N. Khlebtsov, “Gold nanoparticles in biomedical applications: recent advances and perspectives,” *Chem. Soc. Rev.*, vol. 41, no. 6, pp. 2256–2282, 2012.
- [273] M. Hu *et al.*, “Gold nanostructures: engineering their plasmonic properties for biomedical applications,” *Chem. Soc. Rev.*, vol. 35, no. 11, pp. 1084–1094, 2006.

References
